Universidade de Aveiro Departamento de Química
2007

Gil Alberto Batista Gonçalves

Sintese e caracterização de nanocompósitos de TiO_2/celulose

Synthesis and characterization of TiO_2/cellulose nanocomposites

Universidade de Aveiro Departamento de Química
2007

Gil Alberto Batista Gonçalves

Sintese e caracterização de nanocompósitos de TiO_2/celulose

Synthesis and characterization of TiO_2/cellulose nanocomposites

dissertação apresentada à Universidade de Aveiro para cumprimento dos requisitos necessários à obtenção do grau de Mestre em Ciência e Engenharia de Materiais, realizada sob a orientação científica do Professor Associado Tito da Silva Trindade e do Professor Catedrático Carlos de Pascoal Neto do Departamento de Química da Universidade de Aveiro

A todos os meus familiares e amigos um muito obrigado

o júri

presidente

Doutor João Carlos Matias Celestino Gomes da Rocha
Professor Catedrático da Universidade de Aveiro

Doutor Carlos de Pascoal Neto
Professor Catedrático da Universidade de Aveiro

Doutor Tito da Silva Trindade
Professor Associado da Universidade de Aveiro

Doutora Eulália Fernanda Alves de Carvalho Pereira
Professora Auxiliar da Faculdade de Ciências da Universidade do Porto

agradecimentos

Em primeiro lugar quero agradecer aos meus orientadores, o Professor Associado Tito da Silva Trindade e o Professor Catedrático Carlos de Pascoal Neto, pela orientação científica, pelo seu apoio e disponibilidade constantes durante o projecto.

Ao Projecto Europeu Sustainpack pelo suporte financeiro para a realização do projecto

Aos meus colegas de grupo Paula Alexandrina e Ricardo Pinto agradeço a ajuda na realização de alguns ensaios laboratoriais e continuo apoio anímico. Queria também agradecer aos meus amigos Carlos Granadeiro, Jean Conceição e Rui Domingues pelo apoio técnico dado.

Quero também agradecer aos meus colegas de laboratório bem como aos outros docentes do Grupo dos Materiais Macromoleculares e Lenhocelulósicos pelo apoio que me prestaram quando precisei.

palavras-chave

Celulose, dióxido de titânio, nanocompósitos, fotocatálise, actividade antibacteriana.

resumo

O objectivo principal desta tese foi a preparação, caracterização e estudo de possíveis aplicações de novos nanocompósitos de TiO_2/celulose.
Numa primeira fase, os nanocompósitos de TiO_2/celulose foram preparados a partir da síntese *in situ* do TiO_2 na presença de fibras celulósicas. Para esta síntese estudaram-se os parâmetros experimentais que permitem controlar a hidrólise do tetracloreto de titânio ($TiCl_4$) e ureia, na presença de fibras celulósicas. Através desta abordagem *in situ* verificou-se que a concentração de ureia permite controlar a quantidade de TiO_2 e a fase cristalina nos nanocompósitos. Existem evidências que as fibras celulósicas promovem a nucleação e o crescimento das partículas de TiO_2 na sua superfície, conferindo um perfeito revestimento das fibras com nanopartículas de TiO_2, com percentagem de TiO_2 entre 5,6 e 23% (m/m) dependendo das condições de síntese.
Contudo uma contrariedade foi identificada após esta síntese, verificou-se que após exposição solar os nanocompósitos preparados adquiriram uma cor amarelada, o que pode ser indicativo da destruição das fibras da celulose devido às propriedades semicondutoras do TiO_2.
Para proteger o substrato da fotodegradação promovida pelo TiO_2, estudaram-se novas abordagens para a preparação deste tipo de materiais, nomeadamente ligação de nanopartículas de TiO_2 (previamente sintetizadas) à fibra por método de deposição por camadas de polielectrólitos (em inglês Layer-by-Layer (LbL)). Esta abordagem foi aplicada não só a fibras não revestidas mas também a fibras previamente protegidas com diferentes silanos. Dependendo do tipo de silanos usados para proteger a fibra, novas propriedades dos nanocompósitos finais foram obtidas, em particular hidrofobicidade e estabilidade térmica.
Os nanocompósitos e nanoparticulas foram caracterizados por, TEM, SEM, FTIR, TGA e DRX.
Devido às propriedades intrínsecas do dióxido de titânio, estudou-se a possível aplicação destes materiais em fotocatálise e como agentes antibacterianos. Ambos os estudos revelaram que estes novos nanocompósitos possuem propriedades fotocatílticas e antibacterianas interessantes.
Os nanocompositos de TiO_2/celulose podem resultar em interessantes aplicações, como materiais de embalagem ou materiais funcionais, explorando assim as propriedades específicas do TiO_2 tais como o elevado índice de refracção e as características semicondutoras.

keywords

Cellulose, titanium dioxide, nanocomposites, photocatalysis, antibacterial activity.

abstract

The aim of the present thesis was the preparation and characterization of TiO_2/cellulose nanocomposites.

TiO_2/cellulose nanocomposites were first prepared using an in situ methodology based on the controlled hydrolysis of titanium tetrachloride ($TiCl_4$) and urea, in the presence of wood cellulosic fibres. There is evidence from this study that the urea concentration allows to control both the content of TiO_2 and the crystalline phase in nanocomposites. Depending on the experimental conditions used, the cellulose fibres promoted the nucleation and growth of TiO_2 particles on their surfaces, yielding homogeneously coated fibres with TiO_2 content between 5.6 and 23.0% (w/w).

However, one drawback was identified in these new nanocomposites, after light exposure the nanocomposites turned yellowish possibly due to degradation of cellulose fibres due to the photoactivity of TiO_2 nanoparticles.

To protect the substrate from the TiO_2 photodegradation, two different chemical modifications of cellulose surface were performed: Layer-by-Layer (LbL) assembly with polyelectrolyte agents and silanization with functional silane agents. Depending on the type of silane used, new properties of nanocomposite materials were achieved like hydrophobicity and fire retardance. After this cellulose surface treatment, TiO_2 nanoparticles were deposited on top of the protective layer.

All the materials were characterized by TEM, SEM, FTIR, TGA and DRX.

Due to the semiconductor properties of titanium dioxide, these new nanocomposites may find interesting applications namely in photocatalysis and antibacterial applications. Both applications were studied and showed that TiO_2/cellulose nanocomposites may have good performances in those fields.

TiO_2/cellulose nanocomposites materials may have interesting applications, namely as fibres in composites for packing applications or as functional materials, exploring specific properties of TiO_2 such as its high refraction index or its semiconductor nature.

Contents

Abbreviations

AGU	Anhydroglucose
DP	Degree of polymerization
DS	Degree of substitution
Eg	Energy of band gap
FTIR	Fourier transform infrared
ICP	Inductively coupled plasma
LbL	Layer by layer
MB	Methylene blue
OTMS	Octyltrimethoxysilane
P-25	Commercial titanium dioxide (Degussa)
PDDA	Poly(diallydimethylammonium chloride)
PSS	Poly(sodium 4-styrenesulfonate)
PTMS	Phenyltrimethoxysilane
SEM	Scanning electron microscopy
TEM	Transmission electron microscopy
TEOS	Tetraethoxysilane
TEOT	Titanium tetraethoxide
TGA	Thermal gravimetric analysis
UDP	Uridine diphosphate glucose
UV	Ultraviolet
UV/Vis	Ultraviolet-Visible
VOCs	Volatile organic compounds
XRD	X-ray diffraction

List of figures and tables

Figures

Tables

1- General Introduction

1.1- Cellulose

1.1.1- Vegetal cellulose

Cellulose is the most common organic polymer, representing about $1.5x10^{12}$ tons of the total annual biomass production, and is considered to be an almost inexhaustible source of raw material for the increasing demand of environmentally friendly and biocompatible products [1, 2]. Wood pulp remains the most important raw material source for the processing of cellulose, most of which is used for the production of paper and cardboard. The fascination for the cellulose biopolymer is a result of its specific structure. The fusion of both carbohydrate and polymer chemistry in a macromolecule composed by repeating units generates surprising specificity and impressively diverse architectures, reactivities and functions. In contrast to carbohydrates of low molar mass, the reactions and properties of cellulose are determined by intermolecular interactions, cross-linking reactions, chain lengths, chain-length distribution, and by the distribution of functional groups on the repeating units and along the polymers chains [1, 3]. Cellulose is characterized by high chain stiffness and its sensitivity toward the hydrolysis and oxidation of the chain-forming acetal groups, which determine its chemistry and handling.

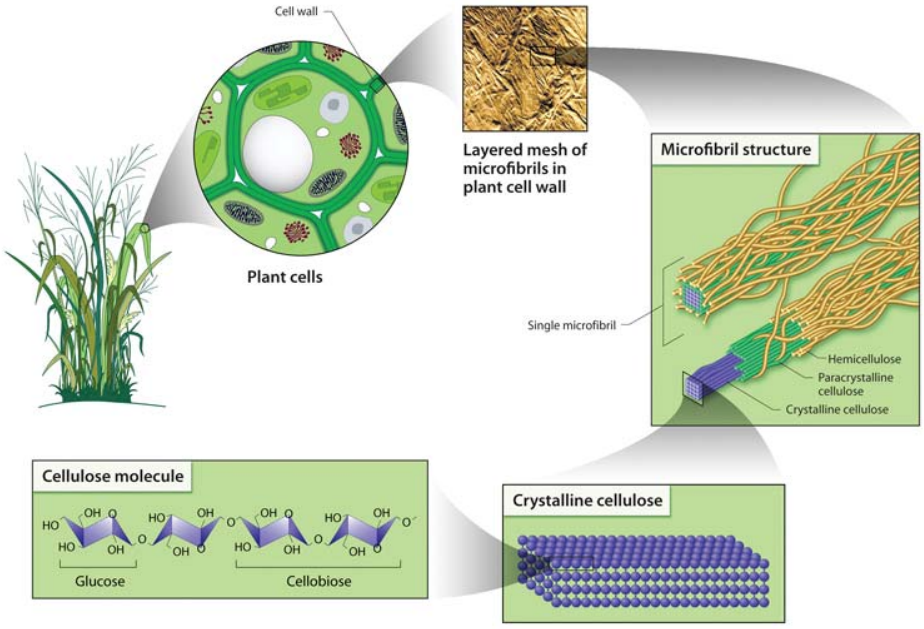

Figure 1 – Schematic representation of cellulose chains from plant cell walls, (Adapted from Cellulose Structure and Hydrolysis Challenges (*http://genomicsgtl.energy.gov)*)

Figure 1 shows the molecular structure of cellulose as a carbohydrate polymer generated from repeating β-D-glucopyranose molecules that are covalently linked through acetal function groups between the equatorial OH group of C_4 and C_1 carbon atom (β-1,4-glucan). As a result, cellulose is an extensive, linear-chain polymer with a large number of hydroxyl groups (three per anhydroglucose (**AGU**) unit) present in the thermodynamically preferred 4C1 conformation. To accommodate the preferred bond angles of the acetal oxygens bridges, every second **AGU** ring is rotated 180º in the plane. In this manner, two adjacent structural units define the disaccharide cellobiose [1-3].

The chain length of cellulose expressed in the number of constituent **AGUs** (degree of polymerization, **DP**) varies with the origin and treatment of the raw material. In the case of wood pulp, the values are typically between 300 and 1700. The molecular structure imparts cellulose with its characteristic properties: hydrophilicity, chirality, degradability and broad chemical variability initiated by the high reactivity of the OH groups. It is also the basis for extensive hydrogen bond networks, which give cellulose a multitude of partially crystalline fibre structures and morphologies. The properties of cellulose are therefore determined by a defined hierarchical order in supramolecular structure and organization.

The hierarchical structure of cellulose, formed by the hydrogen bond network between hydroxyl groups has been the subject of intense research for more than 100 years, marked by frequent controversy over results and consistent supply of new insight. A detailed analysis and modelling of various structural levels of cellulose is essential for synthetic reaction procedures, and for the controlled structure formation and properties of cellulose –based chemical products.

As a first approximation, the crystal structure of native cellulose (cellulose I) can be described as a monoclinic unit cell (space group $P2_1$) which contains chains in a parallel orientation with a twofold screw axis. In the decade of 80 it was discovered that native cellulose is present in two different cellulose I modifications (I_α and I_β), which can be found alongside each other: the I_α/I_β ratio depends on the origin of the cellulose. Some research studies revealed the corresponding crystalline structures to have triclinic (I_α) and monoclinic (I_β) unit cells [1, 3].

Figure 2 shows a schematic representation of the I_β crystal structure. In the side view (figure 2b) of the central chains of a unit cell, two intramolecular, chain-stiffening hydrogen bonds are revealed.

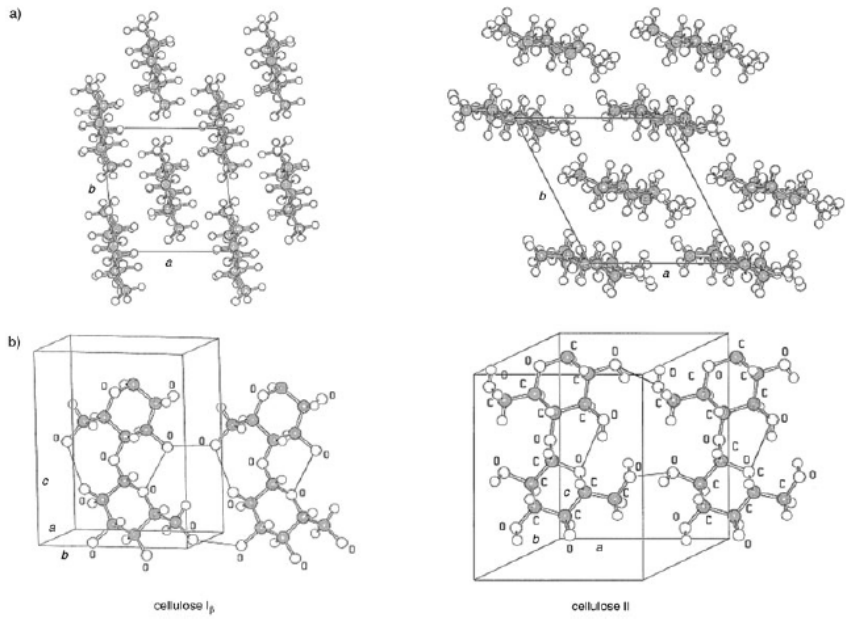

Figure 2 - Crystalline structure of cellulose (I and II) [3].

Apart from the thermodynamically less stable cellulose I, cellulose may occur in other crystalline forms (cellulose II, III and IV) of which cellulose II (figure 2) is the most stable structure of technical relevance. It can be formed from cellulose I by treatment with aqueous sodium hydroxide (mercerization) [4-6] or by dissolution of cellulose and subsequent precipitation/regeneration. This monoclinic crystal structure with two antiparallel chains in the unit cell is characterized by the specific unit cell geometry with a modified H-bonding system.

The biological function and other applications of cellulose are based on its distinct fibre morphology (figure 1 and 3). The morphological hierarchy is defined by elementary fibrils, microfibrils, and microfibrillar bands. The lateral dimensions of these structural units are between 1.5 and 3.5 nm in elementary fibrils, and around 100 nm for microfibrillar bands. The length of the microfibrils is on the order of several hundred manometers. The pore structure can be considered the counterpart of the fibril morphology of cellulose. It is considerably important for the accessibility in chemical reactions and enzymatic degradation. The controlled variation of pore structure enables cellulose

products to meet the needs of a wide range of applications, from highly specialized membranes and carrier materials to consumer goods, such as nonwovens, with excellent absorption properties.

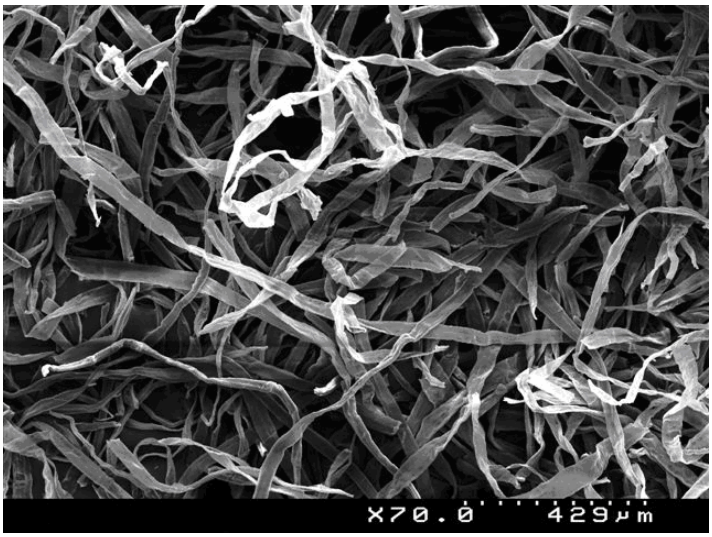

Figure 3 - Micrograph of plant cellulose fibres

Nowadays, chemical modification of natural cellulose fibres is an emerging area. Basically, cellulose reactions are usually more controlled by steric factors than it would be expected on the basis of the inherent reactivity of the different hydroxyl groups. There are three potential hydroxyls groups available on each anhydroglucose ring, so derivatives are usually characterized in terms of the degree of substitution (DS). In most cases, the substitution occurs in the less ordered regions and the crystalline regions remain unreacted. The most popular modifications are esterification, etherification and hydrolysis, however the most important at industrial scale are the acetates [1, 3, 7]. Cellulose derivatives are currently used in many applications such as coatings, optical films, composites, biodegradable plastics and biomedical materials.

1.1.2- Bacterial cellulose

The biosynthesis of cellulose takes place not only in plants but also in bacteria (such as *Acetobacte*r, *Acanthamoeba*, and *Achromobacter spp*.), algae (*Valonia*, *Chaetamorpha spp.*), and fungi [8].

The formation of cellulose by laboratory bacterial cultures is an interesting and attractive access to pure cellulose for both organic and polymer chemists. By selecting the substrates, culture conditions, various additives, and finally the bacterial strain, it is

possible to control the molar mass, the molar mass distribution, and the supramolecular structure. Thus it is possible to control important cellulose properties, and also the course of biosynthesis [3].

Amongst the cellulose-forming bacteria, Acetobacter strains (reclassified as the genus Gluconacetobacter) are especially suitable for the production and investigation of cellulose. These gram-negative and strictly aerobic bacteria form ellipsoidal, straight, or slightly bent rods in the 0.6-0.8x1.0-4.0 μm size range. They are not pathogenic and are commonly found on naturally grown fruits and in fruit products. Strains of the Acetobacter xylinus species produce extracellular cellulose that is easily isolated as fibre material.

Under static immersed culture conditions, a biofilm of varying thickness is produced which helps the colonized bacteria to maintain a high oxygen content near the surface, and that serves as a protective barrier against drying, natural enemies and radiation (figure 4**a)**).

The synthesis of bacterial cellulose occurs between the outer and plasma membranes of the cell by a cellulose-synthesizing complex (terminal complex) starting with uridine diphosphate glucose (**UDP** glucose). This complex is associated with bacterial cell surface pores, which have a diameter of about 3.5 nm. Cellulose synthesis catalyzes the addition of **UDP** glucose to the end of the growing cellulose chain, which exists in the cell as an elementary fibril, and then forms a 3D network with other elementary fibrils through the formation of microfibrils and ribbons (figure 4**b)**). Crystallization and polymerization of elementary fibrils are closely linked.

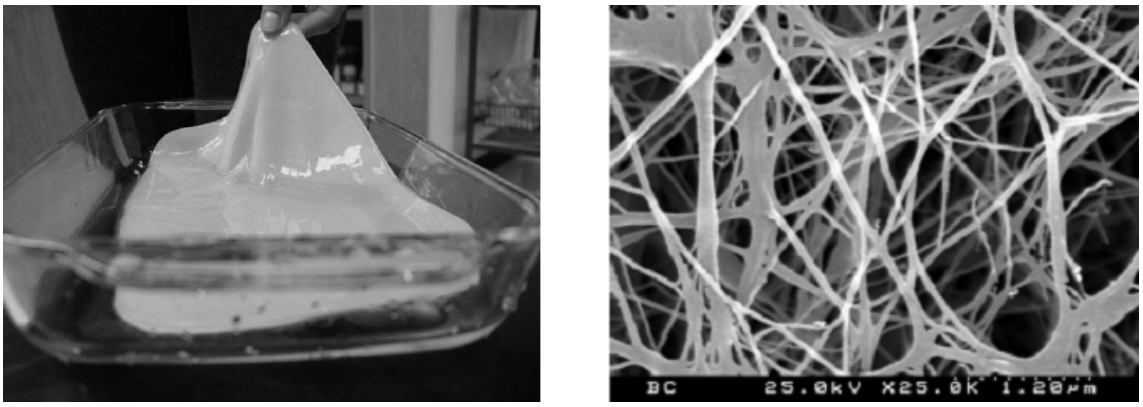

Figure 4 – Bacterial cellulose **a)** Normal photograph ([3, 8]) and **b)** SEM micrograph.

One single cell can convert over 100 glucose molecules into cellulose per hour. As the culture medium contains millions of bacteria, the polymer is synthesized relatively fast. The details of the polymerization catalyzed by cellulose synthase have been the subject of

controversy. The latest studies seem to indicate that the β-(1→4) linkage starts with the formation of cellobiose as an intermediate at a dual **UDP** glucose binding site.

Although identical to cellulose of plant origin in terms of molecular formula, bacterial cellulose is quite different. The degree of polymerization is very high, with **DP** (degree of polymerization) values of 2000-8000. Crystallinity is also high, with values of 60-90%. Bacterial cellulose is characterized by its high purity (no association with accompanying substances like hemicelluloses, lignin, or pectin) and by extremely high water content of 90% or more. Upon complete removal of water by air drying, the bacterial cellulose will only rehydrate to the same low extent as that of plant celluloses after re-exposure to water: about 6%. After gentle freeze-drying, however, it can absorb up to 70% of the original water content by re-swelling.

Through a stepwise exchange of water for other solvents, for instance it is possible to introduce methanol, acetone or n-hexane [3].

Because of its crystalline nano-and microfibril structure, bacterial cellulose has excellent mechanical properties. It is therefore well-suited as a reinforcing agent for paper and fibres made from glass, carbon, phenolic resins and silicon at small quantities (5%). Owing to the high modulus of elasticity in combination with a large internal loss factor, it is also a superior material for headphone and loudspeaker membranes [9].

Over the past few years, there has been an increasing interest in commercial applications of bacterial cellulose. Important examples include supports for proteins, cell cultures and microorganisms, products for temporary skin and tissue replacement, calorie-free food such as “Nata de Coco”, and additives in the production of lattices and paper. These activities are accompanied by the isolation of new bacterial strains, genetic modifications and a wide variation of all laboratory culture parameters. To create a new range of applications for bacterial cellulose it is possible to induce some surface modifications with functional materials.

1.2- Titanium dioxide

1.2.1- Introduction

Titanium is the ninth most abundant element in the Earth’s crust, where normally occurs combined with oxygen. The more important titanium minerals are *Ilmenite* ($FeTiO_3$), *Leucoxene* ($Fe_2O_3.TiO_2$) and *Rutile* (TiO_2). However the largest titanium

reserves in the world are in the form of *Titanomagnetite*, but these cannot be economically used at the present time. Titanium dioxide occurrences in Nature are never pure and are often found with other contaminants metals such as iron. These oxides raw materials can be mined and serve as a source for commercial titanium dioxide [10].

TiO_2 pigments are made from one of two chemical processes - the chloride process which produces TiO_2 products by reacting titanium ores with chlorine gas; and the sulphate process, which produces TiO_2 products by reacting titanium ores with sulphuric acid.

Titanium dioxide is the most important white pigment because of its scattering properties (which are superior to those of all other white pigments), its chemical stability, and lack of toxicity. Titanium dioxide is the most important inorganic pigment in terms of industrial production in the world.

Other applications for TiO_2 includes: catalysis, as a photocatalyst, in solar cells for the production of hydrogen and electric energy, gas sensor, corrosion protection, ceramics, electrical devices such as varistors and in medicine, as bone implants.

1.2.2- Chemical and physical properties

Unravelling the relationship between atomic structure and other physical and chemical properties is probably one of the most important achievements of titanium oxide science, because of the mixed ionic and covalent bonding in metal oxide systems.

Titanium dioxide crystallizes mainly in three different structures; *rutile* (tetragonal a=b=4.584Å, c=2.953Å), *anatase* (tetragonal, a=b=3.782Å, c=9.502Å) and *brookite* (rhombohedrical, a=5.436Å, b=9166Å, c=5.135Å) [11]. Other polymorphs are less important as pigment, for example, *cotunnite* TiO_2 has been synthesized at high pressures and is one of the hardest polycrystalline materials known.

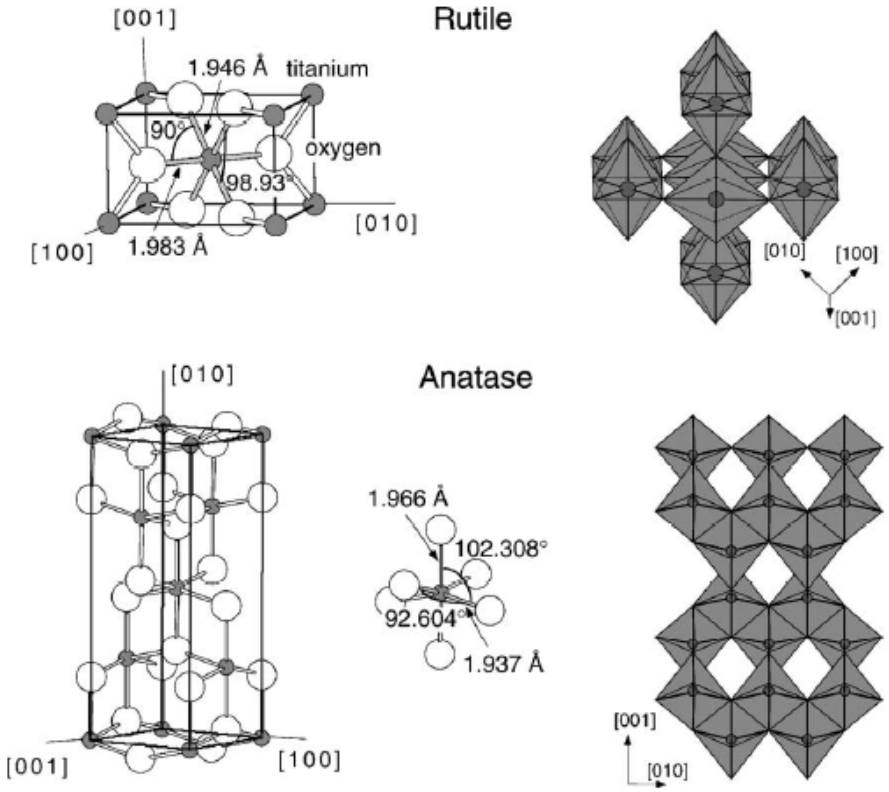

Figure 5 – Crystalline structure of titanium dioxide: Rutile and Anatase ([11]).

The structure of rutile and anatase can be described in terms of the spatial arrangement of TiO_6 octahedra, each Ti^{4+} ion is coordinated to six O^{2-} ions. The two crystal structures differ by the distortion of each octahedron and by the assembly pattern of the octahedra chains. Figure 5 (left) shows the unit cell of *rutile* and *anatase* crystals. The TiO_6 octahedron in *rutile* is not regular, showing a slight orthorhombic distortion. The octahedron in *anatase* is significantly distorted so that its symmetry is lower than orthorhombic. The Ti-Ti distances in *anatase* are greater (3.79 and 3.04 Å vs 3.57 and 2.96Å in *rutile*) whereas the Ti-O distances are shorter than in *rutile* (1.937 and 1.966 Å in *anatase* vs 1.946 and 1.983 Å in *rutile*) [12], as shown in figure 5. In the *rutile* structure each octahedron is in contact with 10 neighbouring octahedra (two sharing edge oxygen pairs and eight sharing corner oxygen atoms) while in the *anatase* structure each octahedron is in contact with eight neighbours (four sharing an edge and four sharing a corner). These structural differences explain the different mass densities and electronic band structures between the two polymorphs of TiO_2 that influence their chemical and physical properties.

One of most important differences is the refractive index, rutile (2.72) and anatase (2.55). Titanium dioxide provides opacity by scattering visible light, in contrast coloured pigments provide opacity by absorption of light. This scattering property is possible because the white pigment is able to bend light. As the light passes though or near the pigment particles, a small amount is absorbed and the rest of the light is refracted and diffracted or scattered.

The interaction between atomic orbitals of titanium (IV) and oxide ions is very important phenomenon that is responsible for titanium dioxide behaviour. It is known that the valence band of titanium oxide is comprised of the 2p orbital of oxygen (O), while the conduction band is made up of the 3d orbital of titanium (Ti), which results in a band gap with 3.2 eV (anatase) and 3.0 eV (rutile) of energy [13]. In this case visible light (400-700 nm) has not enough energy to suppress the band gap and promote electrons from the valence band to the conduction band (no visible light absorption). However, titanium dioxide is a semiconductor material that can be chemically activated by UV-light. When this material is irradiated with photons having energy higher than Eg, electrons are promoted from the valence to the conduction band and electron-hole pairs are generated at the TiO_2 surface and bulk (figure 6). Consequently, as many holes left behind in valence band as the number of excited electrons are created in valence band (figure 6).

The photoexcited state of macrocrystalline semiconductors is normally unstable and can easily relax at room temperature. In the case of titanium dioxide it remains stable even when it is photoexcited, this is an important point that makes titanium dioxide an excellent photocatalyst, particularly anatase.

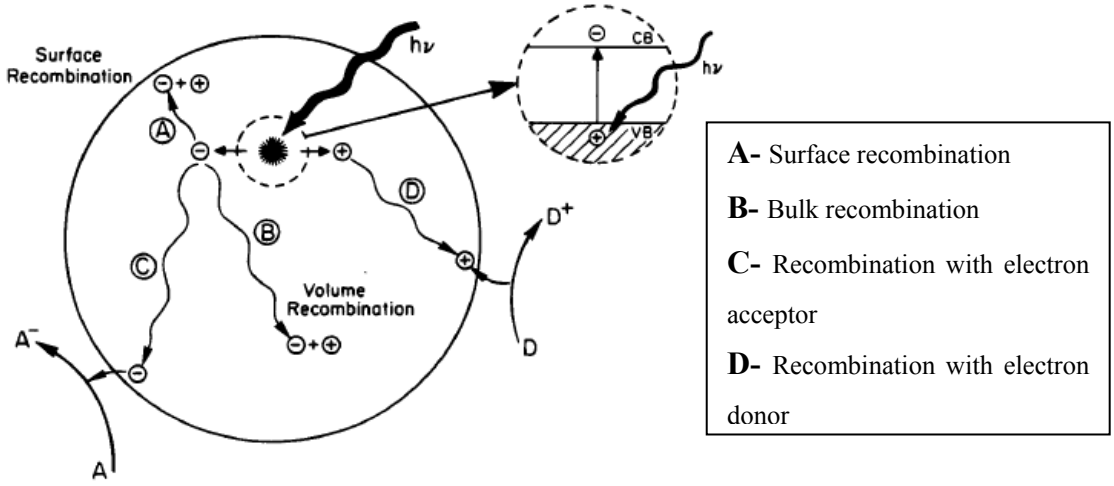

Figure 6 – Schematic representation of photocatalyst TiO_2 reactions [12].

The hole in the valence band can react with H_2O or hydroxide ions adsorbed at the surface to produce hydroxyl radicals ($^{\cdot}OH$), and the electron in the conduction band can reduce O_2 to produce superoxide ions ($O_2^{\cdot-}$). Both, holes and $^{\cdot}OH$ are extremely reactive because they are chemically unstable when in contact with organic compounds [14]. The equations shown below represent all the reaction steps between the titanium dioxide surface (electron-hole pair) and oxygen/water molecule to produce oxidant species:

$$TiO_2 + hv \rightarrow TiO_2 (h^+_{vb} + e^-_{eb})$$
$$O_2 + e^-_{eb} \rightarrow O_2^{\cdot-}$$
$$O_2^{\cdot-} + e^-_{eb} + 2H^+ \rightarrow H_2O_2$$
$$O_2^{\cdot-} + H_2O_2 \rightarrow {}^{\cdot}OH + OH^- + O_2$$
$$e^-_{eb} + H_2O_2 \rightarrow {}^{\cdot}OH + OH^-$$
$$h^+_{vb} + OH^- \rightarrow {}^{\cdot}OH$$
$$h^+_{vb} + H_2O \rightarrow H^+ + {}^{\cdot}OH$$
$$2h^+_{vb} + 2H_2O \rightarrow 2H^+ + H_2O_2$$

Hydroxyl radicals ($^{\cdot}OH$) are among the most reactive radicals known and can be applied as an efficient cell killing agent and in the degradation of organic molecules. High reactivity means that the half life and the effective diffusion lengths of hydroxyl radicals are both short.

1.2.3- Synthetic methods for titanium dioxide nanostructures

An exponential growth of research activities has been seen in Nanoscience and Nanotechnology in the past decades. New physical and chemical properties emerge when the size of the material becomes smaller, down to the nanometre scale. Among the unique properties of nanomaterials, the movement of electrons and holes in semiconductor nanomaterials is primarily governed by the quantum confinement mechanism, and the transport properties related to phonons and photons are largely affected by the size and geometry of the materials.

Properties influencing the behaviour of titania particles have been reported to include surface area, cristallinity, crystallite size and crystal structure [15]. Since the reaction/interaction activity is mostly confined to the surface of the material, its surface area must be increased to maximize the activity [16]. This has been achieved by synthesing

nano-sized TiO_2 particles. Also the amount of the anatase phase must be maximized because the rutile phase shows less photocalytic activity [15].

It is not surprising, in view of the importance of TiO_2 nanoparticles, that a wide variety of approaches for the synthesis of nanosized TiO_2 have been reported, and it remains a particularly active research field.

Literature shows that the properties of TiO_2 significantly depend on the method of synthesis and purification, the presence of dopants and defects in it, and surface morphology. Methods such as sol-gel, sol method, hydrothermal, solvothermal, micelle and inverse micelle, chemical vapour deposition and physical vapour deposition have been widely used [13]. The next table shows a short overview about each method for synthesis of TiO_2 nanoparticles.

Table 1 – Short overview about synthetic methods for titanium dioxide nanostructures

Method	Description	Ref.
Sol-gel	Sol-gel methods are based on the hydrolysis of an alkoxide or halide precursors. Typically a colloid suspension, or a sol, is formed by hydrolysis and condensation reactions of precursors. Complete condensation and loss of solvent leads to the transition from the sol to the gel phase. Several studies have been developed using the sol-gel method for control the size and shape of TiO_2 nanoparticles by changing the reaction parameters. However some additives like amines can be used as shape controllers of TiO_2 nanoparticles.	[13, 17-23]
Sol	Sol method here refers to the nonhydrolytic sol-gel processes and is characterized by the reaction of titanium halide with a high range of oxygen donor molecules, metal alkoxide or organic ether. The condensation between Ti-X and Ti-OR leads to the formation of Ti-O-Ti bridges. The alkoxide groups can be provided by titanium alkoxides or can be formed in situ by reaction of the titanium halide with alcohols or ethers. The variation of X yielded influences in the average particle size, but without a high impact in the reaction rate. Increased the size of the halide resulted in smaller nanoparticles. Surfactants have been widely used to control the size and shape of TiO_2 nanoparticles.	[24-26]

Hydrothermal	Hydrothermal synthesis is normally performed in autoclaves under controlled temperature and pressure with the reaction in aqueous solutions. The temperature can be elevated above the boiling point of water. The amount of solution added to the autoclave and the temperature largely determine the internal pressure. The peptizers and their concentrations influenced the morphology of the nanoparticles. However the morphology can be also influenced by using different surfactants and/or by changing the solvent composition.	[27-29]
Solvothermal	The solvothermal method is almost identical to the hydrothermal method except that the solvent used is nonaqueous. In this case the temperature can be elevated for high values, since a variety of organic solvents with high boiling points can be used. This method allows a better control of the size, shape distribution and crystallinity of the TiO_2 nanoparticles. The use of surfactants increase the variability of shapes achieved for TiO_2 nanoparticles. Moreover the average particle size was smaller and the size distribution narrower in the case of nanoparticles synthesized with surfactant. However, solvents with different physical and chemical properties can also influence the morphology and the crystallization of the TiO_2 nanoparticles.	[30-32]
Micelle and Inverse Micelle	Aggregates of surfactant molecules dispersed in a liquid are called micelles when the surfactant concentration exceeds the critical micelle concentration (CMC). In micelles, the hydrophobic hydrocarbon chains of the surfactant are oriented toward the interior of the micelle, and the hydrophilic groups of the surfactants are oriented toward the surrounding aqueous medium. In case of reverse micelles are formed in nonaqueous media, resulting in an inverse orientation of surfactants. The shape of a micelle and respectively the TiO_2 nanoparticles is a function of the molecular geometry of its surfactant molecules and solution conditions such as surfactant concentration, temperature, pH, and ionic strength. The materials prepared by these techniques normally are amorphous and calcination is necessary in order to increase the crystalinity.	[33-35]

Chemical and Physical Vapour Deposition	Vapor deposition refers to any process in which materials in a vapour sate are condensed to form solid materials. Vapor deposition processes usually take place within a vacuum chamber. If during this process chemical reaction occurs is named chemical vapour deposition (CVD), in case of no chemical reaction the process is named physical vapour deposition (PVD). The crystalline phase and morphology of TiO_2 nanostructures can be controlled with reaction conditions: temperature, pressure and relative percentage of gases.	[36-38]

In the present work the preparation of TiO_2/cellulose nanocomposites was based in sol-gel method. Sol-gel reactions allow good control from the molecular precursor to the final product, which makes possible to achieve at low temperature materials with high purity and high homogeneity and desired size and shape. Moreover, in the case of sol-gel method it is possible to preserve the integrity of the substrate. Nucleation and growth of TiO_2 nanostructures at cellulose surface avoid the using of extreme conditions of temperatures and pH.

1.2.4- Applications

The most important function of titanium dioxide is in powder form as a pigment for providing whiteness and opacity. Titanium dioxide is by far the most widely used white pigment due to the very high refractive index – surpassed only by diamond. The refractive index determines the opacity that the material confers to the matrix in which the pigment is used. Hence, with its high refractive index, relatively low levels of pigment are required to achieve a white opaque coating.

The high refractive index and bright white colour of titanium dioxide make it an effective opacifier for matrix with low refractive index. The material is used as an opacifier in glass and porcelain, cosmetics, sunscreens, paper and paints. One of the major advantages of the material for exposed applications is its resistance to discoloration under **UV** light.

Environmental pollution has drawn attention to the vital need of totally new and environmental friendly technologies. There are no limits to the possibilities and applications of titanium dioxide photocatalysts, which operate at room temperature, clean manner (water and carbon dioxide are the reaction products) and the energy source is not

expensive - sun light. There are many studies that describe the degradation of a wide range of organic compounds by titanium dioxide photocatalysts under **UV** radiation [39-42].

The photocatalytic oxidation of organic compounds in aqueous solution containing a suspension or/and supported titanium dioxide is a potential method in the treatment of both waste and drinking water. Several laboratory tests were performed to evaluate these new potentialities [40, 43-48].

The photocatalytic reactivity of titanium dioxide under **UV** light can be also used for the reduction or elimination of pollutants in air such as volatile organic compounds (**VOCs**). They are found not only in industrial and manufacturing sites but also in commercial workplaces and domestic households. Many of these compounds are not only irritants, but also suspected carcinogens and pose a significant health risk. Several research reports, have been published in the last decade about this topic and, in general, they demonstrate that TiO_2 catalyst can be an effective solution for the degradation of volatile organic compounds [39, 44, 49-51].

When exposed to sunlight or ultraviolet light, TiO_2 also exhibits antimicrobial activity due to its strong oxidizing properties. This important behaviour of titanium dioxide may be applied in the medical field, genetic laboratories, processing food factories, pharmaceutics, in microbiological laboratories and places where regular and thorough disinfection of surfaces is required in order to reduce the risk of infections caused by bacteria [52, 53].

Maness et al [54] demonstrated for the first time, that lipid peroxidation of polyunsaturated phospholipids in E. Coli occurs as a result of oxidative reactions exerted by TiO_2 and **UV** light at room temperature. Initiation of lipid peroxidation is known to require some form of radical attack, after that the reaction propagates by generating a peroxy radical intermediate that can continue peroxidation with another unsaturated lipid molecule. It has also been suggested that superoxide ions react with the intermediate hydroperoxide to initiate new radical chain reactions that degrade lipid phase which is the cell membrane. After some reaction time the radical can penetrate inside the cell and lead to destruction. This idea can be applied to all life forms as well, because all have a cell membrane made up of a variety of lipids with various degrees of unsaturation and rely on their structures to carry out essential functions.

A new generation of TiO_2 nanomaterials is described in the recent literature, the main objective is to increase the performance of TiO_2 nanomaterials by increasing their optical activity, shifting the onset of the response from the **UV** to the visible region [13, 41, 55].

Titanium dioxide can only use 3-4% of the solar spectrum that reaches the Earth. Several works showed an increase of the quantum yield, presumably by decreasing the rate of hole/electron recombination, and/or to increase the minimum irradiation wavelength required to improve the performance.

Therefore, the chemical composition of TiO_2 can be altered by doping. Specifically the metal (titanium) or the non-metal (oxygen) component can be replaced in order to alter the material optical properties; however it is important to maintain the integrity of the crystal structure of the material. For this propose a critical amount of metal (W, V, Ce, Zr, Fe and Cu) or non-metal (B, C, N, F, S, Cl and Br) was used to dope TiO_2, and such changes can favour the photocatalytic activity of TiO_2 in the visible [13].

1.3- TiO_2/cellulose nanocomposite materials

Functional hybrid materials contain both organic and inorganic components whose unusual properties allow the development of new applications [56, 57]. In designing such materials, the aim is two fold: to bring out the interesting properties of the individual components and also to enhance the properties resulting from synergistic effects due to interactions between the inorganic and organic components [57, 58]. In the last years, there has been great interest in designing hybrid nanocomposites, i.e. materials in which, at least one component, is at the nanoscale level and interacts chemically with the other component.

While considerable progress has been done on nanocomposites based on synthetic polymers [59-61], comparatively less has been done on the use of natural occurring biomacromolecules. However, there are important applications involving natural polymers to fabricate wide spread composite materials, such as the use of cellulose in the paper industry. This motivated the investigation of hydrolytic methods for the *in situ* synthesis of inorganic nanoparticles in the presence of wood cellulosic fibres. Due to their relevance in the paper making technology, we have started to focus on titanium dioxide (TiO_2) loaded materials. TiO_2 has been used as a white pigment whose high refractive index (2.72 rutile; 2.55 anatase) improves the brightness and opacity of paper materials. In papermaking

process, TiO_2 particles are mechanically mixed with cellulosic fibres. However, nanosized TiO_2 pigments, mechanically mixed with fibres, are poorly retained in fibres, unless agglomeration is promoted by means of polyelectrolytes or other retention aids thus decreasing the optical efficiency of the pigment. Recently, the synthesis of TiO_2/cellulose nanocomposites using the controlled hydrolysis of titanyl sulphate has been proposed as an interesting approach to improve the performance of TiO_2 in paper materials [62]. Apart from its optical properties, which justify its wide usage not only in papermaking but also in painting industry, TiO_2 is also a semiconductor widely used in photocatalytic applications [63-67].

We have been interested in developing synthetic strategies which provide the tools to control the morphological and chemical characteristics of the final cellulosic nanocomposites and hence their final properties. In the literature, distinct methods have been used to synthesise TiO_2 particles, but sol-gel techniques have been mostly used due to the ability to control the particle size distribution [68-70]. These methods generally involve the controlled hydrolysis of titanium (IV) alkoxides followed by a subsequent calcination step to promote crystallinity and remove organic residues [15, 16, 71-73]. However, calcination above 280–300 ºC precludes the use of such procedures in the preparation of cellulosic nanocomposites containing TiO_2. Several authors have reported that the hydrolysis of Ti (IV) species from $TiCl_4$ or $TiOSO_4 \cdot xH_2O$, under specific controlled conditions, can produce morphological well-defined TiO_2 nanoparticles at room temperature [63, 66, 74, 75]. Also, chemical additives, such as urea, acetyl acetone or acetic acid can be used in the reaction medium to control the final crystalline phase [16, 63]. In particular, the synthesis of TiO_2 in the presence of urea caught our attention because the reacting conditions seem compatible with the soft cellulosic fibres used as the composite matrices.

Therefore, the hydrolysis of $TiCl_4$ and urea to coat cellulosic fibres with a specific TiO_2 polymorph (synthesis ***in situ***) is reported in this thesis. Moreover, a possible mechanism for the growth of TiO_2 at the cellulosic fibres will be discussed. Other synthesis approach was followed to protect the substrate against the titanium dioxide photo-attack. For this purpose, a thin layer of organic molecules (silanes and polyelectrolytes) is used has a chemical barrier.

The photocatalytic activity of a selected anatase/cellulose nanocomposite was tested by methylene blue degradation under UV illumination and compared with that of "commercial photocatalytic-grade TiO_2", which is commonly used as basis for comparison with photocatalyts prepared by other procedures. Moreover the antimicrobial activity of TiO_2/cellulose nanocomposites was also studied for different types of microorganisms: *Staphylococcus aureus*, *Klebsiella pneumoniae* and *Escherichia coli*.

2- Preparation and characterization of TiO_2/cellulose nanocomposites

2.1- Introduction

The ***in situ*** preparation of TiO_2/cellulose based nanocomposites (i.e. the synthesis of TiO_2 in the presence of cellulosic fibres) will be presented in this section. The hydrolysis of $TiCl_4$ in water was selected as first approach to prepare these nanocomposites.

A second approach to prepare TiO_2/ cellulose nanocomposites involving the layer-by-layer assembly of TiO_2 particles on modified cellulose fibres surfaces using polyelectrolytes will also be presented. One of the main advantages of this method consists in the simplicity of the procedures.

.

2.2- TiO_2/cellulose nanocomposites by *in situ* preparation of TiO_2

In the present study, it was possible to precipitate TiO_2 nanoparticles at the cellulose fibres surfaces, yielding nanocomposite materials, through a simple method based on the hydrolysis of $TiCl_4$ in the presence of urea.

The percentage of TiO_2 retained in the fibres determined by elemental analysis (ICP) and the TiO_2 crystalline phase identified by XRD in the final nanocomposites are presented in Table 2. For the synthesis of these nanocomposites, all the experimental conditions were kept constant, except the urea concentration.

Table 2 - Synthesis conditions for the nanocomposites, the results of TiO_2 crystalline phase detected and % TiO_2 retained in the final products (synthesis *in situ* – $TiCl_4$ hydrolysis).

Sample	m (urea)/ g	Urea/Ti^{4+} molar ratio	Final pH	TiO_2 phase	% TiO_2 in final nanocomposite
U1	0	-	< 0	**Rutile**	23.0
U2	0.5	0.8	0	**Rutile + Anatase**	21.2
U3	1	1.7	0	**Anatase + Rutile**	16.7
U4	1.5	2.5	0.1	**Anatase**	11.2
U5	3	5	0.7	**Anatase**	9.4
U6	4.5	7.5	0.9	**Anatase**	6.2
U7	6	10	1.0	**Anatase**	5.6

As it can be seen from Table 2, the percentage of TiO_2 retained in the final nanocomposite decreased with the increase of the urea concentration in the reaction

medium. These results are confirmed by the visual analysis of experimental synthesis that showed a faster initial visible turbidity of the solutions, for the ones without or with less amount of urea. This can lead us to the preliminary conclusion that the presence of urea in the synthesis medium inhibits or retards the precipitation of titanium dioxide.

From Raman spectroscopy (figure 7) and X-ray diffraction (figure 8) it was possible to identify the TiO_2 crystalline phases present in the final nanocomposites. The results show that in the absence of urea, TiO_2 crystallized at the fibres surface as rutile; when the molar ratio urea/Ti^{4+} in the reaction mixture was 0.8, TiO_2 crystallized as a mixture of rutile and anatase with a predominance of the former; for urea/Ti^{4+} molar ratio equal to 1.7, a mixture of phases was also obtained but with inverted relative intensities; for urea/Ti^{4+} ≥ 2.5 the rutile phase was no longer observed by Raman or XRD, thus only anatase is present.

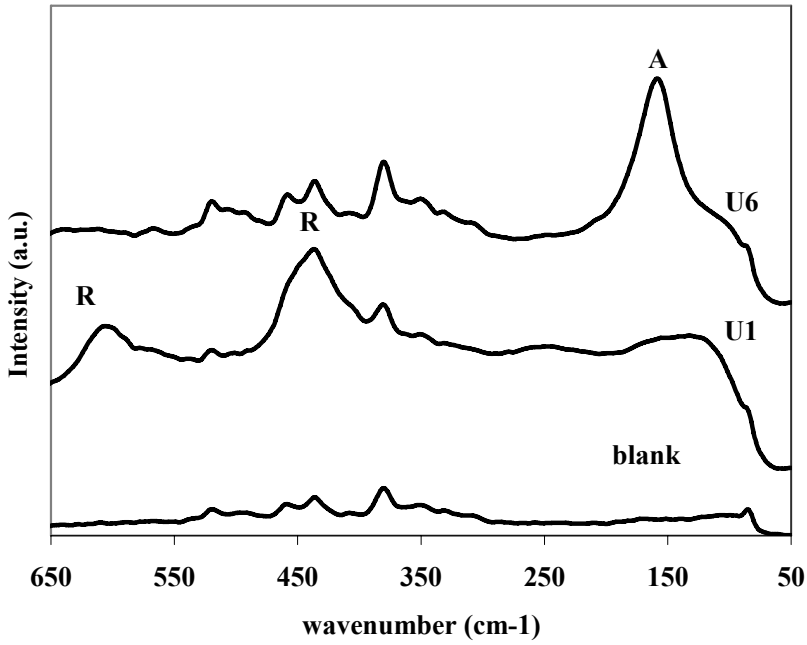

Figure 7 - Raman spectra of TiO_2/cellulose nanocomposites U1, U6 together with blank cellulose fibres. Rutile (r) has two major lines at 442 and 607 cm^{-1}, while anatase (a) shows its most intense line at 143 cm^{-1}.

Figure 7 illustrates the Raman spectra of the nanocomposites U1 and U6, together with the blank Raman spectrum for the cellulose fibres. Rutile has two major bands at 442 and 607 cm^{-1} and others at 143, 236, and 825 cm^{-1} while anatase shows an intense band at 143 cm^{-1}, with bands of less intensity at 194, 326, 393, 512, 635 and 749 cm^{-1} [62].

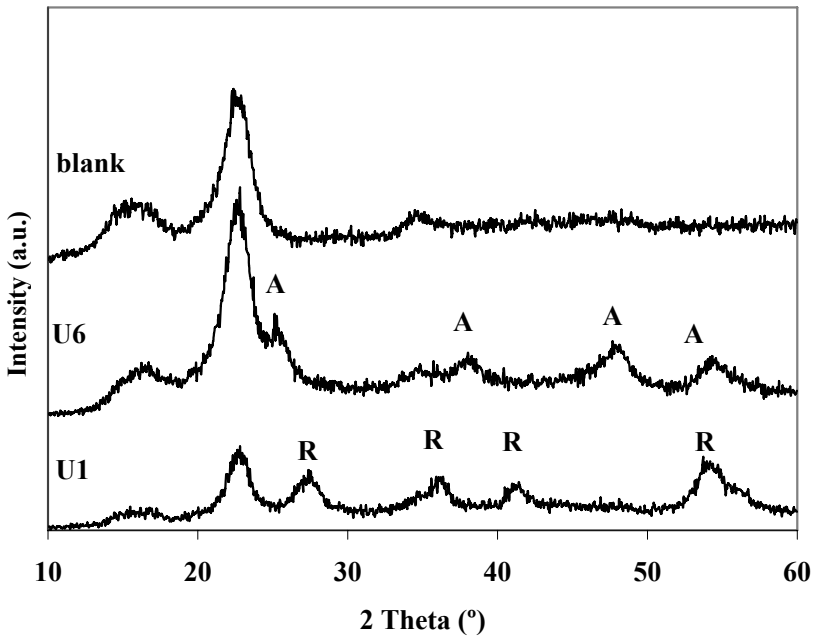

Figure 8 - XRD patterns of samples U1 and U6 together with the RXD of cellulose blank fibres. The "a" assigns the anatase and "r" the rutile bands.

Figure 8 shows the XRD patterns of samples U1 and U6 together with the XRD of the blank fibres. These results show that, rutile is predominant in the nanocomposite U1 while anatase is mainly present in U6, in agreement with the Raman spectra (figure 7). All the diffraction peaks of the sample prepared by aqueous hydrolysis of $TiCl_4$ without urea (U1) can be assigned to the rutile crystalline phase, 2θ= 27º, 36º, 41º and 54º; for the sample prepared in the presence of urea (U6) the XRD peaks are characteristic of the anatase phase, 2θ= 25º, 37º, 47º and 54º [76].

These results show that in the method described here, the crystalline TiO_2 phase present in the final nanocomposite can be controlled during the synthetic step, without any further thermal treatment, which for cellulose fibres based materials would be always a limitation.

Although the synthesis of TiO_2 in the presence of cellulose fibres deals with low pH values in solution, no apparent degradation of the cellulose fibres was detected as can be seen in figure 9**a)**. This image show a general view of the TiO_2 coated cellulose fibres prepared with a urea/Ti^{4+} molar ratio of 2.5 (U4). In figure 9**b)** to 9**d)**, higher magnification micrographs of the nanocomposite surface show a homogeneous coverage of the fibres with the TiO_2 coating with particles sizes ranging from 15 to 60 nm. SEM observation of

nanocomposites obtained with other urea/Ti^{4+} ratios showed identical morphology. In the absence of urea some particles agglomeration was observed, probably due to the higher TiO_2 content in this material.

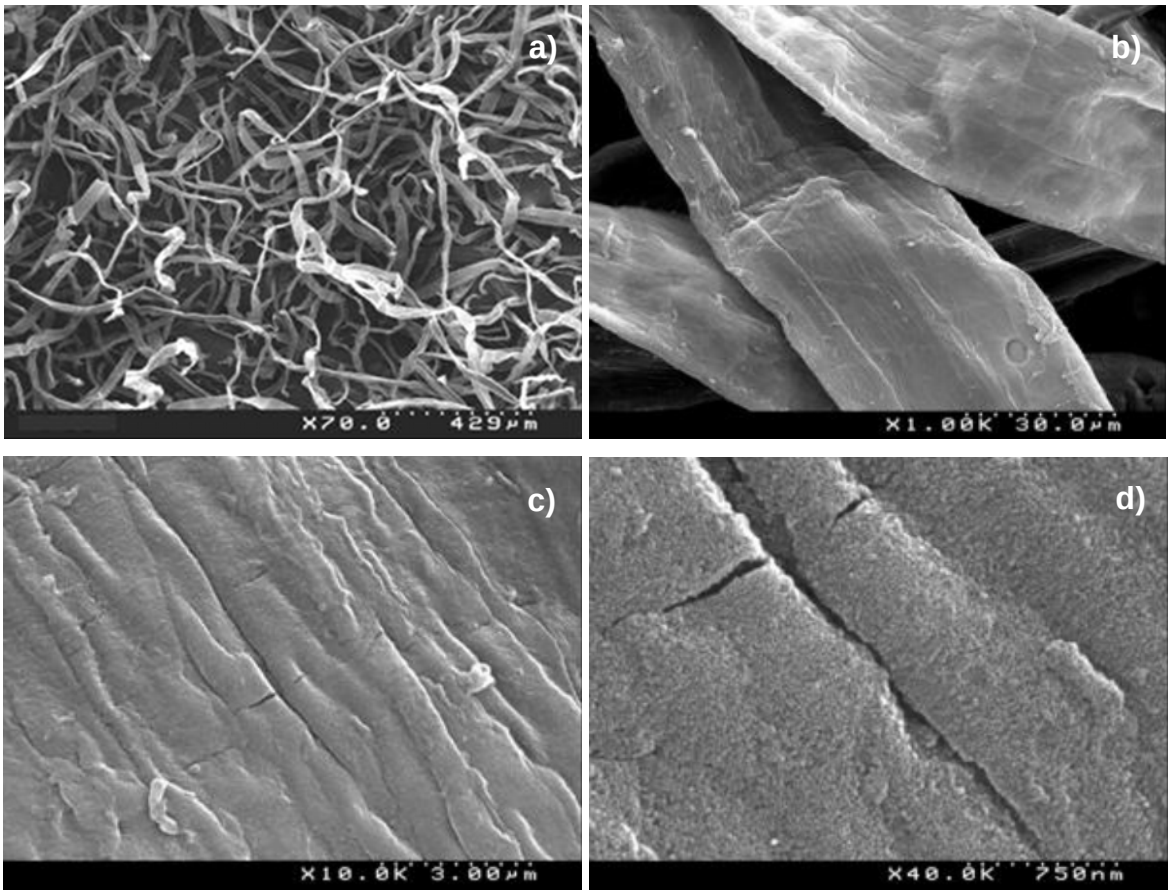

Figure 9 - SEM micrographs of TiO_2/cellulose nanocomposite (U4) showing different magnifications of the nanocomposite surfaces.

The TiO_2/cellulose nanocomposites showed the typical visible reflectance spectra of the TiO_2, figure 10 shows the UV-Vis spectra of U4 together with the spectrum of commercial TiO_2 (anatase). The commercial Degussa P25 TiO_2 was used as experimental control material. P25 TiO_2 is mostly in the form of anatase and has a BET surface area of $50m^2/g$, corresponding to a mean particle size of 30 nm [77]. The spectrum of the nanocomposite shows the expected reflectance of a TiO_2 based material. Thus, there is a high reflectance across the visible region (ca. 82%) and strong absorption in the UV region, i.e. for wavelengths lower than 350nm. Note that the visible reflectance of the TiO_2/cellulose nanocomposite is lower than that one of TiO_2 P25. This could be resulted to the presence of cellulosic fibres

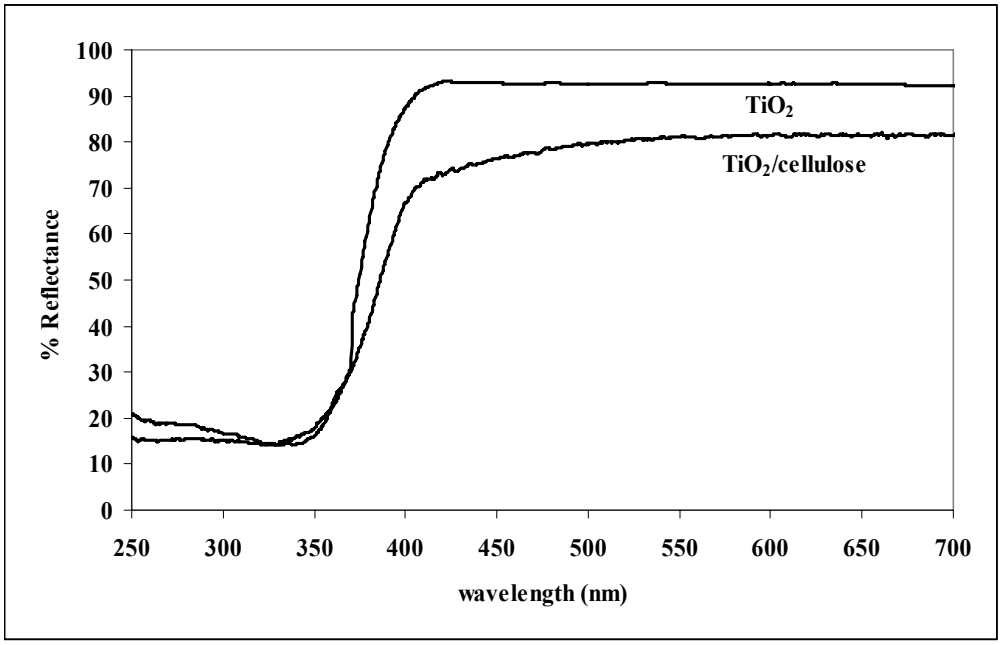

Figure 10 - Visible reflectance of TiO_2/cellulose nanocomposite (U4) and of commercial anatase (Degussa P25).

The present nanocomposites have a short range of particle size distribution from 15 to 60 nm. Concerning the optical properties, TiO_2/cellulose nanocomposites prepared by $TiCl_4$ hydrolysis in the presence of urea are not very interesting. In previous studies Marques et al [62] prepared TiO_2/cellulose nanocomposites from the so-called sulphate process with a wider particle size distribution from 70 to 350 nm, and the percentage of reflectance in visible region was higher, approximately 90%. Since the light scattering depends on the particle size, the maximum scattering occurs when the size of the particle is about one-half the wavelength of light [64]. Since the visible range is ~400-700 nm, the maximum visible light scattering should occur when the particle size is ~200-350 nm ($\lambda/2$). This justifies the increase of reflectance at visible light for the nanocomposites prepared from the sulphate method.

In order to understand the formation of TiO_2 at the cellulose fibres, attempts were made to suggest a possible mechanism. After the addition of $TiCl_4$ to ice-cold distilled water, a white precipitate forms in solution due to the hydrolysis of titanium (IV) species and in some cases yellow precipitates were also observed. After 15 minutes under vigorous stirring, the solution became then optically clear. Chu et al [66] referred also the presence of transient yellow precipitates attributing them to $TiO(OH)_2$ species. When the reacting

solution became colourless, $TiOCl_2$ predominates in solution [66, 78, 79]; this solution remaining stable at low temperatures for long periods of time. By heating the solution, $TiOCl_2$ species will react by a two-step process involving hydrolysis (1) and condensation (2) leading to the formation of TiO_2 according to the equations **A** or **B**, depending on the pH.

$TiOCl_2(aq) + H_2O(l) \rightarrow Ti(OH)_2^{2+}(aq) + 2Cl^-(aq)$	(1)	**(A)**
$Ti(OH)_2^{2+}(aq) \rightarrow TiO_2(s) + 2H^+(aq)$	(2)	
$TiOCl_2(aq) + 3H_2O(l) \rightarrow Ti(OH)_4(aq) + 2HCl(aq)$	(1)	**(B)**
$Ti(OH)_4(aq) \rightarrow TiO_2(s) + 2H_2O(aq)$	(2)	

It is reported in the literature [80] that $Ti(OH)_2^{2+}$ is the predominant species for pH < 2.45 whereas $Ti(OH)_4(aq)$ predominates for pH > 2.45. In the present conditions employed in this synthesis, the pH was always less than 1, thus equations (A) should be considered.
The change in pH during the sol gel process for the formation of uniform TiO_2 particles is mainly governed by the adsorption and desorption of hydroxide ions or protons [18, 81, 82]. Those results are in agreement with the results presented in Table 2, that showed when the pH increase the quantity of TiO_2 retained in the cellulosic fibres decrease from 23 to 5.6%.
One may find that the formation rate of TiO_2 significantly increases with the reduction of pH, especially in the acidic range. Lee et all [71] intensively studied the influence of acid concentration in the hydrolysis of $TiCl_4$ to form TiO_2 nanoparticles and they concluded that the higher the concentration of acid, the shorter the time needed for condensation reaction and crystal growth.

Although the hydrolytic synthesis of TiO_2 has been investigated intensively by several authors [63, 74, 79, 83, 84], the role of urea in this process is still poorly understood. In this context some efforts were made to understand the influence of urea in the hydrolysis of titanium species. For that purpose, the precursor solution containing the $TiCl_4$ and urea is isolated before heating. This solution was analysed by FTIR and ^1H NMR spectroscopies. For these analyses two solutions were prepared with different concentrations of titanium (IV) (TiU1-0.2M and TiU2-0.5M); the concentration of urea

was constant (1M). FTIR spectra of precursor solutions showed some kinds of interactions between the titanium (IV) and urea (figure 11).

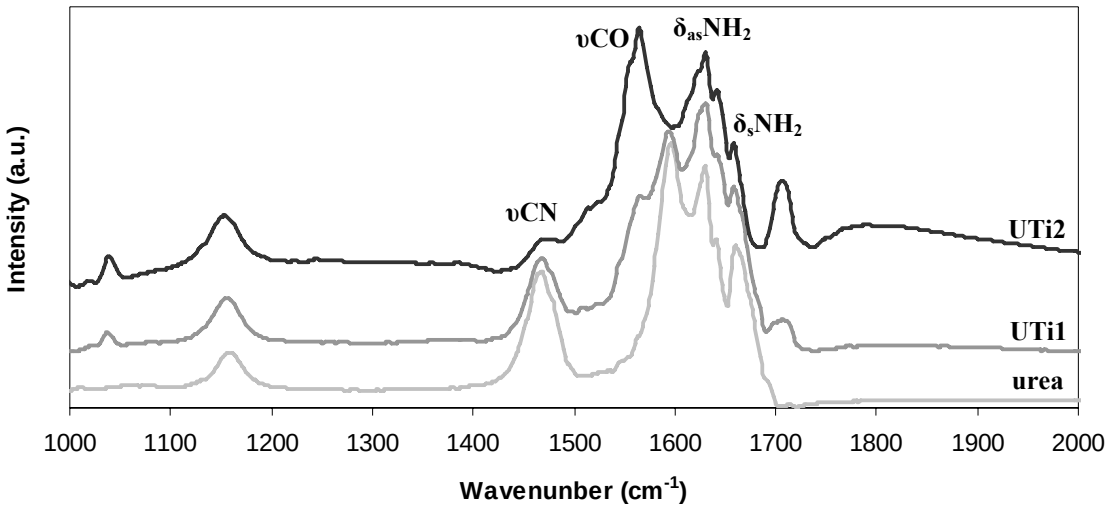

Figure 11 - FTIR analysis of several water solutions with: urea, UTi1 (0.2M Ti^{4+}) and UTi2 (0.5M Ti^{4+}). The concentration of urea in water solution is constant (1M)

Based on FTIR studies reported by Grdadolnik [85] on aqueous solutions of urea, insights can be made for the system titanium-urea-water. Table 3 shows the characteristic vibrational bands reported by these authors for urea in water. Our studies have shown, some similarity regarding the interactions of water-urea solution. However when titanium tetrachloride was added to the reaction medium some important shifts were assigned.

Table 3 - FTIR bands of urea and urea complexes with titanium in aqueous solution.

Assigments	**Literature** ([85])	**Experimental**		
	urea	**urea**	**UTi1**	**UTi2**
-	-	-	1043	1043
ρNH_2	1157	1163	1160	1161
υCN	1466	1471	1471	-
υCO	1599	1606	1573	1566
$\delta_{as}NH_2$	1629	1637	1631	1631
$\delta_{s}NH_2$	1668	1662	1660	1660
-	-	-	1712	1710

The band at 1606 cm^{-1} of urea shifts for lower wavenumbers when the titanium (IV) ion was added to the urea aqueous solution: 1573 cm^{-1} (0.2M) and 1566 cm^{-1} (0.5M). The FTIR show an important interaction between titanium (IV) ion and urea that was mainly

governed by the C=O→Ti^{4+} interaction and not the by H_2N→Ti^{4+} interaction. The presence of titanium (IV) species in the complex structure also shows one important influence on the C-N vibrations of urea, at 1471 cm^{-1}. The intensity of that band is significantly reduced when the concentration of titanium (IV) increases, which means that the molecule becomes more rigid and some vibrational states characteristic of urea disappear.

Urea is a perfect symmetric molecule due to its relative symmetry to the C=O group, but when influenced by a titanium (IV) ion the urea molecule partially loses the symmetry associated with NH_2 vibrations. By analysing the characteristic vibrations of NH_2 in the urea molecule, it is clear that, when titanium tetrachloride is added, the relative intensity of the asymmetric vibrations 1631 cm^{-1} ($\delta_{as}NH_2$) when compared with the symmetric vibrations 1660 cm^{-1} (δ_sNH_2) increases significantly. These results can be attributed to the foreign molecule ($TiOCl_2$) with high electronic density that disturbs the space orientation of the urea molecule, generating new repulsions between the atoms in the complex structure.

The ^1H NMR spectrum of the urea aqueous solution shows a narrow peak at 5.6 ppm assigned to N-H. After "complexation" with titanium (IV) a broad peak is obtained, this is indicative of a fast proton transfer or conformational exchange in water solution. These results suggest that there is an interaction between titanium (IV) and urea, however that also showed that it is mainly governed by electrostatic interactions.

Following the evidence from FTIR and ^1H NMR analysis we propose a possible mechanism for the formation of titanium-urea complexes that are responsible for the different kinetics of TiO_2 formation and consequent TiO_2 anatase phase obtained.

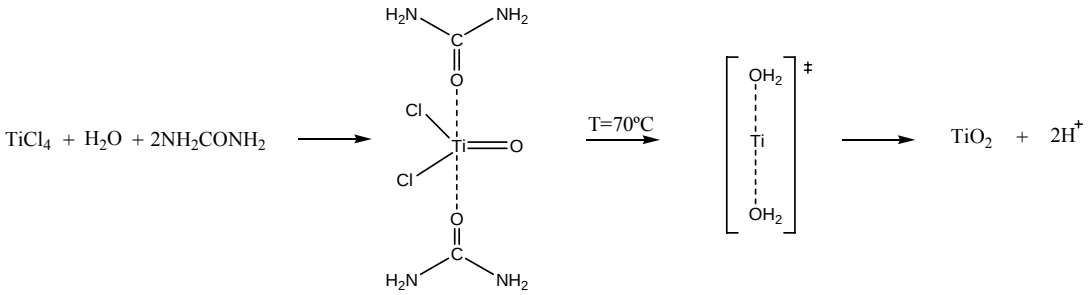

The fast hydrolysis of $TiCl_4$ in aqueous solutions results in the formation of $TiOCl_2$ species, these species will establish the interaction between two urea molecules to form the

intermediate specie $TiOCl_2(NH_2CONH_2)_2$, that after hydrolysis at 70ºC results in TiO_2 nanoparticles.

To further study the interaction between titanium species and urea, another study was conducted, for that we performed the synthesis of a solid complex $TiCl_4(NH_2CONH_2)_2$ and then hydrolyse it in presence of cellulose fibres. The synthesis of $TiCl_4(NH_2CONH_2)_2$ was performed in glove box with low concentration of water and O_2 (<1ppm), that avoid the fast hydrolysis of $TiCl_4$ compound into titanium oxide intermediate species.

After synthesis, Elemental analysis and ICP of titanium(IV) complex showed that the relative percentage of each element is, 15.0 Ti, 18.14 N, 7.25 C, 9.61 O, 3.82 H and 46.18 Cl %wt. These results are in agreement with the work of Roland Rivest [86], which is indicative of the same molecular structure proposed for titanium(IV)-urea complex, $TiCl_4(NH_2CONH_2)_2$.

The FTIR spectra of $TiCl_4(NH_2CONH_2)_2$ in solid state showed a preferential coordination of urea to titanium (IV) by the C=O bond (figure 12). The band at 1589 cm^{-1} characteristic of C=O shift considerably to lower wavenumbers 1512 cm^{-1}, these results are in agreement with the results described for the complex in aqueous solutions. It is also evident the disappearance of the band at 1458 cm^{-1} of C-N when titanium (IV) is in a complex structure. The increase of asymmetric vibrations of $\delta_{as}NH_2$ at 1629 cm^{-1} relative to the decrease of symmetric vibrations of δ_sNH_2 at 1674 cm^{-1} is also confirmed.

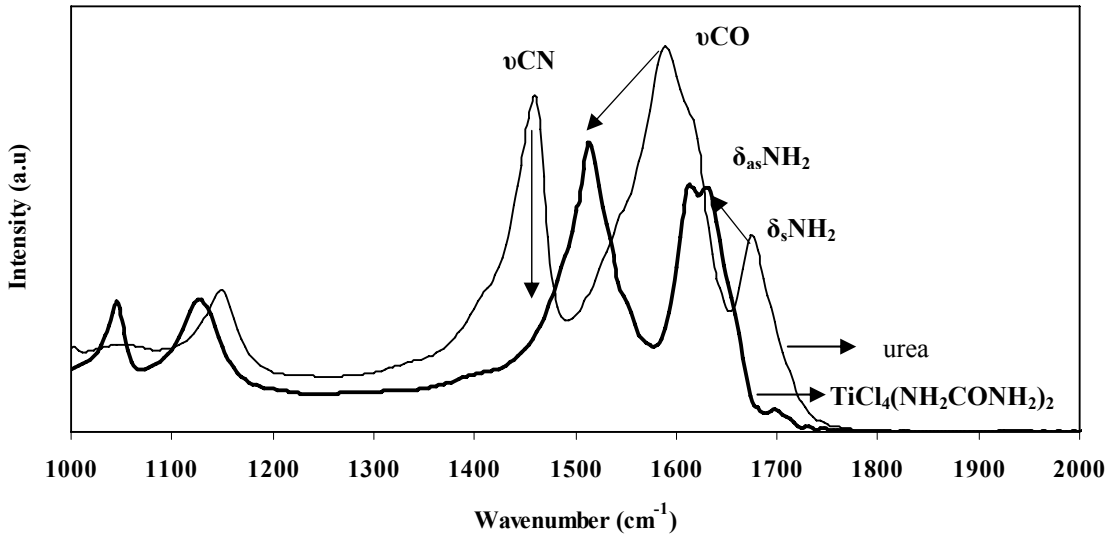

Figure 12 - FTIR analysis of the solids: urea and urea-titanium complex.

The synthesis of this solid complex showed the effective interaction between titanium species and urea molecules. The hydrolysis of this solid titanium (IV) complex in aqueous solution was then performed in the presence of cellulosic fibres using the same initial [Ti^{4+}] concentration that was used to prepare the samples referred in table 2. It resulted in a TiO_2/cellulose nanocomposite with TiO_2 retained in cellulosic fibres of 12.1%wt.

Raman analysis of the resulting nanocomposite showed the presence of anatase phase due to the most intense band at 143 cm^{-1} and less intense bands at 194, 326, 393, 512, 635 and 749 cm^{-1}[62]. XRD patterns of sample showed the diffraction peaks can be assigned to the presence of anatase crystalline phase, 2θ at 25º, 37º, 47º and 54º [76]. These results show that, when the titanium (IV) is complexated with urea the preferential TiO_2 polymorph formed is anatase.

SEM images show a perfect cover of cellulose fibres with TiO_2 nanoparticles (figure 13). The morphology of TiO_2 film at cellulose surface obtained from the previously formed solid complex is quite similar to the results attained for the nanocomposites synthesized from the direct dissolution of $TiCl_4$ and urea in aqueous solution.

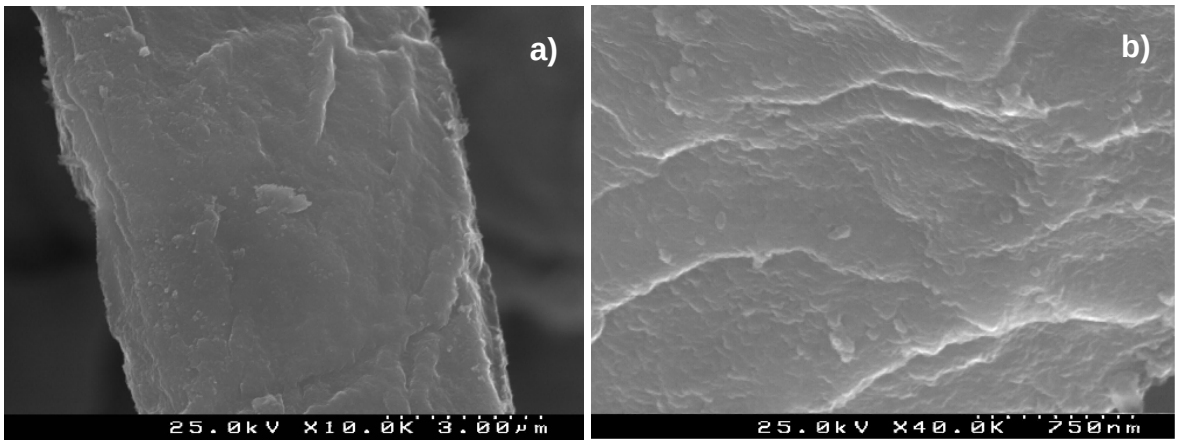

Figure 13 - SEM micrographs of TiO_2/cellulose nanocomposite prepared by hydrolysis of solid complex $TiCl_4(NH_2CONH_2)_2$ showing different magnifications of the composite surfaces.

Both approaches for the study of urea-titanium interaction arrived to the same final result. This shows that, in fact, the hydrolysis of the titanium (IV) complex is responsible for the anatase formation in cellulose surfaces.

Now is considered the effect of substrate in the nucleation and growth of TiO_2 films. This work shows that the presence of hydrophilic substrates seems to accelerate the

formation of TiO_2 without any effect on the crystalline phase obtained, compared to experiments in which fibres were not used. Hence the influence of these substrates is on the chemical kinetics and not in the thermodynamics of the crystalline solids.

In addition, TiO_2 nanoparticles were strongly attached to the cellulose fibres; strong mechanical agitation of aqueous suspensions of the TiO_2/cellulose nanocomposites was applied without lowering the inorganic content. This is in agreement with the strong chemical interactions between the polysaccharides (cellulose and glucuronoxylan) of the fibres and the TiO_2 particles surfaces, rather than a simple adsorption phenomenon.

A possible explanation involves the adjacent hydroxyl groups in anhydroglucose or anhydroxylose units, or the carboxyls in the uronic acid moieties, as electron donor sites for the complexation of cationic Ti(IV) species, thus promoting the nucleation of TiO_2 particles.

In conclusion, TiO_2/cellulose nanocomposites were successfully prepared from in situ synthesis of TiO_2 in the presence of cellulose fibres. There is evidence from this study that the urea concentration allows to control both the content of TiO_2 and the crystalline phase in the final nanocomposites.

2.3- TiO_2/cellulose nanocomposites prepared by the layer-by-layer technique

The main idea of the LbL assembly is to build up new nanocomposite materials based on electrostatic interactions between three charged components: cellulose fibres, synthetic polyelectrolytes and TiO_2 nanoparticles.

The so called LbL (Layer-by-Layer) technique was used here to assembly TiO_2 at cellulose modified surface with polyelectrolytes. This new approach consists in the consecutive adsorption of polyanions and polycations at cellulose surface for the fabrication of multilayer system (figure 14).

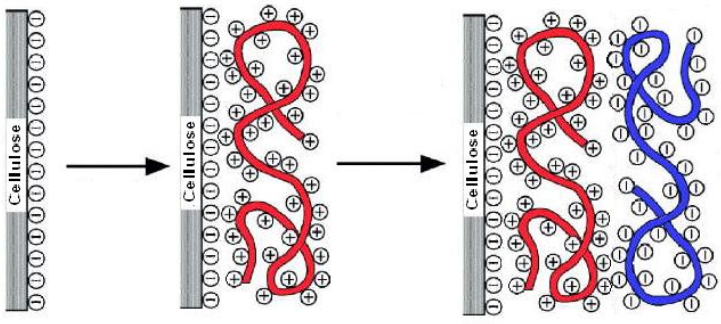

Figure 14 - Schematic representation of the working principle of polyelectrolytes at the cellulose surface.

Decher et al demonstrated that strong electrostatic attraction occurs between a charged substrate and an oppositely charged polyelectrolyte in solution. The adsorption of polyelectrolytes at substrates surface allows the repulsion of equal charged molecules and the adsorption of molecules with reverse charges. Cyclic repetition of both adsorption steps leads to the formation of multilayer structures [87].

This method has been applied to build up diverse inorganic/organic nanostructures in order to obtain nanocomposites with new properties or new functional groups [87-91].

To prepare the TiO_2/cellulose nanocomposites using the LbL approach the first step is synthesize the TiO_2 particles. The synthesis and characterization of these particles are described in the following section.

2.3.1- Synthesis and characterization of TiO_2 particles

Many studies have sought to produce TiO_2 nanoparticles with controlled size and shape [17, 23, 67, 92-97]. One of the most important methods for the synthesis of titanium oxide particles is the hydrolysis of alkoxides in aqueous/alcohol solution. In this method, interfacial electrochemical properties and dispersion stability of particles are strongly influenced by the surface structure. TiO_2 spherical particles were prepared using the controlled hydrolysis and condensation of titanium tetraethoxide (**TEOT**) in an aqueous-alcohol solution [97]. The critical precipitation parameters such as the reactant concentration, the concentration ratio of water and **TEOT**, reaction temperature and ageing conditions have an effect on the particle size, size distribution, morphology and degree of agglomeration. The time required to observe an initial turbidity may be assumed to be a good indication of the induction time for the particle nucleation.

Among all the parameters that have been described in the literature to influence the properties of the TiO_2 nanoparticles, temperature was not referred to our knowledge.

In this work the effect of the synthesis temperature in the morphology and internal arrangement of nanocrystallites in TiO_2 aggregates was investigated. Two interesting kinds of aggregates are achieved, both with different densities and porosity, presenting extreme dependence with the temperature. Figure 15**a)** shows the TiO_2 particles synthesized at 10ºC, where it is possible to observe that the surface is rough and it seems like small nucleus have grown around TiO_2 particles. When synthesis temperature increases to 20ºC,

figure 15**b)**, the TiO_2 particles are spherical and smooth. At 30ºC, figure 16, the particles do not have a well defined morphology and the size is completely random. It is possible to observe that, in this case, small particles aggregate in large agglomerates. All different types of particles were calcinated at 500ºC.

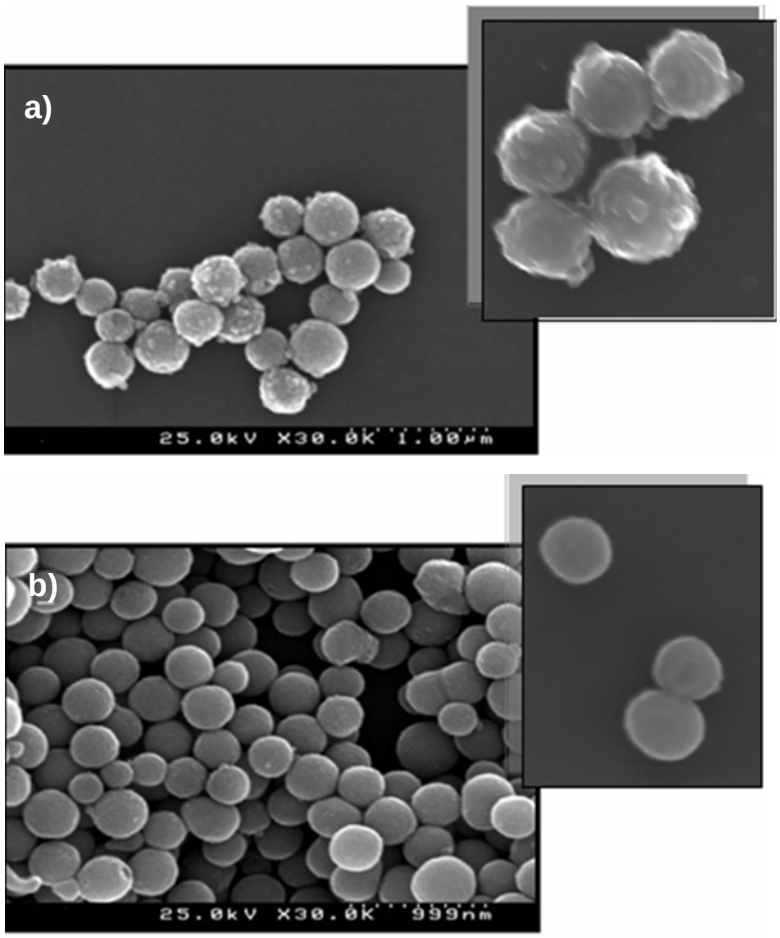

Figure 15 - SEM micrographs of TiO_2 showing the different surface of particles **a)** synthesized at 10ºC and **b)** synthesized at 20ºC.

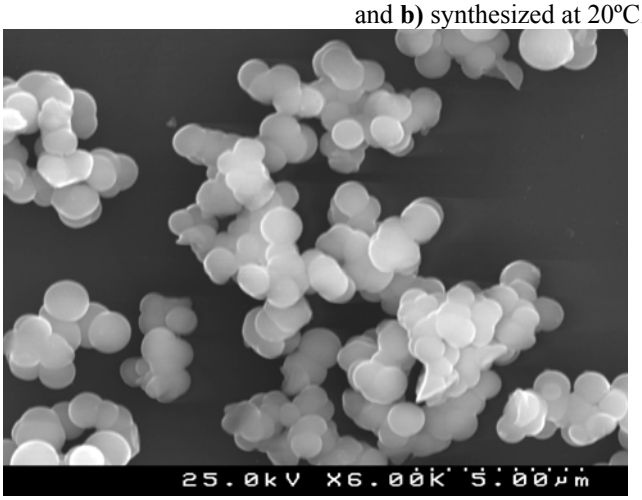

Figure 16 - Aggregates of TiO_2 particles

Figure 17 shown TEM images of TiO_2 particles synthesized at 10ºC. Both images show that the particle is an aggregate of smaller nanocrystallites which range from 10 to 30 nm. The size of the aggregate is around 300 nm and seems to be loosely packed.

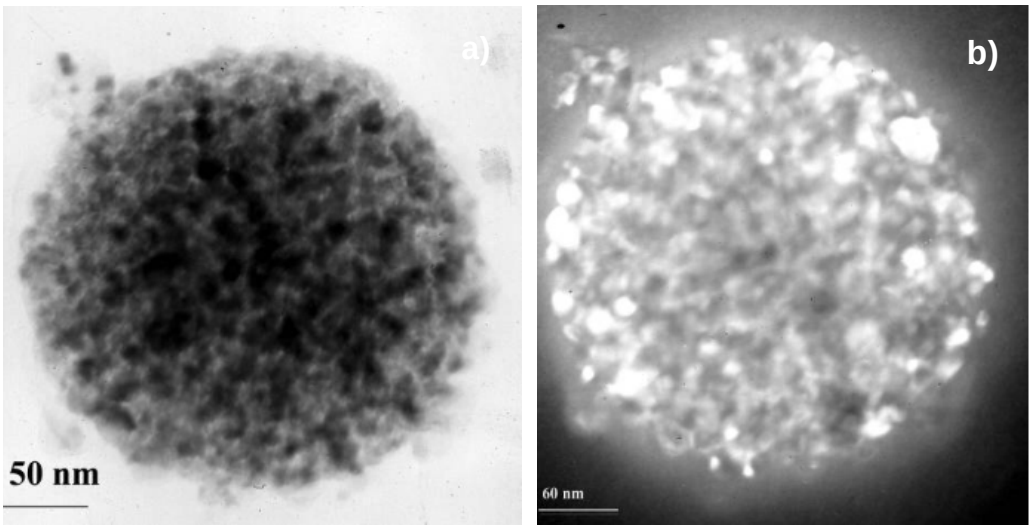

Figure 17 - TEM images of TiO_2 particles synthesized at 10ºC, **a)** dark field image and **b)** bright field image.

TiO_2 particles synthesized at 20ºC are shown in figure 18, where one important reduction of the sizes of the particles, between 200-250 nm can be observed. A magnified image shows that the particles have a smooth surface and the packing of nanocrystallites inside the TiO_2 particles is higher than the particles synthesized at 10ºC.

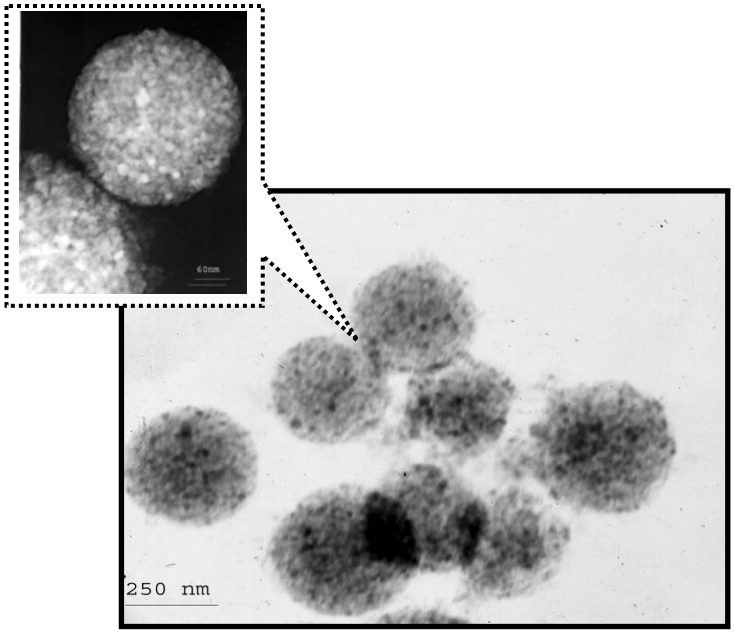

Figure 18 - TEM image of TiO_2 particles synthesized at 20ºC.

Based on TEM and SEM images it is possible to conclude that, the synthesis temperature has an influence in the surface morphology and nanocrystallites arrangements in the final aggregates.

The sizes of both types of particles were evaluated by DLS analysis and the data collected is shown below (figure 19).

Figure 19 - DLS report of the particle size distributions **red**) smooth particles (20ºC) and **green**) rough particles (10ºC).

Figure 19 represents the percentage of particles (number) in function of the particle size, in which the Z-Average corresponds to the maximum value of each peak. The red line corresponds to the rough particles that have an average size of 342 nm. In the case of the green line, the average size of spherical particles is lower, 315 nm. The Gaussian shape of the peaks indicates a good distribution of the particle size in both cases.

Comparing those results with those of SEM and TEM for the same samples, the DLS analysis shows bigger particles size in both cases. This is probably due to the presence of large aggregates in solution that can significantly increase the average size.

BET analyses clearly show the difference of the surface area between the particles synthesized at 10 and 20ºC. Particles synthesized at 20 ºC have a surface area of 24,267 m^2/g and a total porous volume of 0,036 cm^3/g (figure 20**b)**) and particles synthesized at 10ºC have a surface area of 35,154 m^2/g and total porous volume of 0,0538 cm^3/g (figure 20**a)**).

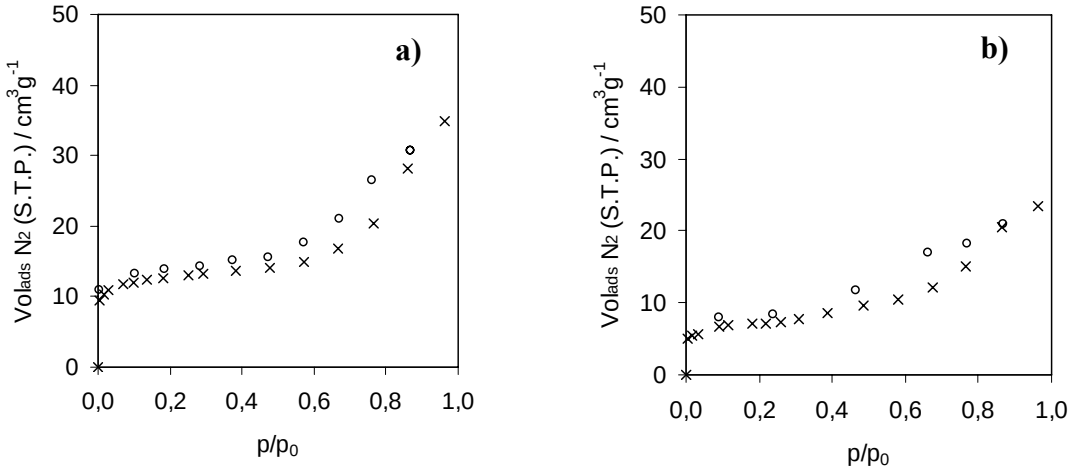

Figure 20 - BET analysis of smooth (10ºC) **a)** and rough (20ºC) **b)** particles of titanium dioxide.

Particles synthesized at 10ºC showed an adsorption of N_2 almost two times higher than the particles synthesized at 20ºC, that means the internal porosity of particles synthesized at 10ºC are higher and density is lower. These results are in agreement with the last predictions, and confirm that the arrangement of nanocrystallites inside the colloidal particles depends of the synthesis temperature and not only of the calcination temperature.

From the Raman spectroscopy it was possible to identify the TiO_2 crystallographic phase as anatase. Figure 21 illustrates the Raman spectrum of the synthesized TiO_2 particles (spectrum is similar for the particles synthesized at different temperatures).

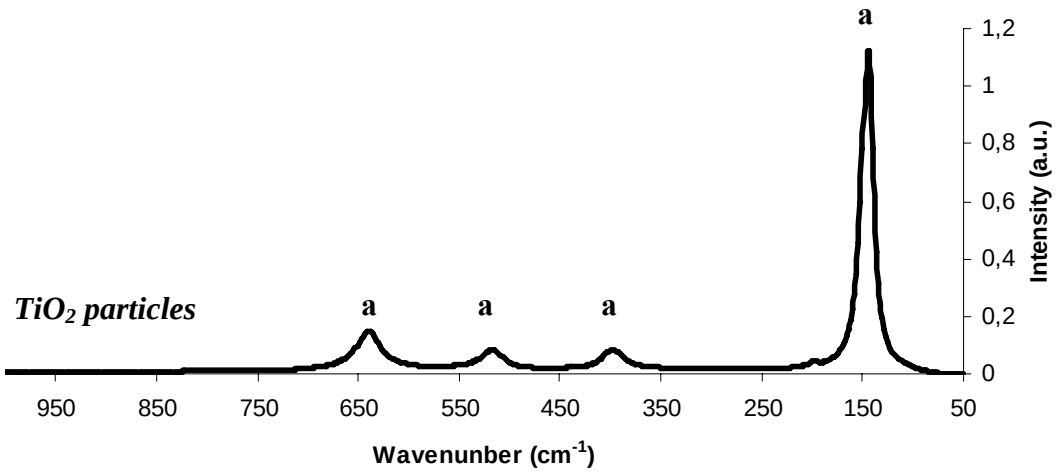

Figure 21 - Raman spectrum of titanium dioxide particles, "**a**" means anatase.

Anatase shows its most intense bands at 143 cm^{-1}, and smaller bands at 393, 512, and 635 cm^{-1} [62], that are similar for the two sample since the calcination temperature is the same 500ºC for both cases.

The TGA curve recorded under air (figure 22) indicates the weight loss in function of temperature. There are two stages, one for weight loss and other for weight gain. The first one starts at room temperature until to 400ºC, with a weigh loss of approximately 13.5%, whereas the second one is in the range of 400-450ºC, with an increase of weight of 1.5%.

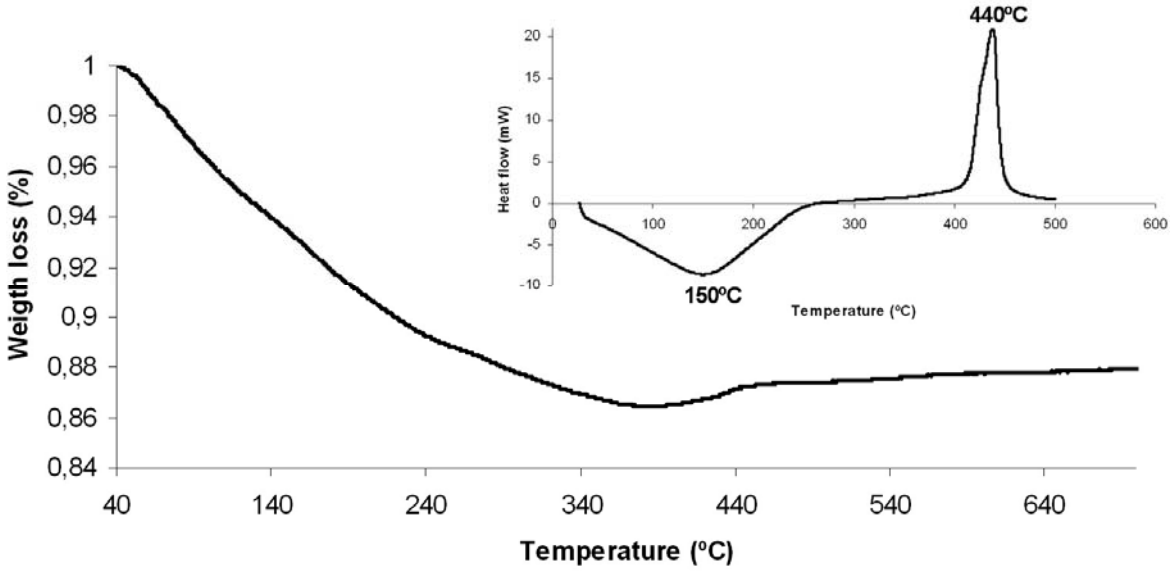

Figure 22 - TGA and DSC of titanium dioxide particles.

The weight loss in the first stage can be attributed to the degradation of organic vestiges and to adsorbed water that can be removed during this stage [96]. Above 400ºC the increase of weight can be attributed to the oxygen gain from air. It is supposed that a possible rearrangement of the TiO_2 structure occurs at 400ºC, leading to some oxygen inclusion from air, what justifies the weight increase.

The broad endothermic peak at 150ºC in the DSC curve (figure 22) should be attributed to the decomposition of organic vestiges and the loss of adsorbed water. The sharp exothermic peak at 440ºC corresponds to the transition from amorphous phase to anatase. These results are in agreement with the TGA analysis performed in these materials.

XRD studies on the effect of temperature on the crystallization of titanium particles was done (figure 23). The results showed that titanium dioxide particles start to crystallize

at 400ºC. Before this temperature the results showed that titanium dioxide particles are amorphous.

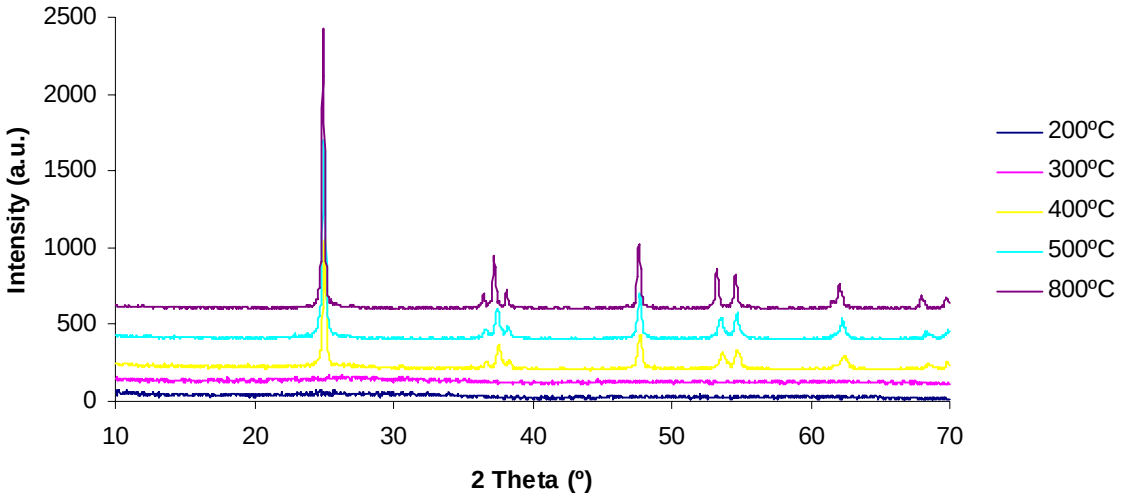

Figure 22 - XRD patterns of TiO_2 particles in function of temperature.

All the XRD peaks of the sample prepared by hydrolysis of titanium tetraethoxide are assigned to the anatase crystalline phase, 2θ = 25º, 37º, 47º and 54º [76]. It is interesting to see that when the calcination temperature increases the intensities of the peaks also increase. However no change of crystalline phase is achieved until 800ºC.

Let us consider the chemistry of the process in solution to try to interpret the above results. The possible reaction mechanism of the titanium alkoxides is described in the literature [98, 99] by a two step reaction consisting in hydrolysis (**A**) and condensation (**B**):

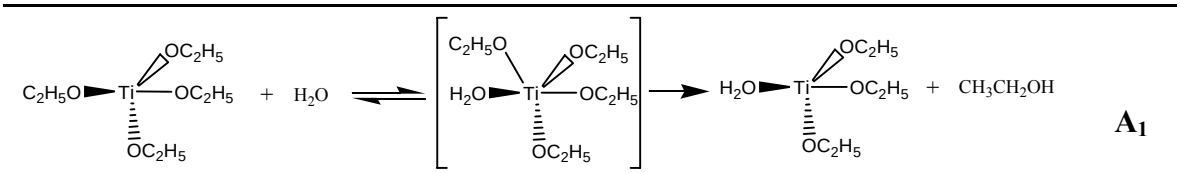

A1

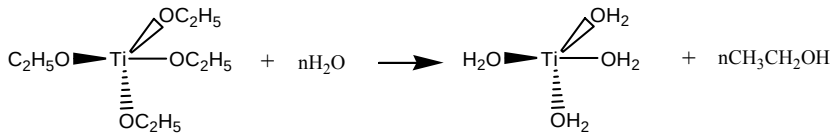

A2

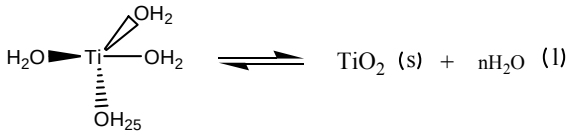

B

In general, the mechanism of ligand substitution through the bimolecular reaction path depends on the behaviour of the leaving group and entering group. One possible mechanism is proposed by Park et al. - associative mechanism [99], in which the entry of the hydroxy group occurs first and then hydrolysis of the ethoxy group, resulting in a intermediate species with an expanded coordination number (**A_1**).

However, the most common mechanism proposed in literature is the hydrolysis of ethoxy groups ($–OC_2H_5$) to form hydroxyl groups (–OH) (**A_2**). That reaction is performed by four steps that correspond to the initial number of $–OC_2H_5$ that coordinates the titanium (IV) ion.

The condensation reaction (**B**) is the way by which the hydrolysis species polymerize to form higher molecular weight products. Condensation proceeds either through water or an alcohol elimination reaction. The water elimination rate is expected to be faster than the alcohol elimination reaction, the dominant mechanism depends on the relative rates of the hydrolysis and condensation reactions and the number of hydroxyl groups on the major hydrolysis species.

The temperature controls the kinetic mechanisms of the reaction and this parameter controls the velocity of the hydrolysis of the alkoxide and aggregation of the primary particles [97]. When synthesis is carried out with temperatures above 30ºC, individualized particles are not obtained; with temperature around 20ºC the resultant particles shown smooth surface and high density, while at temperatures lower than 10ºC the resultant particles shown a rough surface and low density.

At lower temperature, TiO_2 surfaces were probably only partially covered with organic molecules. Therefore, the growth becomes difficult and in this case, the packing or assembling process should proceed in a much more random way and an uncontrolled branching of Ti-O-Ti may occur at several sites or locations. In the case of the particles synthesized at 20ºC, they possess enough energy to well organize the Ti-O-Ti lattice and obtain preferential particle morphology. After the hydrothermal treatment, the structure exhibits the thermodynamically preferred form of morphology (spherical) [96].

The last described work clearly shows that it is possible to modify the internal organization of nanocrystallites and the morphology of TiO_2 aggregates by changing the synthesis temperature. Synthesis temperature controls the reaction of the titanium

precursor from the molecular level until the nucleation and growth of TiO_2 particles. This result was supported by the analysis of the several characterization techniques described.

To continue with the preparation of TiO_2/cellulose nanocomposites, the TiO_2 particles synthesized at 20ºC were chosen due to their more uniform morphology.

2.3.2- Assembly of TiO_2 particles at cellulose surface

TiO_2/cellulose nanocomposites were built based in electrostatic interactions between the cellulose fibres, polyelectrolytes and titanium dioxide spherical particles (synthesized at 20ºC). The density of negative charges at cellulose surface is due to the presence of free hydroxyl groups (zeta potential of cellulose low than zero [2]), allows the electrostatic interaction with PDDA (positive charges - figure 24). Igor L. et al [89] studied the interactions between cellulose surfaces and colloidal particles using AFM technique, and they conclude that, in most situations, Van der Walls interactions have been responsible for cellulose films anchored to cationic polyelectrolyte layer.

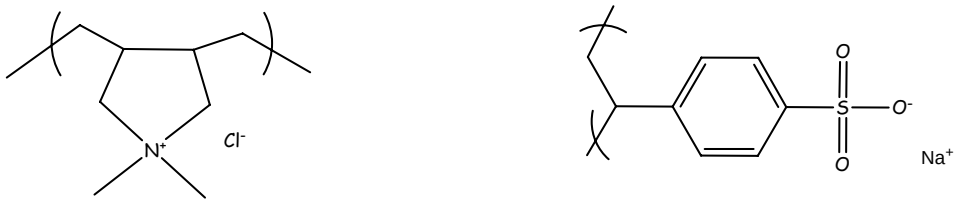

poly(diallydimethylammonium chloride)
PDDA *(MW 100000-200000)*

poly(sodium 4-styrenesulfonate)
PSS *(MW 70000)*

Figure 24 - Chemical structure of two types of polyelectrolytes with positive charges **(PDDA)** and negative charges **(PSS).**

Then, to stabilize the positive layer a new negative layer is prepared with PSS (negative charges - figure 24), and at the end a new layer of PDDA is used. The interactions between the three layers of polyelectrolytes (**PDDA-PSS-PDDA**) are mainly governed by the reverse charges.

The chemical structure of the polyelectrolytes represented before shows the different charge surface and that different charges tend to attract one another to form a chemical bond. This last positive layer allows electrostatic interactions between TiO_2 aggregates since these particles are negatively charged, as shown in figure 25, for the work region (pH 6-8).

Metal oxide particles suspended in water are known to be amphoteric [101]. In titration experiments, metal oxide suspensions behave as if they were simple diprotic acids. In the case of TiO_2, the principal amphoteric surface functionality is the titanol moiety, >TiOH. Hydroxyl groups on the TiO_2 surface are known to undergo the following acid-base equilibrium:

$$>TiOH_2^- \leftrightarrow >TiOH + H^+ \ (\mathbf{pK_{a1}})$$

$$>TiOH \leftrightarrow >TiO^- + H^+ \ (\mathbf{pK_{a2}})$$

Where >TiOH represents the titanol surface group, pK_{a1} is the negative log of the microscopic acidity constant for the first acid dissociation and pK_{a2} is the negative log of the acidity constant for the second acid dissociation.

The titanium dioxide particles in aqueous solution are covered by hydroxyl groups, and that groups are high electronegative, resulting in a negative zeta potential for the particles. This property allows the electrostatic interactions between **PDDA** and TiO_2 particles.

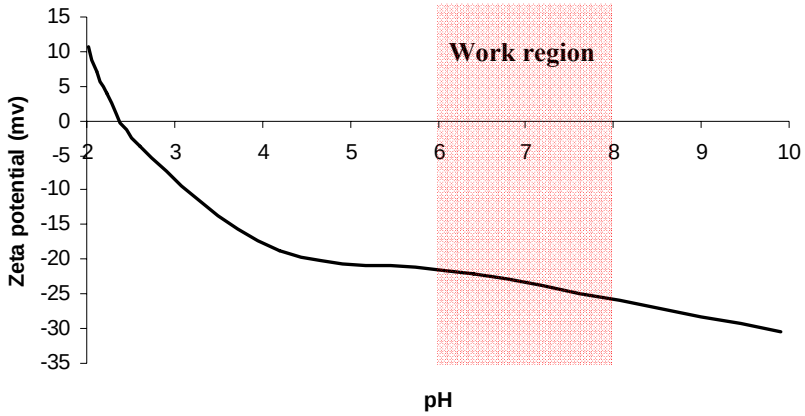

Figure 25 - Zeta potential of TiO_2 nanoparticles (synthesized at 20ºC) as of function of the pH.

SEM images, figure 26, show a good distribution of TiO_2 particles at the surface of the cellulose fibres. It is possible to observe that the layer-by-layer system is an effective method to achieve a good distribution and homogeneity of nanocomposite materials.

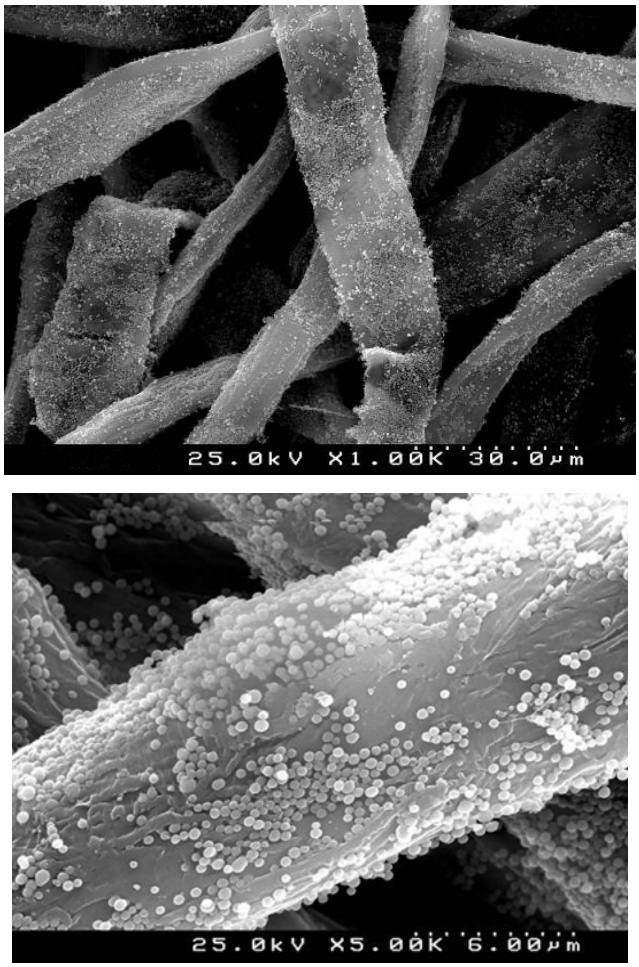

Figure 26 - SEM images of TiO_2 nanocomposites build up by the LbL method, at different amplifications.

Figure 26 shows the surface morphology of cellulose modified with TiO_2 particles having a size of approximately 300 nm.

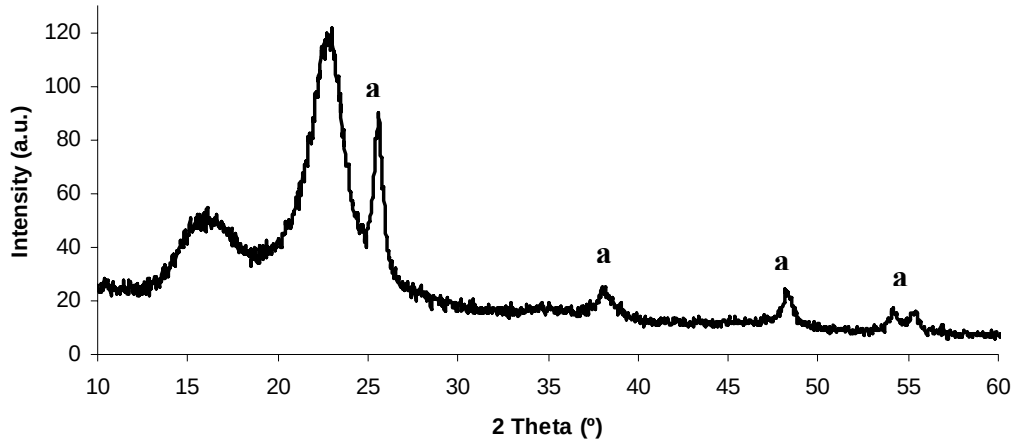

Figure 27 - XRD spectra of TiO_2 nanocomposite obtained by the LbL method (**a** – anatase crystalline phase).

The presence of TiO_2 particles in the nanocomposite can also be confirmed by Raman analysis. These bands were also confirmed in the nanocomposite but with lower intensities due to the superposition with the Raman bands of cellulose. Figure 27 shows the XRD patterns of the nanocomposite, as can be seen the crystalline phase that is present in this nanocomposite is anatase as expected.

ICP analysis showed that the average amount of titanium dioxide in the cellulose fibres was 12 wt%. If the quantity of titanium dioxide particles in the aqueous suspension was increased, the quantity in the final nanocomposites would still be the same. One possible explanation is the number of free active places at the surface of the polyelectrolyte, which means that the density of free charges per area determines the maximum quantity of titanium dioxide in nanocomposite materials.

To evaluate the optical properties of these new nanocomposite materials, the UV/Vis spectra were recorded. Figure 28 shows the diffuse reflectance of two different nanocomposites: **LbL** system and synthesis ***in situ*** (U4 - 11.2 wt%) and commercial TiO_2 pigment (P25). Titanium dioxide pigment P25 was used as comparing sample (morphological properties described before).

Comparing the percentages of reflectance of the nanocomposite build up by the **LbL** method with the ones of the nanocomposite obtained by syntheses ***in situ*** it is clear that better optical properties are achieved with the **LbL** system.

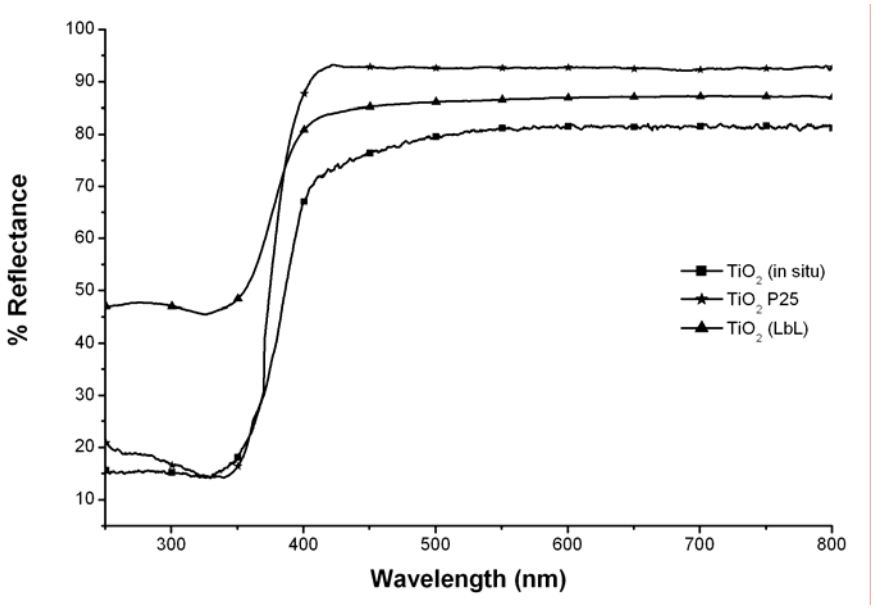

Figure 28 - Visible reflectance of TiO_2/cellulose nanocomposites and titanium dioxide particles P25.

This behaviour is expected, due to the theoretical principles described earlier, which showed that the size of TiO_2 particles influence the reflectance properties. In the case of **LbL,** the particles have a size of approximately 300nm that corresponds to the region of maximum visible light scattering (λ/2 of visible light), in case of synthesis ***in situ*** the particles are 15-60 nm of size which reduces visible light scattering.

Other important parameter is the quantity of TiO_2 in the nanocomposites; in the **LbL** case we have 12%w/w of TiO_2, while in the synthesis ***in situ*** we have also 12%w/w of TiO_2. Better reflectance properties in the first case with same quantity of titanium dioxide, which is also one important economical factor. TiO_2 pigment is expensive, so if the TiO_2 particles have an optimized size it is possible to reduce the quantity used and increase the optical properties of TiO_2/cellulose materials.

LbL method has other important advantages relatively to ***in situ*** method. First of all, during synthesis, acid conditions and high temperature are not used avoiding the degradation of cellulose fibres. **LbL** deposition of TiO_2 nanoparticles via polyelectrolytes results in nanocomposites containing discrete and spherical TiO_2 particles at the fibres surfaces. This methodology offers the possibility to control both the diameter and the final load of TiO_2 particles in the nanocomposite materials.

However, one important advantage of the ***in situ*** method must be considered; the formation of thin film at the cellulose surface is one important parameter that increases surface area of the nanocomposites. This is one important property for the increment activity of the photocatalytic papers that will be discussed in the last chapter.

3- Preparation and characterization of TiO_2/cellulose nanocomposites using surface modified cellulosic fibres

3.1- Introduction

TiO_2 pigment is only used in some kinds of special papers in order to increase the optical properties such as opacity. However to avoid the self degradation of this products the titanium dioxide is covered with a thin layer of silica or alumina.

In order to extend the utility and value of paper products, some companies have recently announced products with photocatalytic activity that can decompose organic pollutants and kill bacteria. The main idea is to increase the optical properties and at the same time obtain new functionalities.

However, it is well known that photocatalytic papers may have a short lifetime because of the photocatalytic decomposition of cellulose fibres. For example, Iguchi et al. compared the strength loss of irradiated sheets with and without TiO_2 [102]. Results show a high reduction of strength (30%) after 240 h of exposure at UV radiation.

This problematic was recently referred by Pelton in a revision paper [101]. This author refer that every photocatalityc paper involves the use of an agent to stick the TiO_2 to the substrate, since there is little natural adhesion between rather rough colloidal TiO_2 particles and cellulose. From the perspective of substrate stability, the most challenging applications will be when the photocatalytic paper is immersed in water. The cellulose will swell, thus degrading adhesive joints between the TiO_2 and the support. Flowing water could actually carry away the TiO_2 catalyst [101]. In fact is observed that, the TiO_2/cellulose nanocomposites prepared by the in situ methodology aquired a yellow colour after several days of direct sunlight exposure. This was probably due to the TiO_2 photo-attack to the cellulose fibres (organic phase).

In this context and to further improve the properties of the TiO_2/cellulose nanocomposite materials, novel TiO_2/cellulose nanocomposites were prepared having the fibre surface covered with silane agents. The use of silane layers separating the TiO_2 particles from the cellulose seems to be an efficient strategy. Further interesting properties of these materials, like hydrophobicity and thermal stability were achieved depending of silane used.

3.2- Coating of cellulose fibres with silica

As described in the literature silica has high thermal stability and excellent mechanical strength [103, 104]. Such advantage can help us in the protection of cellulose fibres against the possible titanium dioxide photo-attack. The preparation of SiO_2/cellulose nanocomposite materials can originate interesting new materials since coated fibres can act as a support to numerous applications.

The so-called "Stöber method" [105] is a reference method for the synthesis of silica particles. This method is based on the hydrolysis of tetraalkyl silicate and subsequent condensation in a homogeneous alcoholic medium in the presence of ammonia. The reaction leading to the silica formation from tetraethoxysilane (**TEOS**) may be described by the following simplified equations (this reaction is obvious a simplification of very complex processes):

$$Si(OEt)_4(l) + 4\ H_2O(l) \rightarrow Si(OH)_4(aq) + 4\ EtOH(l) \quad (\mathbf{1})$$

$$Si(OH)_4(aq) \rightarrow SiO_2(sol) + 2\ H_2O(l) \quad (\mathbf{2})$$

The Stöber method was adopted by Pinto et al [106] to build new SiO_2/cellulose nanocomposites [106]. We followed this new research work as one possible way to protect the cellulose fibres.

As shown in figure 29, the synthesis of SiO_2 in the presence of cellulosic fibres originated a homogeneous coating at the fibres surface. From SEM analysis it is possible to observe that the surface of the cellulose fibres is completely coated with SiO_2 film.

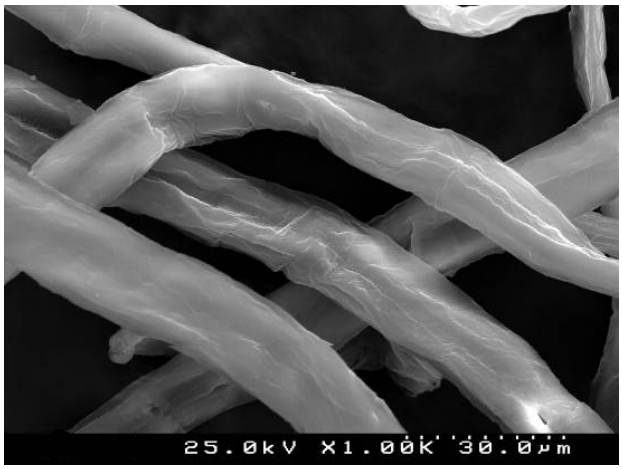

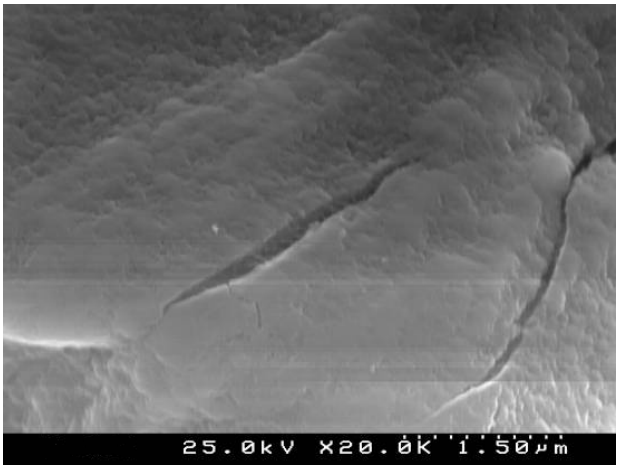

Figure 29 - SEM images of SiO_2/cellulose *nanocomposite* obtained from the *in situ* synthesis.

As it can be seen, SiO_2 nanoparticles nucleated and grown at the fibres surface. Since these materials were subject to vigorous washing and stirring treatment, it is believed that SiO_2 nanoparticles are strongly fixed to the fibres. FTIR spectra confirmed the presence of SiO_2 nanoparticles at the surface of the cellulose fibres, displaying bands due to the Si-O vibrations located at 1000–1100 cm^{-1}. These bands are absent in the blank fibres as shown in figure 30.

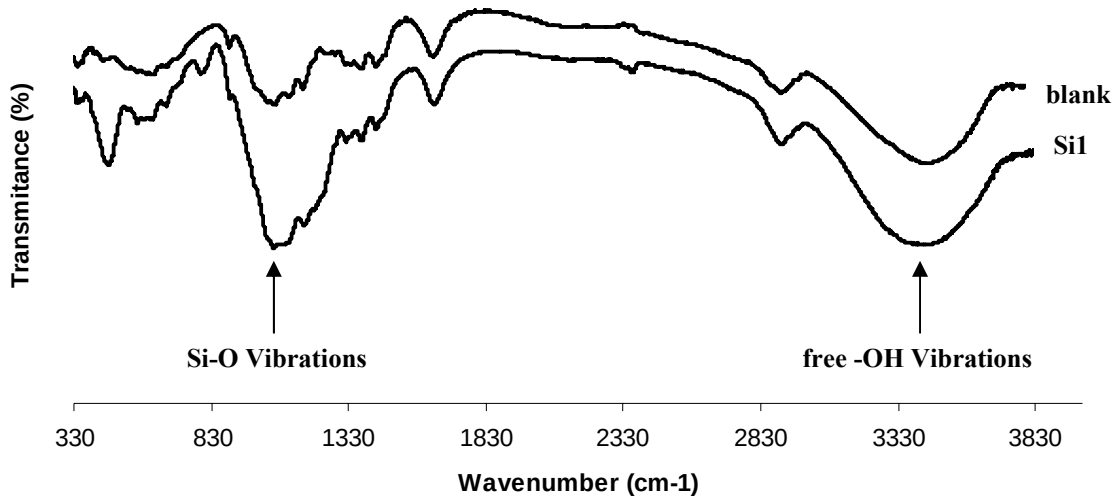

Figure 30 - FTIR spectra of SiO_2/cellulose nanocomposite and blank (cellulose)

Thermogravimetric analyses of SiO_2/cellulose and blank samples were performed at air atmosphere at heating rate of $10^{o} \cdot min^{-1}$, from room temperature until 800 ºC with 1 hour landing at this temperature. From these analyses it was possible to estimate that the deposited SiO_2 represents about 25% (w/w) of the nanocomposite weight (figure 31).

However, it is possible to observe that the silica layer does not change the thermal stability of the materials, the high decrease of weight loss at 350ºC is similar in both cases.

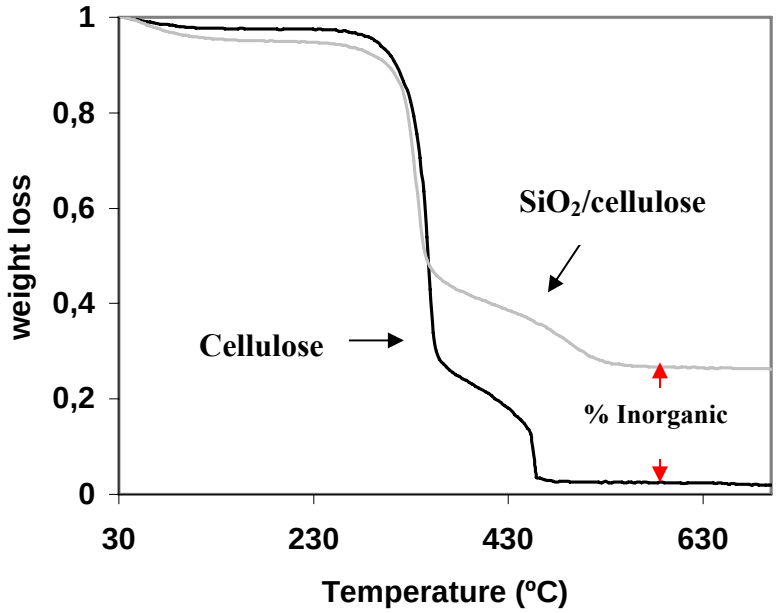

Figure 31 – Termogravimetric behaviour of SiO_2/cellulose and blank

After the modification of cellulose with a silica layer, functionalization of the new substrate with TiO_2 nanoparticles was performed. For this purpose, several methodologies were followed. Table 4 describes the methodology followed to build up each nanocomposite and the inorganic percentage of silica and titanium dioxide. The TiO_2 particles used to prepare the LbL composites were the same described in section 2.3.1.

Table 4 - Percentage of inorganic oxides for each nanocomposite material build up by different methodologies: **B**, **C** and **D**.

Sample	Description	%TiO_2	%SiO_2	% Inorganic
A	cellulose	-	-	-
B	TiO_2/cellulose [*in situ*]	12	-	12
C	TiO_2//SiO_2/cellulose [*LbL*]	11	19	30
D	TiO_2/SiO_2/cellulose [*in situ*]	6	19	25

***In situ* -** the synthesis of the inorganic phase was done in the presence of cellulosic fibres using $TiCl_4$ as precursor.
LbL - "Layer by layer", that is, inorganic particles were connected to the fibres through polyelectrolytes.
X/Y/cellulose - the cellulose fibres were first covered with Y and then with X; one bar (/) means that the deposition was made *in situ*; two bars (//) means that the deposition was made through LbL

Results in table 4 confirm that the saturation point of polyelectrolytes is, independently of the substrate, approximately 12% w/w (sample **C**) relatively to TiO_2 particles. The most interesting point is the low quantity of TiO_2 that nucleated and grown at the silica surface, only 6% (sample **D**). In the first approach of the synthesis *in situ* without a silica layer, the explanation for the nucleation and growth of TiO_2 nanoparticles at the cellulose surface was the presence of free electron donors (OH-cellulose). In fact, silica has higher density of OH groups at the surface it is expected a higher percentage of TiO_2, but less amount was obtained. One possible explanation is that the silica layer reduces the rough surface of cellulose fibres and less amount of titanium dioxide can nucleate and grow on top of silica layer. However, there are no evidences that help us to better understand which factor is responsible for this phenomenon.

The presence of titanium dioxide in the anatase crystalline structure can be confirmed by XRD analysis (figure 32), characteristic peaks position was discussed before and confirmed here.

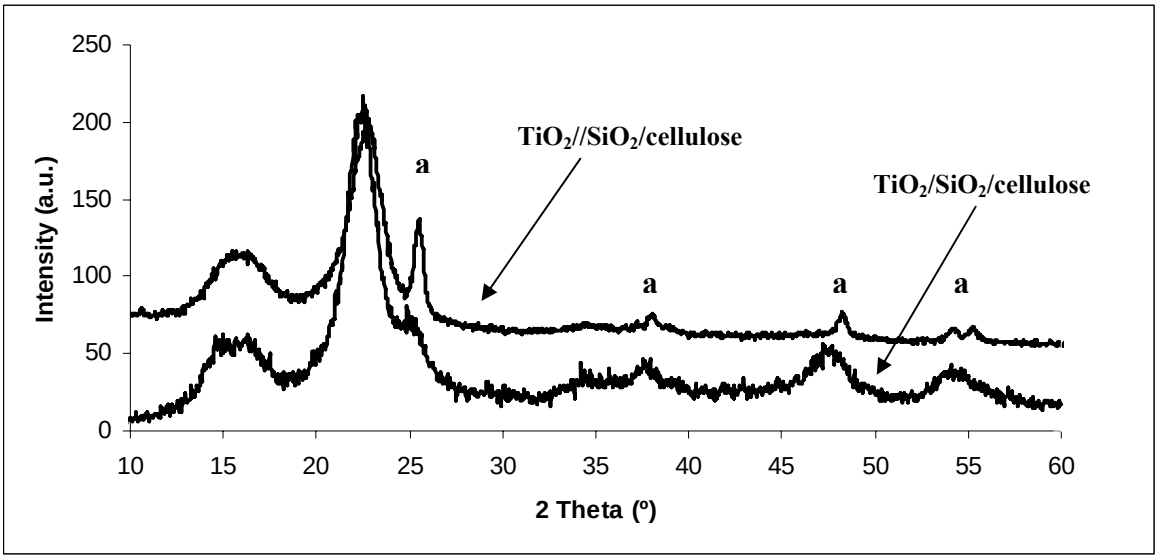

Figure 32 - XRD patterns of two different composites: TiO_2/SiO_2/cellulose - all inorganic oxides deposited by synthesis *in situ*, $TiO_2//SiO_2$/cellulose - Silica deposited by the synthesis *in situ* and titanium oxide by the LbL method

The SEM images shown below (figure 33) help us to better understand the differences achieved for each nanocomposite surface correlated with the methodology followed to build up each one. It is also possible to see that the TiO_2 particles are

effectively attached to the silica layer, and that cellulose fibres were not destroyed after this new treatment.

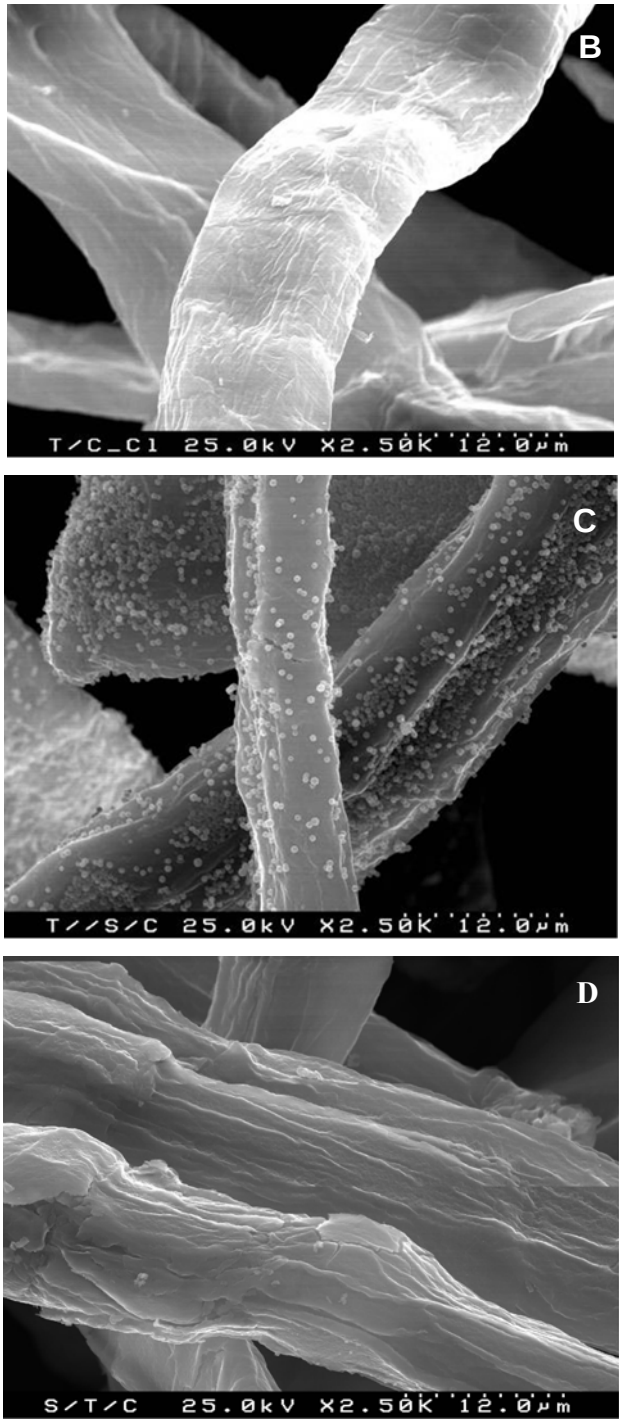

Figure 33 - SEM images of the new surface of cellulose modified by three different methods, **B**, **C** and **D**.

The resulting nanocomposites coated with TiO_2 were exposed to direct solar light during two weeks together with a TiO_2/cellulose nanocomposite prepared from $TiCl_4$

hydrolysis in the presence of urea (**U4**). The results clearly show that the silica barrier between cellulose fibres and TiO_2 is effective against the yellowing of the fibres as can be observed in figure 34.

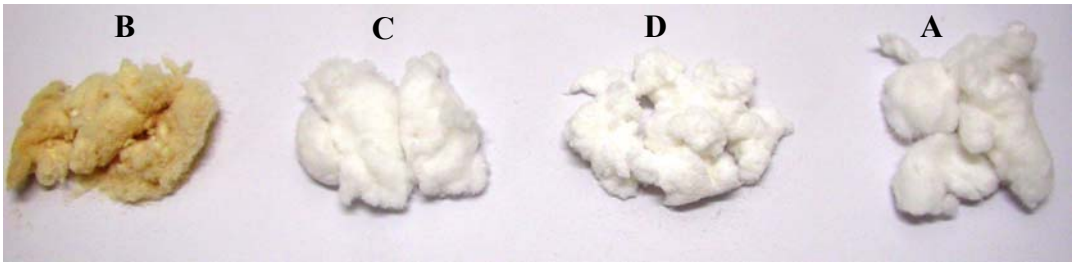

Figure 34 - Real image of the effect of titanium oxide in the cellulose with (C and D) and without (B) the silica layer protection after solar exposure.

Fibre **B** suffered yellowing compared with fibre **A** (blank), which can be attributed to photodegradation promoted by the presence of titanium dioxide at the cellulose surface with exposition at sun light. However, when the cellulose fibres were first covered with one silica layer the same effect is not achieved (fibre **C** and **D**). These results showed that the silica layer is an efficient protection against photo-degradation promoted by titanium dioxide.

The change of colour is attributed to the production of hydroxyl radicals ($OH^{\cdot}$) at the TiO_2 surface [41, 52], when irradiated with UV radiation. Radical species are thermodynamically unstable and have a good affinity for organic molecule like cellulose substrate. The reaction between radicals and cellulose can result in the formation of new chromophore groups at the cellulose surface (yellow colour). This sample was analysed by FTIR but no new bands were obtained, maybe due to the fact that this new bands have very low intensity relatively to the characteristic bands of cellulose.

These oxidation-reduction reactions are responsible for the degradation of cellulose fibres, since the interaction between hydroxyl radicals, that are chemically unstable, and cellulose chains can promote the transference of electrons that destroy covalent bonds between carbon atoms. The structure of cellulose is mainly constituted by single or double bonds between carbon atoms.

Good results were achieved by modifying the cellulose fibres with **TEOS** in order to protect them against titanium dioxide photo-attack, showing that it is possible to use new types of silanes.

3.3- Modification of cellulose fibres with functional silanes

To increase the potentialities of protection layer against TiO_2 photo-attack, another type of functional silanes were used, the purpose is to achieve new properties for the nanocomposite materials.

By definition, a silane coupling agent will act at an interface between an inorganic substrate (such as glass, metal or mineral) and an organic material (such as an organic polymer, coating or adhesive) to bond or couple the two dissimilar materials [107].

Organosilanes are a unique class of organic silicon based functional group, SiR_n. They can react with both inorganic and organic substrates as well as with themselves and other silane by complexes hydrolysis-condensation reactions to form a variety of hybrid organic –inorganic structures. The R groups in organosilanes can be non functional constituents, like $-O-CH_2CH_3$ in **TEOS**, or functional, like hydrocarbon, phenylcarbon, nitrocarbon or fluorocarbon chains. These types of silanes are frequently used as release agents for protective coatings of various substrates. But normally, almost one of the R groups can be a reactive substituent with a terminal functional group capable of specific chemical reactions. The R constituents on silicon, -Cl, $-NH_2$, $-OCH_3$, $-O-CH_2CH_3$, or esters such as $–O_2CCH_3$, are usually readily hydrolysable, so that they can form $R-Si-(OH)_n$ silanol intermediates by reaction with water, for instance **TEOS** has four reactive groups. To increase the possibilities of a chemical bond between silane and substrate, most of the silanes used are trifunctional, with respect to their hydrolysable groups. Normally the monoalkoxysilanes can only form a monolayer, whereas the trialkoxy and dialkoxysilanes (after hydrolysis to their silanol forms) lead to multi-layered interphases.

The silanes considered in this work were **OTMS** (octyltrimethoxysilane) and **PTMS** (phenyltrimethoxysilane), and their chemical structures are represented in figure 35. With this new approach, besides fibre protection, the final materials may acquire hydrophobic and thermo stability properties, due to the intrinsic characteristics of the carbon chain.

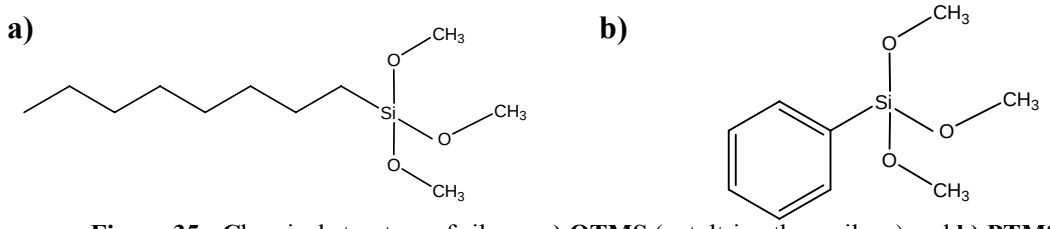

Figure 35 - Chemical structure of silanes **a) OTMS** (octyltrimethoxysilane) and **b) PTMS** (phenyltrimethoxysilane).

The interaction between silane-based reagents and cellulose is described in the literature [108, 109]. Briefly, the silanes dissolved in a water-ethanol solution hydrolyse giving the corresponding silanol intermediate R-Si-$(OH)_3$ as described before. Afterwards the resulting hydroxyl groups are able to establish hydrogen bonds with the hydroxyl groups of cellulose, and finally, chemical condensation is promoted during solvent evaporation, leading to siloxane bridges.

A second approach was developed in order to increase the compatibility between silanes and substrate, consisting in coat first the cellulose fibres with a thin layer of SiO_2, and then promote the reaction between the last described silanes and silica surface (figure 36).

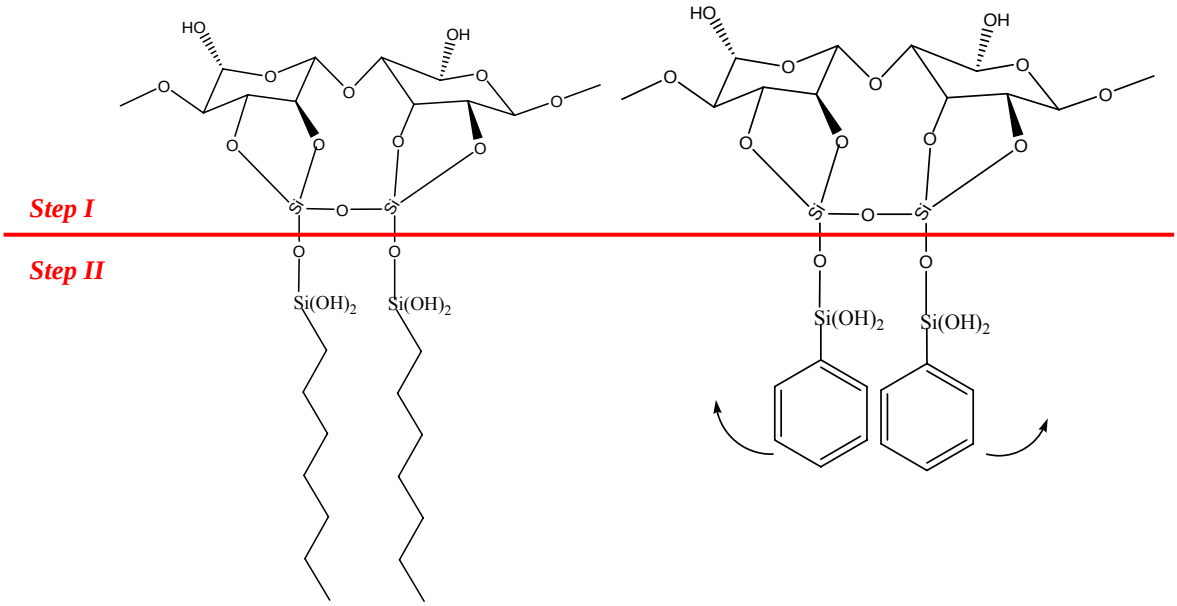

Figure 36 - Schematic representation of the nanoengeniring project of modification of cellulose surface: **step I** - silica layer and **step II** - silane layer.

It is important to emphasize that the schematic representation is only to better understand the principal steps performed for the modification of the cellulose surface. **Step I** corresponds to the modification of cellulose surface with a thin layer of silica particles and **step II** corresponds to the condensation of silanes at the silica surface. The picture can suggest a perfect molecular distribution with covalent bonds between the agents involved, however no evidences lead us to conclude that.

Since each monomer has three functional groups, the silanol groups may not only undergo condensation reaction with the substrate hydroxyl groups, but also self

condensation to form a polysiloxane network on the surface [109]. Further condensation reactions lead to gel like networks, which precipitate in the form of colloidal particles. Both the hydrolysis and condensation reactions of the methoxy groups are affected by the structure of the organic part of the silane, water in solution and reaction temperature. By simply following the reaction it is possible to conclude that the two silanes used have distinct ways of reacting with the cellulose or silica substrate: **OTMS** is mainly governed by the hydrolysis reactions and **PTMS** by the condensation reactions. Because we observed the formation of some precipitates in the bulk solution of **PTMS** reaction flask, while in the case of **OTMS** reaction no precipitation was verified.

^{29}Si MAS NMR is of great interest to acquire further information about the structure of the oligomeric species. The chemical shift of silicon is determined by the chemical nature of its neighbours, namely, the number of siloxane brigdes attached to a silicon atom, being **M**, **D**, **T** and **Q** structures commonly used notation corresponding to one, two and four Si-O- briges, respectively. Figure 37 shows the coordination of the Si atom for each structure.

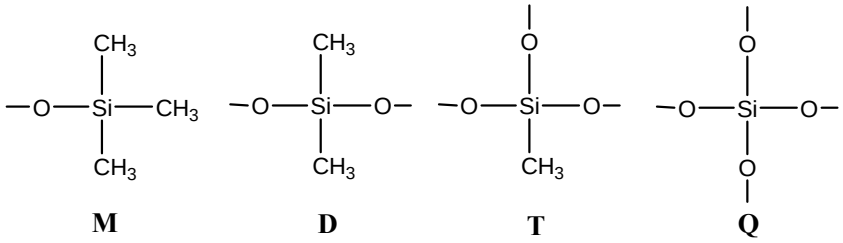

Figure 37 - Schematic representation of the several number of siloxane bridges attached to a silicon atom – **M** (one), **D** (two), **T** (three) and **Q** (four)**.**

There are five types in the case of **Q** structures, designated $\mathbf{Q_0}$ (single tetrahedron), $\mathbf{Q_1}$ (end group), $\mathbf{Q_2}$ (middle group), $\mathbf{Q_3}$ (branching site) and $\mathbf{Q_4}$ (cross-linking group) that can be present in the ^{29}Si NMR spectrum. The typical chemical shifts in the **Q** region are: $\mathbf{Q_0}$= -72 to -82 ppm; $\mathbf{Q_1}$= -82 to -89ppm; $\mathbf{Q_2}$= -92 to -96 ppm; $\mathbf{Q_3}$= -100 to -104 ppm and $\mathbf{Q_4}$~-110ppm [110-112].

In the case of **T** structures there are only four types, that can be characterized by only one organic Si-R side group and three siloxane briges that can be differentiated between Si-OSi and Si-OR groups. The characteristics chemical shifts for these structures are: $\mathbf{T^0}$= -37 to -39; $\mathbf{T^1}$= -46 to -48 ppm; $\mathbf{T^2}$=-53 to -57 ppm and $\mathbf{T^3}$= -61 to -66ppm [109, 110].

After this brief discussion, it is possible to interpretate the results achieved for the condensation of silanes at the cellulose surface. Figure 38 contains the ^{29}Si MAS NMR spectra of cellulose modified with **PTMS** and **OTMS**.

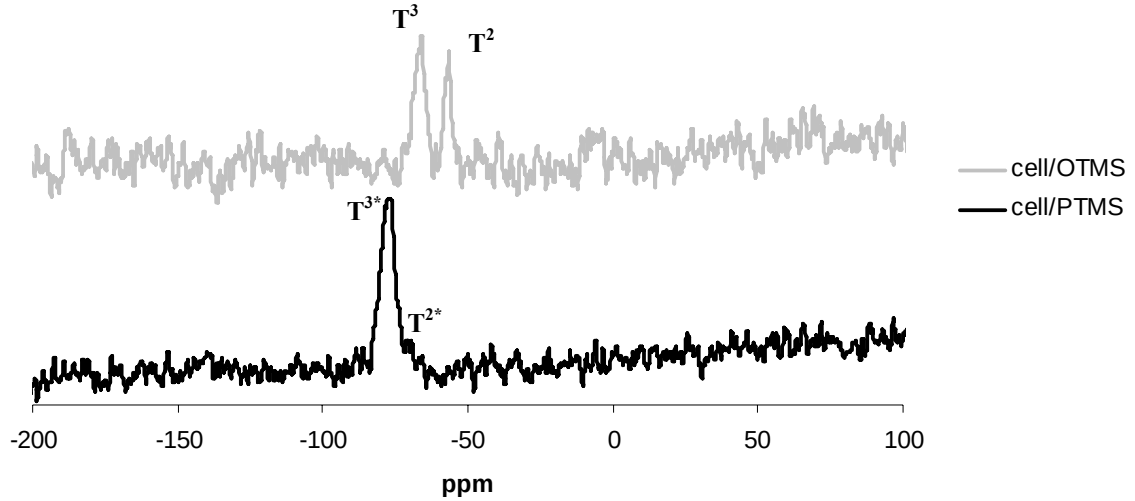

Figure 38 - ^{29}Si MAS NMR spectra of cellulose modified with OTMS and PTMS

^{29}Si MAS NMR spectra correspond to the analysis of samples: OTMS/cellulose and PTMS/cellulose. The peaks observed for OTMS/cellulose at -56 and -66 correspond to **T** structures $\mathbf{T^2}$ and $\mathbf{T^3}$, respectively. In the case of $\mathbf{T^2}$, the chemical structure is described in the literature as R-**Si**-$(OSi)_2$-OR, meaning that the silica atom in analysis is surrounded by two –OSi groups and one O-R group, while in the case of $\mathbf{T^3}$ the chemical structure is described by R-**Si**-$(OSi)_3$, wich means that the Si atom is surrounded by three –SiO groups [109]. By the relative intensity of the peaks we can conclude that the two types of complexation have the same impact in the final structure.

When the cellulose is modified with **PTMS**, the correspondent peaks are also **T** structures. However, for $\mathbf{T^{3*}}$ and $\mathbf{T^{2*}}$ structures a chemical shift of 10 ppm is obtained, at -77 and -71 ppm, respectively. Thomas et al refer that this chemical shift is due to the formation of ring structures between the –SiO groups [110]. In this case, the relative intensity of the peaks is completely different showing a predominance of $\mathbf{T^{3*}}$ structures.

The ^{29}Si MAS NMR analysis is also used to study the second synthesis approach OTMS/SiO_2/cellulose and PTMS/SiO_2/cellulose and the results are shown in figure 39.

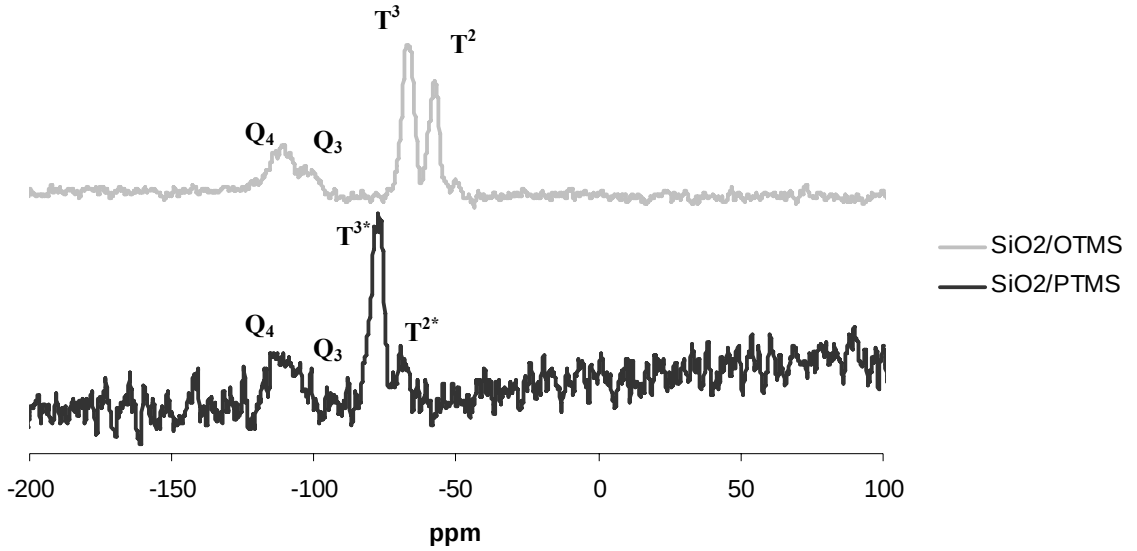

Figure 39 - ^{29}Si MAS NMR spectra of cellulose modified with silica layer and OTMS or PTMS.

The ^{29}Si MAS NMR analysis showed the presence of two new peaks, **Q_3** and **Q_4** at -106 and -111 ppm for both cases. These peaks are described in the literature as O-**Si**-$(OSi)_3$ for **Q_3** and **Si**-$(OSi)_4$ for **Q_4**. These structures correspond to the formation of silica particles [111, 112]. This result confirms that the silica layer remains in nanocomposite materials after the hydrolysis of silanes.

The **T** structures are also identified in these nanocomposites, -66 (**T^3**) and -56 (**T^2**) for OTMS/SiO_2/cellulose and -77 (**T^{3*}**) and -71 (**T^{2*}**) for PTMS/SiO_2/cellulose. It is possible to conclude that the functionalization of cellulose fibres with a silica layer does not change the condensation mechanism of silanes.

SEM images show a different morphology between the two silane-cellulose nanocomposites, which clearly confirms the different ways of polycondensation. A continuous film is observed at the fibres surface modified with **OTMS** (figure 40**a)**), and the same is observed in the modification with **PTMS** but with rough appearance (figure 40**b)**). This feature is due to the SiO_2 agglomerates resulting from the polycondensation of silane.

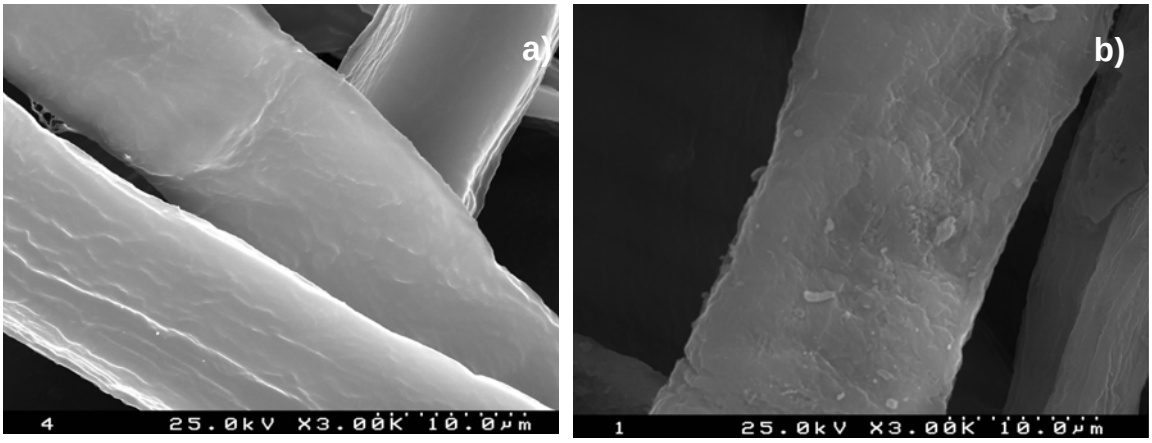

Figure 40 - SEM images of cellulose surface modified with **a)** OTMS and **b)** PTMS.

The FTIR analysis allows the confirmation of the presence of silanes at the cellulose surfaces. Figure 41**a)** and 41**b)** shows, respectively, the spectra of OTMS/cellulose and PTMS/cellulose, together with blank cellulose fibres for comparison. An intense band with a complex structure at ~1100-1040 cm^{-1} appears in both spectra, that can be assigned to the formation of siloxane species (Si-O vibrations) on the surface [113]. Both, the Si-O-Si and Si-O-C asymmetric stretching vibrations absorb at the same wavenumber area [114].
Besides, cellulose bands absorb in this region as it can be observed in the cellulose blank fibres spectrum. Due to this overlapping, the correct distinction of the bands in this area is a difficult task.

In the OTMS/cellulose spectrum (figure 41**a)**), the bands at ~2920, 2850 cm^{-1} ($\upsilon(CH_2)$), and ~1460 cm^{-1} ($\delta(CH_2)$) are consistent with the appearance of alkyl groups on the surface [113]. Two less intense bands at 3740 and 2940 cm^{-1} can be attributed to residual Si-O-H and Si-O-CH_3 groups, respectively [113, 115]. In the PTMS/cellulose spectrum (figure 41**b)**) the presence of the aromatic ring is detected at 1125-1000 cm^{-1}, due to planar ring vibrations having some Si-C stretching character. Other phenyl bands are found near 1430, 730 and 695 cm^{-1} [114].

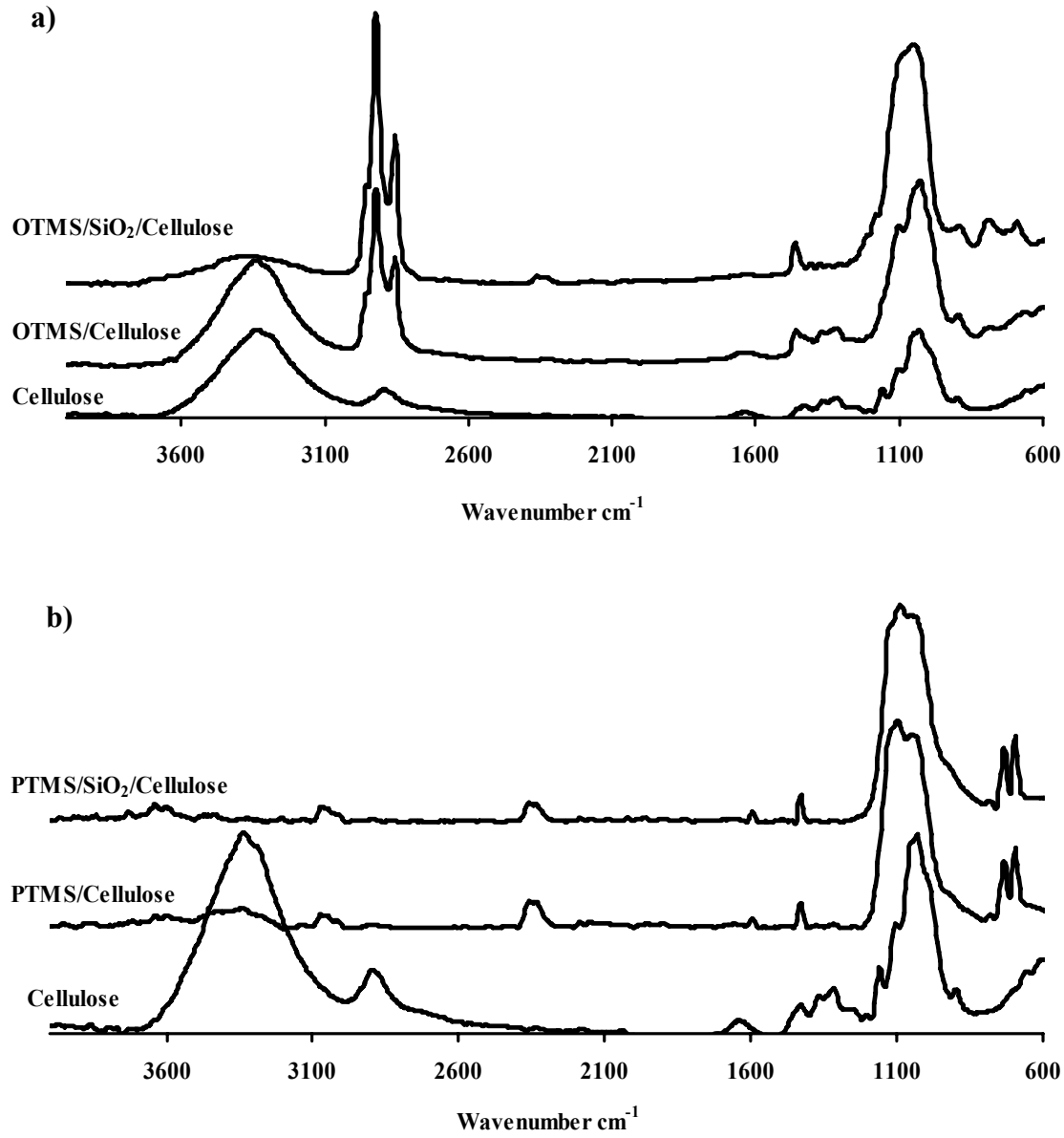

Figure 41 - FTIR spectra of cellulose modified with **a)** OTMS/cellulose and OTMS/SiO_2/Cellulose and **b)** PTMS/Cellulose and PTMS/SiO_2/Cellulose.

The present chemical grafting involves functionalised silane coupling agents, commonly used for many purposes, like water repellent and thermal stability. Now it is described the results obtained for the new nanocomposite materials. For this propose the hydrophilic and the thermal properties of these materials were studied.

Cellulose fibres in aqueous medium normally swell. The presence of polar groups such as carboxyl and hydroxyl at the cellulose surface promotes a good affinity for polar

solvents like water. As the fibres swell, intermolecular bonds (hydrogen bonds) are broken as the result of internal stresses produced by swelling.

The change of the cellulose surface properties after the modification was ascertained by contact angle measurements. The contact angles measurements should be ideally, made on smooth, flat surfaces, because contact angles are significantly influenced by surface roughness, chemical heterogeneities and are known to dramatically change between the wet and dry states of a material [116]. Because of this, the fibres were previously conditioned in a dessicator and after pressed in a mould to obtain pellets with flat surfaces. Water contact angles were measured on these substrate surfaces and the results are summarized in figure 42. From the results obtained and bearing in mind that cellulose is a highly hydrophilic substrate (water contact angles around 50º), it is evident that the present modifications with silanes reversed this behaviour.

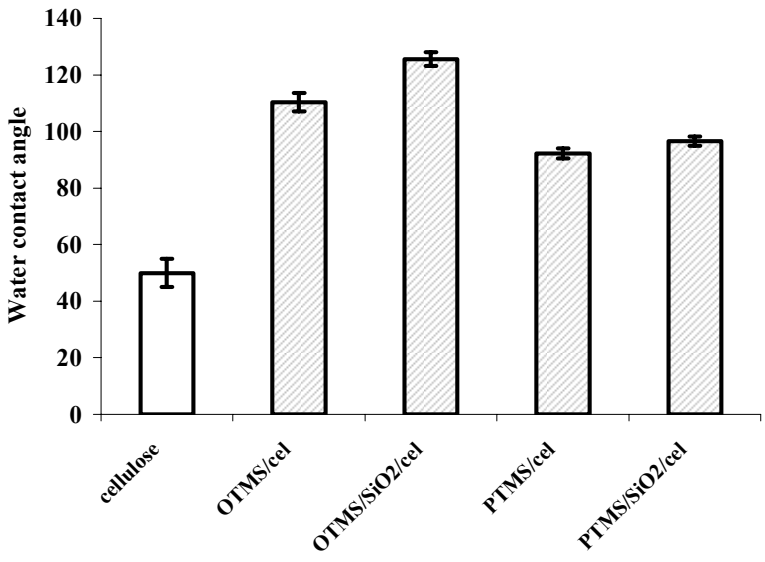

Figure 42 - Water contact angles of silanes/cellulose nanocomposites

The higher hydrophobicity was obtained when the substrates were previously coated with silica before the reaction with silanes. This is a strong indicator of a good coverage of fibres surface by silanes molecules, since SiO_2/cellulose is a highly hydrophilic surface. Due to the rapid absorption of the water droplet on the SiO_2/cellulose substrates, this measure was impossible; this is due to the highly hydrophilic nature of untreated SiO_2 surfaces [117].

The refereed difference in the contact angles is probably related with the orientation of the alkyl and phenyl radicals. When the fibres are modified with SiO_2 the alkyl chains may adopt a preferential orientation perpendicular to the cellulose surface, creating a more homogeneous layer. In the case of phenyl radicals, the high volume and high electronic density of these groups may create some repulsions, and some distortion is probably verified at the cellulose surface. However, as discussed before the **PTMS** silane forms some silica agglomerates during the condensation process at the cellulose surface. These silica moieties are hydrophilic and reduce the water contact angle of the materials.

The thermal degradation behaviour of the silane-treated cellulose fibres was accessed by thermogravimetric analysis. The TG thermograms and dTG curves of these fibres together with blank cellulose and SiO_2/cellulose fibres are presented in figure 43. Table 5 resumes the temperatures at maximum degradation rates (peak temperatures, T_d) and the final residue percentage. The weight loss below 100 ºC, due to the adsorbed moisture in all compounds, was not considered.

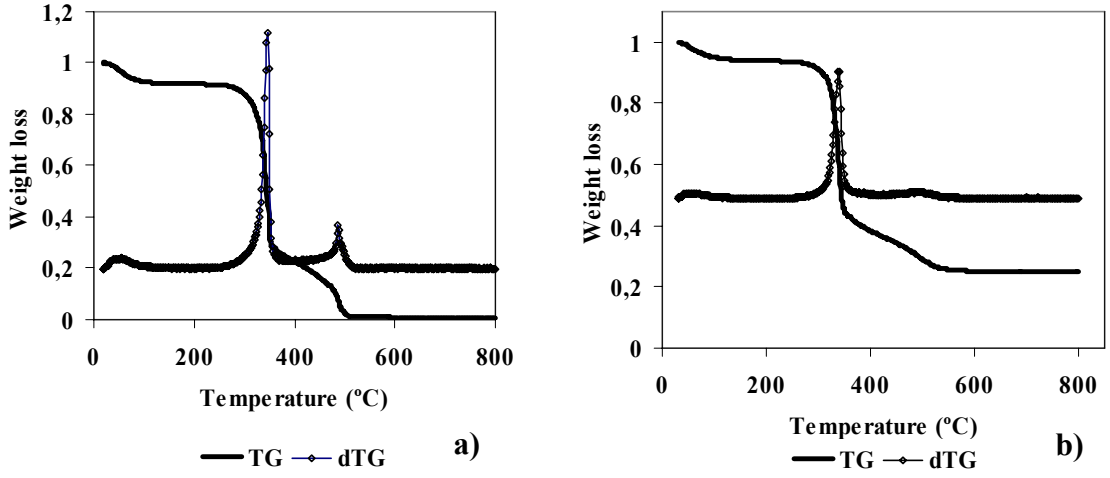

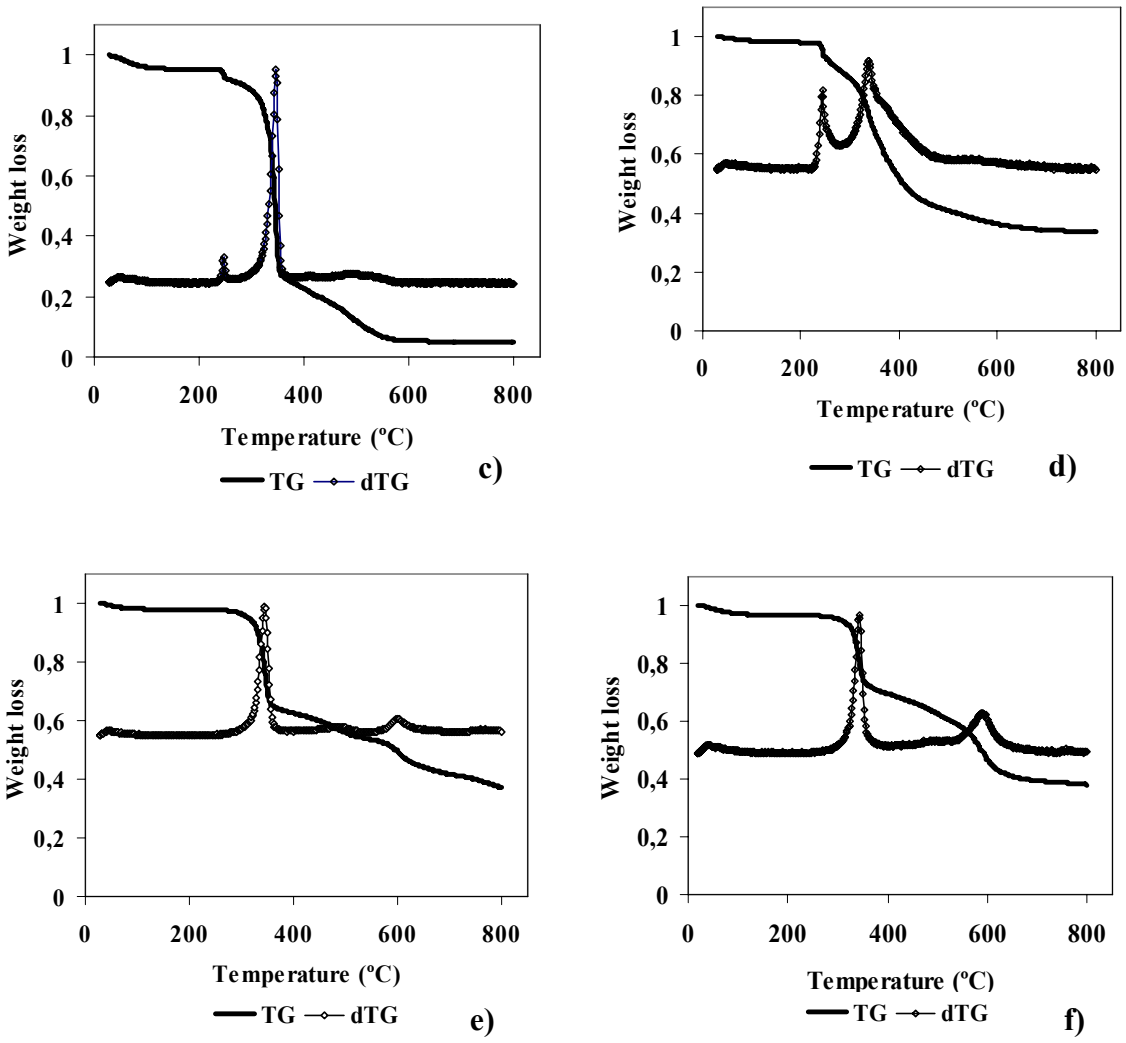

Figure 43 - TG and dTG of cellulose **a)**, SiO_2/cellulose **b)**, OTMS/cellulose **c)**, OTMS/SiO_2/cellulose **d)**, PTMS/cellulose **e)** and PTMS/SiO_2/cellulose **f)**.

Table 5 -Thermogravimetric features of cellulose and surface modified cellulose fibres. T_{dX} (X = O, C and P) correspond to OTMS, PTMS and Cellulose respectively while X refers to the temperature at maximum degradation rate (from dTG))

Sample	T_{dO} (ºC)	T_{d1C} (ºC)	T_{d2C} (ºC)	T_{dP} (ºC)	% residue
Cellulose	-	347	488	-	0
SiO_2/cellulose	-	339	499	-	25
OTMS/cellulose	247	347	496	-	5
OTMS/SiO_2/cellulose	243	340	478	-	34
PTMS/cellulose	-	344	*489*	595	37*
PTMS/SiO_2/cellulose	-	346	*490*	602	38

For reference, the TG thermogram of cellulose blank fibres was performed at the same conditions as the composite fibres. As expected, the TG curve obtained at air shows

two main stages of weight loss (figure 43**a)**). The first stage (T_{d1C} = 347 ºC) corresponds to the thermal degradation of cellulose. At this stage, the decomposition leads to the generation of volatile flammable products. The second stage (T_{d2C} = 488 ºC) may be ascribed to the thermal oxidation of volatile products [118].

The SiO_2 coating slightly modified the thermal stability of the cellulose fibres (figure 43**b)**). Also the same conclusion can be made to the **OTMS** coating. Although in the thermograms of OTMS/cellulose and OTMS/SiO_2/cellulose (figure 43**c)** and 43**d)**), an initial peak appears at 247 ºC it is probably due to structural rearrangements leading to dehydration that results from the previous incomplete reaction between OH groups from the silane molecules and cellulose (or silica) resulting in covalent bonding.

Interesting changes in the cellulose thermal stability were observed with **PTMS** coatings. When compared with the thermogram of blank cellulose fibres, **PTMS** and PTMS/SiO_2/cellulose composites exhibit a retarded thermal oxidation step denoting a higher resistance to thermal degradation (figure 43**e)** and 43**f)**). A possible explanation to this behaviour can be that, during the first degradation step, a thermally stable char is formed that acts as an outer layer to prevent the further degradation of the bulk and thus may improve the flame retardancy. At the end of the thermogravimetric analysis (800 ºC), the stabilization of weight loss was not achieved. The increased thermal stability of **PTMS** modified composites can be attributed to the presence of aromatic groups since these structures can improve thermal stability due to their ability to inhibit ignition and promote char formation [119, 120]. Further calcinations tests were performed by heat treating all the composite fibres in a furnace at a heating rate of 10 ºC/min until 850 ºC and keeping this temperature constant during 6 hours. After this treatment, the final residue percentage was the same as determined in the TG analysis with the exception of PTMS/cellulose, where the final residue percentage was 26% but still incomplete due to dark residues. This result shows an interesting retardant action of the thermal decomposition of this material.

3.3.1- Assembly of TiO_2 particles at cellulose modified surface

To build up new nanocomposites with titanium dioxide these new materials were tested for the different techniques described in the last chapter, ***in situ*** and **LbL**, but the results are not so good. In the first case, syntheses ***in situ***, its reaction medium is extremely

acid and destroys the organosilane molecules, while in second case (**LbL**), the organosilane molecules do not have charges at the surface and the polyelectrolytes do not attach.

An unexpected interaction between TiO_2 particles suspended in water and cellulose fibres previously modified with **OTMS** and **PTMS** was verified. After removing the fibres from the TiO_2 aqueous suspension, 6%w/w of TiO_2 particles remained in the fibres (ICP analysis). SEM analysis shows the TiO_2 particles at the cellulose surface (figure 44).

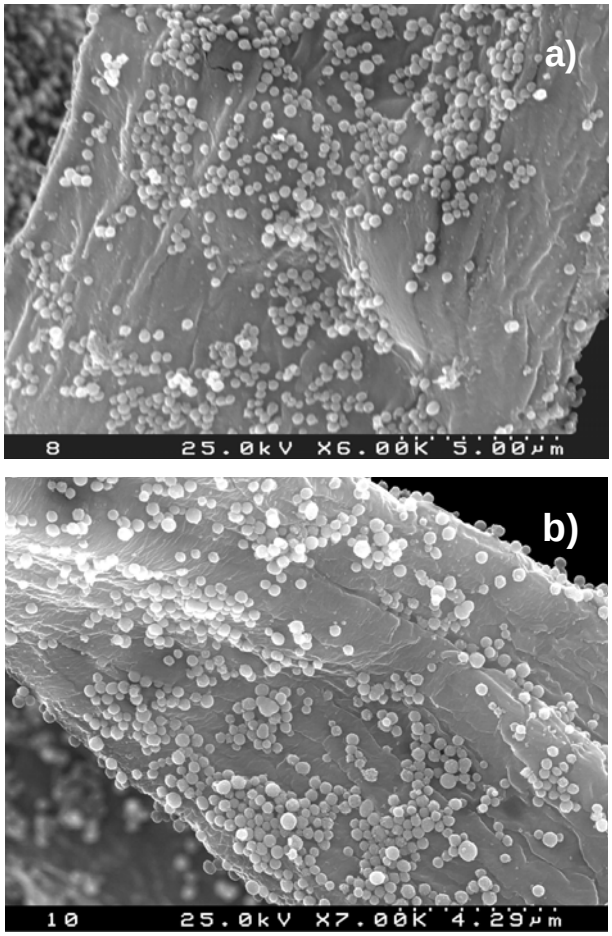

Figure 44 - SEM images of TiO_2/silane/cellulose composites, **a)** PTMS and **b)** OTMS

Titanium dioxide particles in aqueous solution are negatively charged due to the formation of Ti-OH groups at the particles surface, which have very strong polar interactivity. For other side the surface modification of cellulose fibres with silanes showed a high hydrophobicity, that is expected a low compatibility between those materials.

The most interesting point of this study is the ability of modified cellulose fibres with silanes to attach to TiO_2 particles. This behaviour is not well understood but can have one

possible explanation for the interaction of silanes and TiO_2 particles. The hypothesis consists in some free hydroxyl groups at the surface of silanes that can establish some interactions with titanium dioxide. The OH- groups and TiO_2 are hydrophilic and this similarity can increase the compatibility between the two materials.

Hydrophobicity and thermal stability properties of these new nanocomposites materials, TiO_2/silane/cellulose, were also studied. Concerning the hydrophobic properties, the materials showed a decrease of approximately 10º. This behaviour can be understood due to the high hidrophobicity of TiO_2 particles. The thermal stability of **PTMS** nanocomposites showed a similar behaviour to the nanocomposites without TiO_2. These results showed that titanium dioxide particles do not have significant influence in this property.

After this study it is possible to conclude that, new properties were achieved with modification of cellulose fibres with silane agents **OTMS** and **PTMS**, hydrophobicity and fire retardancy, respectively. This new approach showed a new range of potentialities for cellulose fibres; first, we suppress the natural behaviour of cellulose fibres hydrophilicity with the **OTMS** modification that can avoid the well know phenomenum of swelling, that sometimes can be a problem in the development of new materials. Secondly, fire retardancy achieved by the cellulose modified with **PTMS** can avoid flame propagation in new materials based in cellulose fibres.

4- Preliminary assessment of photocatalytic and antibacterial activity of TiO_2/cellulose nanocomposites

4.1- Introduction

Semiconductor photocatalysis with a primary focus on TiO_2 has been applied to a variety of problems of environmental interest like as water and air purification. It has been shown to be useful for the oxidation of organic compounds, destruction of microorganisms such as bacteria and viruses, for the inactivation of cancer cells, for odor control, for the photosplitting of water to produce hydrogen gas, for the fixation of nitrogen and for the cleanup of oil spills [39-42, 121, 122].

Various chalcogenides (oxides and sulphides) have been used: TiO_2, ZnO, CeO_2, ZrO_2, SnO_2, $SbrO_4$, CdS, ZnS, etc…. As generally observed, the best photocatalytic performances with maximum quantum yields are always obtained with titanium dioxide. In addition, anatase is the most active polymorphic form among the various forms available, either natural or artificial. Anatase is thermodynamically less stable than rutile, but its formation is kinetically favoured at lower temperatures (<600ºC) [121]. This lower temperature could explain the higher surface area and a higher surface density of active sites for adsorption and for catalysis.

When titanium dioxide is irradiated with UV light, this semiconductor also exhibits strong bacterial activity. To evaluate the antibacterial activity of TiO_2/cellulose nanocomposites some studies was performed for inactivation of some microorganisms: *Staphylococcus aureus*, *Klebsiella pneumonide* and *Escherichia coli*.

4.2- Photocatalitic behaviour of TiO_2/cellulose nanocomposites

Since TiO_2 is one of the most efficient photocatalyst (special focus in the anatase phase) with wide application, we decided to evaluate the possible photocatalytic activity of TiO_2/cellulose nanocomposites (***in situ*** and **LbL**) using TiO_2 **Degussa P-25** as the reference photocatalyst.

Aiming to test the photocatalytic activity of the TiO_2/cellulose nanocomposite, the conditions used for the synthesis of the nanocomposites **U4** and TiO_2//cellulose (**LbL**) were selected for a scale-up experiment. For this composition, a larger amount of anatase was obtained in the nanocomposite, which has been reported as the TiO_2 polymorph with

higher photocatalytic activity [68]. The scale-up procedure allowed the preparation of TiO_2/cellulose nanocomposites with around 12% of inorganic content and with the same characteristics as the lower scale synthesis.

The study of the photocatalytic activity of TiO_2/cellulose photocatalysts, degradation of methylene blue (**MB**) was carried out under irradiation of UV-ligth [123]. The reaction temperature was maintained at 298K. The UV-visible absorbance spectrum of the reaction mixture containing organic dye solution and catalyst with respect to the irradiation time was recorded in order to determine the concentration of **MB** in solution after separating the catalyst. A decrease in the intensity of bands at 609 and 668nm was observed with respect to the radiation time during the evolution of photocatalytic reaction (figure 45).

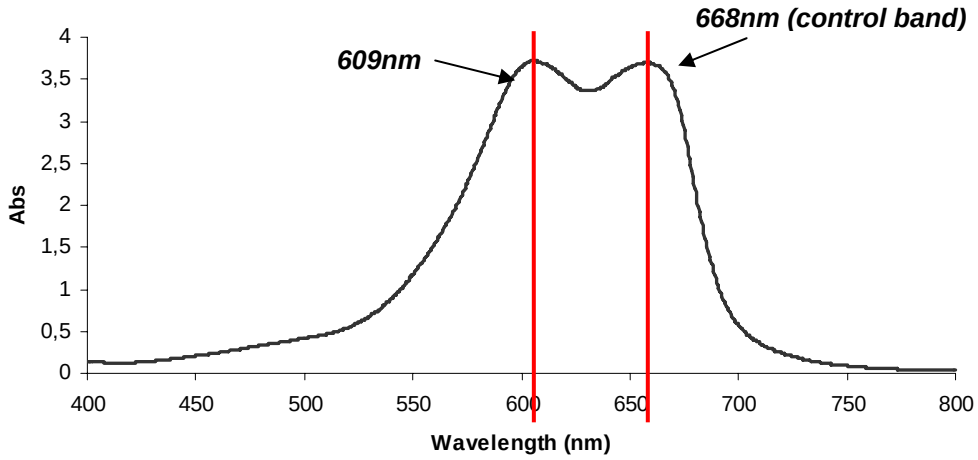

Figure 45 - UV-Vis spectra of Methylene Blue (**MB**) solution with a 50ppm of concentration.

To avoid adsorption phenomenum, the nanocomposite was first saturated with a 50 ppm methylene blue solution. Some studies were carried out with cellulose fibres and we concluded that capacity to absorb dye is approximately 95% for the blank fibres and 50% in the case of TiO_2/cellulose nanocomposite, for a solution with a 50ppm of concentration. These results can clearly show the high affinity of cellulose for organic dyes and can suggest some draughts about what type of phenomenum is responsible for removing the organic dye from the aqueous solution (adsorption or degradation) [101, 124, 125].

Temporal changes in the concentration of **MB** were monitored by examining the variations in maximal absorption in the UV-visible spectra. The latter absorption band was selected to monitor the temporal concentration changes of **MB** in aqueous solution, since

the band at 668 nm shifted considerably towards the blue region during the course of photoassisted degradation (figure 46).

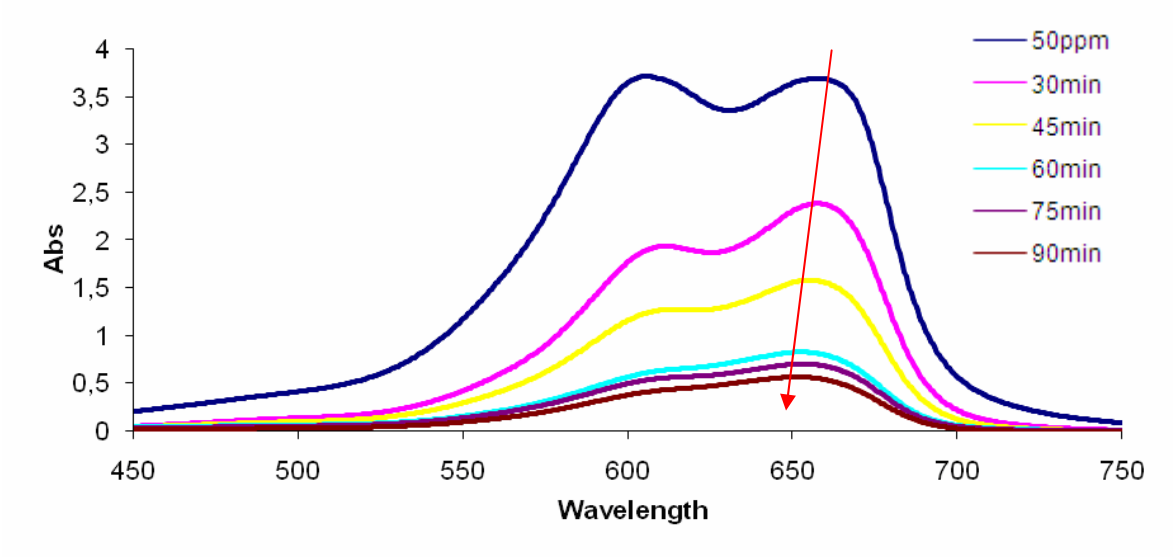

Figure 46 - Temporal spectral changes of MB in aqueous solution with TiO_2/cellulosenanocomposite (*in situ*) under UV illumination (0–90 min)

The colour of **MB** solutions becomes less intense when all or part of the auxochomic groups (methyl or methylamine) degrades. Figure 46 also shows that the spectral band at 668nm blue-shifts by as much as 18nm from 668 to 650 during the course of the photodegradation.

The first approach to explain the photodegradation of **MB** by TiO_2 is described by T. Zhang et al [125]. The process of N-demethylation of MB is described in figure 47.

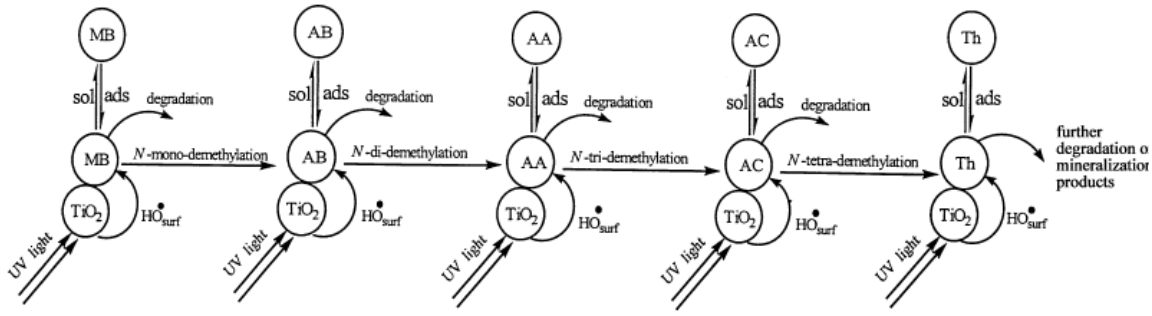

Figure 47 - Scheme depicting the N-demethylation of MB and the dynamic equilibrium of MB and N-demethylated species between the bulk solution and the TiO_2 particle surface during the photodegradation of MB (**MB**- methylene blue, **AB**- Azure B, **AA**- Azure A, **AC**- Azure C and **Th**- Thionine) [125].

N-demethylation of **MB** occurs through the mechanism represented in figure 47, where **AB**, **AA**, **AC** and **Th** refer to the various structures of the N-demethylated intermediates.

As weak electron-donor substituents, methyl groups can facilitate the attack on **MB** by electrophilic species (OH^-) in the demethylation process; this is also likely to be a major step in the photocatalytic oxidative degradation of **MB**. Examination of the spectral variations in figure 49 suggests that **MB** was N-demethylated in a stepwise manner; methyl groups were removed one at a time as confirmed by the gradual band wavelength shifting towards the blue region.

Absorption bands of N-demethylated analogs of **MB** in the visible range are seen [125] at 648-655nm for Azure B (blue color in aqueous solution), at 620-634nm for Azure A (blue color in aqueous solution), at 608-612nm for Azure C (blue color in aqueous solution) and at 602.5nm for Thionine (first yields a blue color, then a violet solution). These characteristics bands are responsible for the shift of the maximum band of MB spectrum. The color of TiO_2-nanocomposites turned from white to a grayish blue color, caused by the mixture of colored intermediates adsorbed on the surface of the TiO_2-nanocomposites and undergoing partial or complete N-demethylation and deamination during the irradiation time.

To better understand the degradation capability of nanocomposite materials, all absorbance values obtained were converted to concentration values by the **Beer-Lambert** equation. For this purpose, it is necessary to build up the calibration curve of **MB** (figure 48). Each point of the calibration curve is the mean value of three independent measures.

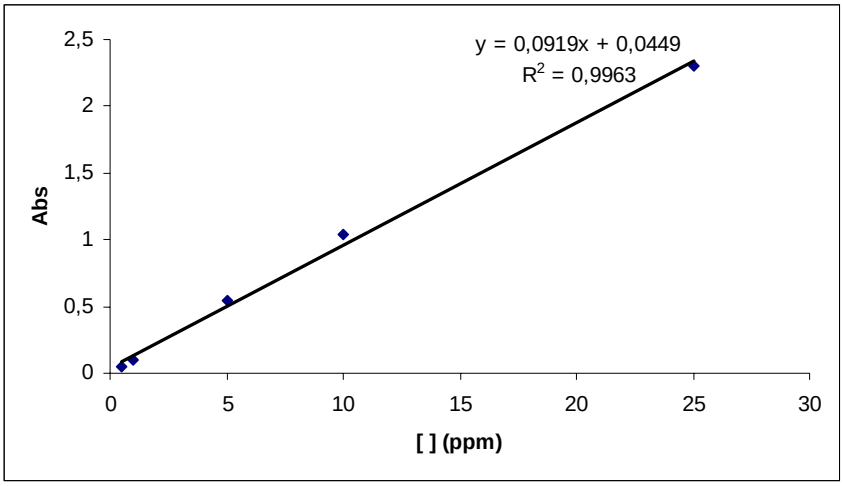

Figure 48 - Calibration curve of MB for several concentrations

Figure 49 shows the degradation of methylene blue using TiO_2/cellulose nanocomposite (***in situ*** and **LbL**), **Degussa P-25** and a mixture of **Degussa P-25+blank**

fibres. The experimental values used to draw the curves are mean values of three independent experiments. From these results, it is clear that the reaction rate of **MB** decomposition due to the TiO_2/cellulose nanocomposite (***in situ***) is the highest; approximately 100% of degradation was obtained after 90 min of reaction time. In the case of **P25** and **P25+blank fibres** only 80% of degradation was obtained after 175min, while in case of **LbL** only 45% of degradation is achieved after 150 min.

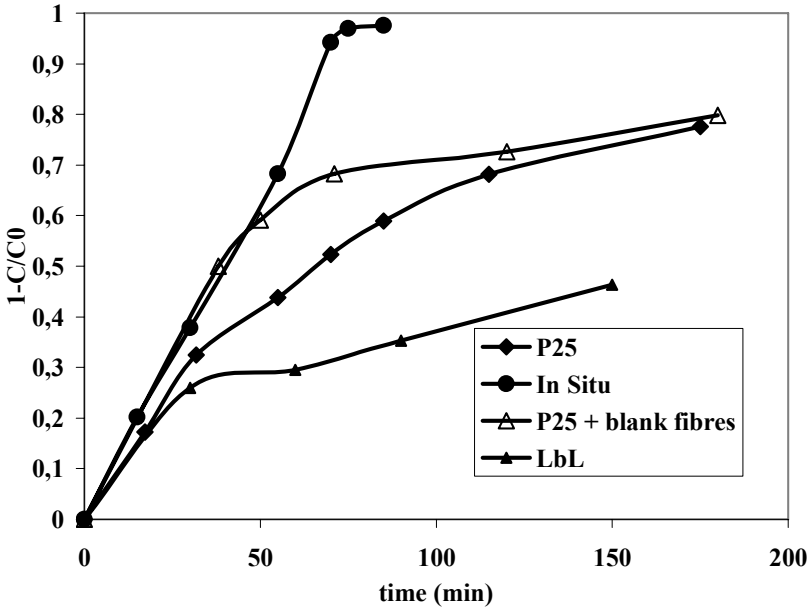

Figure 49 - Degradation of **MB** using nanocomposites and P25 catalysts under UV light irradiation.

The photoactivity of a sample depends on a large number of parameters including particle size, surface area and ratio between amorphous and crystalline phases [68]. It is generally accepted that anatase is the most active photocatalyst, and that a combination of high crystallinity and large specific surface area improves the photocatalytic performance. Degussa P-25 is made of 80% anatase and 20% rutile phase, its specific area is 50 $m^2 \cdot g^{-1}$ and it consists in a powder whose particles have a 30 nm diameter [68]. The TiO_2 phase in the nanocomposite is mainly anatase, as detected in the XRD, with the particle size diameter ranging between 15 and 60 nm [126]. However, since these nanoparticles are supported in the fibres, their available surface area decreases. Nevertheless, the morphology of the particles also provides an important contribution for the enhanced photoactivity of a sample therefore the irregularity of the particles size distribution at

cellulose surfaces and heterogeneous morphologies of these particles are certainly responsible for an increase of the available surface active sites.

From the above experiments, it is evident that some adsorption of methylene blue occurs. By comparing the results achieved for **P25** and **P25+blank fibres**, the initial decrease in **MB** concentration rate is higher in the second case, although after 100min the behaviour of the two materials are similar. These results can be explained by initial adsorption phenomenum at the cellulose surface.

The lowest photocatalytic activity is achieved for the nanocomposite materials made by the **LbL** technique. These results are not very well understood since the quantity of TiO_2 is similar to other samples. One possible explanation is that both (**PDDA** and **MB**), have positive charges at the surface, and repulsion phenomena can occur. On the other hand, particle size is bigger, approximately 300nm, which diminishes the specific surface area and consequently, the number of active sites.

This work showed the high photocatalytic activity achieved for TiO_2/cellulose nanocomposites (syntheses ***in situ***) when compared with reference **P25**. In fact, TiO_2/cellulose nanocomposite has other advantage, since it is one supported catalyst that avoids many problems correlated with the recovery of the catalyst for new application. In the case of homogeneous catalyst it is necessary to centrifuge in order to recover the powders.

TiO_2/cellulose nanocomposites could be successfully used in gas-phase heterogeneous photocatalysis for the degradation of organic compounds. These nanocomposites will be tested in future work.

4.3- Antibacterial activity of TiO_2/cellulose nanocomposites

Titanium dioxide, as a result of the direct absorption of incident light photons, near-UV light, can participate in surface photochemical processes that lead to complete oxidation of most organic molecules, that organic molecules can be the cell membrane of microorganisms, promoting the destruction of that forms of life. To evaluate the antibacterial activity of TiO_2/cellulose nanocomposites, the same samples tested for photocatalysis were tested here (**LbL** and ***in situ***). Both samples have the same contents in TiO_2 approximately 12%wt.

The results achieved for the inactivation of mioorganisms, *Staphylococcus aureus*, *Klebsiella pneumoniae* and *Escherichia coli* in the presence of nanocomposites is described in table 6. The contact time between bacterias and nanocomposites was 24h and nanocomposites were activated by UV-light during this period.

Table 6 - Antibacterial activity of TiO_2/cellulose nanocomposites (LbL and in situ) against three different types of bacterias, *Staphylococcus aureus, Klebsiella pneumoniae and Escherichia coli*. The method used for count the bacterias was CFU (Colony Forming Units).

Samples	***S. aureus* ATCC 6538 Gram +**			***K. pneumoniae* ATCC 4352 Gram -**			***E. coli* ATCC 4352 Gram -**		
	CFU T_0	CFU 24 h	% red 24 h	CFU T_0	CFU 24 h	% red 24 h	CFU T_0	CFU 24 h	% red 24 h
Vegetal Cellulose	27×10^4	31×10^4 35×10^4	**0** **0**	5×10^5	92×10^6 90×10^6	**0** **0**	18×10^4	12×10^7 12×10^7	**0** **0**
TiO_2/cell (***in situ***)		0 0	**100** **100**		0 0	**100** **100**		39×10^2 35×10^2	**99,99** **99,99**
TiO_2/cell (**LbL**)		0 0	**100** **100**		12×10^7 13×10^7	**0** **0**		61×10^3 73×10^3	**99,95** **99,94**

The antibacterial activity has been evaluated as percentage bacteria reduction. Due to the intrinsic variability of the antibacterial tests, at least 90% reduction (corresponding to 1 log reduction of CFU values) was considered necessary to claim an antibacterial effect. The antibacterial activity can be distinguished in:

- **bacteriostatic effect**, when only an inhibition of bacterial growth is obtained (the number of initially inoculated bacteria is not affected, in our experiments: a value around 3×10^5 CFU was used.
- **bactericidal effect**, when inhibition of growth and reduction of the number of initially inoculated bacteria is obtained. In some cases completely killing of bacteria can be registered.

Antibacterial tests have been also carried out on control fibre samples (vegetal cellulose), without the presence of the photoactive TiO_2 nanoparticles. That control sample has not produced any reduction or growth inhibition of bacterias, that results showed that cellulose substrate do not have any influence in the killing mechanism process of bacterias studied (figure 50 **a)** and **b)**).

Sample ***in situ***, where the nanoparticles have been synthesised directly on the fibre surface have shown high antibacterial activity towards the three microorganisms tested, completely killing (bactericidal) for *S. aureus*, for *K. pneumoniae* and for *E. coli* (figure 50 **c)** and **d)**).

Sample **LbL**, TiO_2 connected to the fibre through polyelectrolites, was following different behaviour, and has produced completely killing for *S. aureus* and both inhibition of growth and some bactericidal activity for *E. coli* but no activity at all toward *K. pneumoniae*.

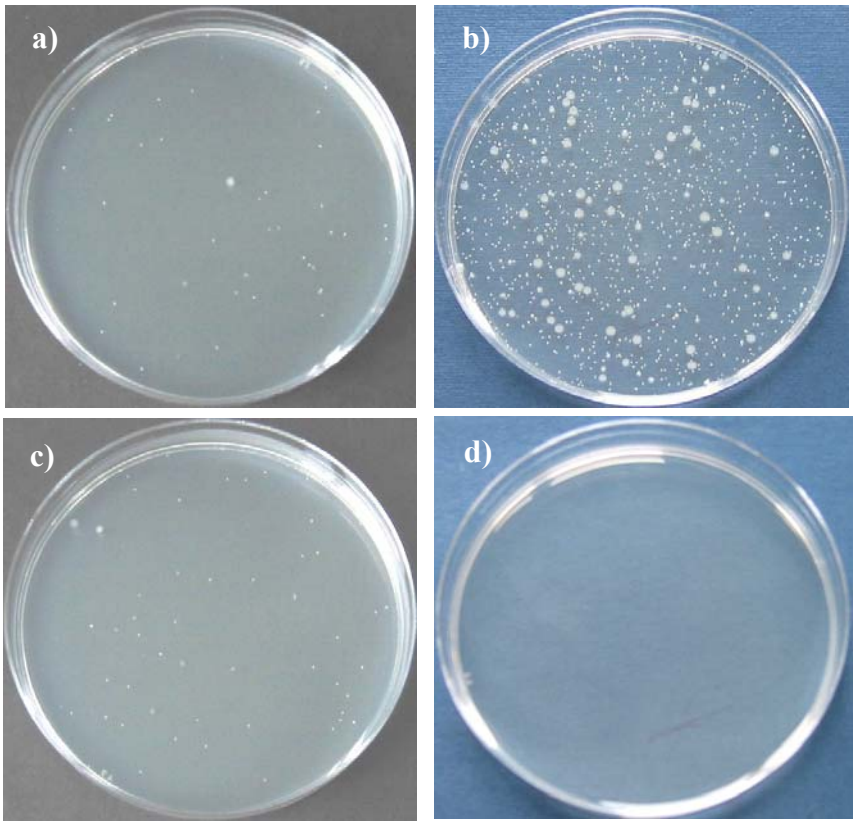

Figure 50- *E. coli* colonies in contact with control cellulose sample, **a)** 0 and **b)** 24h. *E. coli* colonies in contact with a TiO_2/cellulose sample **c)** 0 and **d)** 24h.

In general, the best result was achieved for Sample ***in situ***, synthesized by chloride method. In case of chloride method the particle size of samples is significantly lower then the **LbL** method, 15-60 and ~300nm respectively. That morphological property allows a higher specific surface area for the samples prepared by the chloride method. Properties influencing the behaviour of titania particles have been reported to include surface area, cristallinity, crystalline size and crystal structure [15]. Since the reaction/interaction activity is mostly confined to the surface of the material, its surface area must be increased to maximize the activity.

The antibacterial behaviour depends on the different treatments and on the different bacteria tested. In general gram + bacterium *S. aureus* showed to be the most sensible to the TiO_2 photoactivity and *K. pneumoniae* the most resistant one. Maness et al [54] suggested that superoxide ions initiate the mechanism of lipid peroxidation of cell

membrane, and after some reaction time the radical can penetrate inside the cell and lead to destruction. Based on that, the bacterial resistance depends predominantly of the cell membrane thickness.

Further tests could be useful to better highlight the antimicrobial activity mechanisms and efficiency, such as kinetic studies of photo-activation in the dark and bacteria reduction with respect to TiO_2-bacteria contact time. Assessment of efficiency toward other microorganisms, such as spore forming bacteria and fungi, could be also interesting.

5- Conclusions

TiO_2/cellulose nanocomposites have been prepared using different approaches. In situ synthesis of TiO_2/cellulose nanocomposites using the controlled hydrolysis of titanium tetrachloride with and without addition of urea was performed. The nanocomposites show a surface homogeneously coated with TiO_2 nanoparticles. It was found that, controlling the amount of urea in the system, it is possible to control both: the load and the crystalline phase of TiO_2 in the final nanocomposites.

The Layer-by-Layer (**LbL**) multilayer film deposition method, one of the most widely used techniques for the fabrication of functional materials due to its simplicity and versatility, showed to be an effective way to build up TiO_2/cellulose nanocomposites. Particles of titanium dioxide were synthesized by the ethoxy method which makes it possible to control the size and shape. Polyectrolytes works like bridges to attach the TiO_2 particles to cellulose surface by electrostatics bonds. This method is a good choice when the size of TiO_2 particles is a critical parameter, for instance, the reflectance capability of titanium dioxide depends on its size.

A selected TiO_2/cellulose nanocomposite (**U4**) was effective in the photocatalytic degradation of methylene blue offering the possibility of using these nanocomposites in photocatalytic applications without the need of filtration after the reaction to recover the catalyst (in aqueous systems) and in gaseous photocatalysis such as in the purification of indoor air. Moreover, that TiO_2/cellulose nanocomposite showed to have good antibacterial properties. The preliminary studies realized showed a completely killing (bactericidal) of the three different bacterias: *Staphylococcus aureus*, *Klebsiella pneumoniae* and *Escherichia coli*.

A silica nanolayer at the cellulose surface demonstrated to be an efficient protection of the substrate against photo-attack by the TiO_2 nanoparticles. This inorganic barrier prevents the migration of $OH^{\cdot}$ radicals from the titanium dioxide surface to the cellulose avoiding the destruction of the organic structure.

In this work, novel TiO_2/cellulose composites with a silane barrier between TiO_2 and cellulose fibres were prepared and characterized. This barrier was effective on the protection of cellulose fibres against TiO_2 photo-attack. Interesting properties arise from these composites depending on the nature of the silane used: **OTMS** and **PTMS** confer

hydrophobic characteristics to the resulting materials. This property results from a decrease in the fibres surface energy, improving their compatibilization with common nonpolar polymer matrices; **PTMS** coated fibres improved the thermal resistance of the cellulose fibres, which is a very important feature of cellulose based materials.

The increasing demand for materials based in recyclable resources can open the doors for applications of these new nanocomposites. I hope that this work can contribute for the development of new materials based on natural polymers.

6- Future work

The cellulose fibres modified with TiO_2 nanoparticles will be incorporated in polymeric matrix. The main idea is to evaluate the compatibility between the modified cellulose fibres/polymers system and study if the new properties achieved by cellulose modified (photocatalyis, antibacterial, hydrophobicity and fire retardant) remain in composite materials (polymer-modified cellulose fibres).

All the synthesis performed for vegetal cellulose will be tested for the bacterial cellulose, also with the same proposes, to functionalise the bacterial cellulose with inorganic materials (TiO_2).

7- Experimental

7.1- Instrumentation

Scanning electron microscopy (SEM) images were obtained using a FEG-SEM Hitachi S4100 microscope operating at 25 kV. Transmission electron microscopy (TEM) was performed using a Hitachi H-9000 operating at 300 kV. The samples for TEM were prepared by depositing an aliquot of the colloid onto a carbon coated copper grid and then, letting the solvent to evaporate.

X-ray powder diffraction (XRD) was performed, using a Philips X_Pert instrument operating with Cu K*a* radiation (*k* = 1.54178 A˚) at 40 kV/ 50 mA.

Raman spectra were recorded using a Brucker RFS100/S FT-Raman spectrometer (Nd:YAG laser, 1064 nm excitation).

The FTIR spectra for solid samples were recorded with a BRUKER IFS-55 FTIR spectrometer equipped with a single horizontal golden gate ATR cell with resolution 8 and 128 interferograms. In case of liquid samples HATR TROUGH Plate ZnSe 45 degrees (PIKE) was used with a crystal size of 80mm and 4mm thickness. ATR measurements (128 interferograms) were collected and apodised with a triangular function. The spectral resolution was 4 cm^{-1}.

The UV/visible spectra were recorded using a Jasco V-560 UV–vis spectrophotometer; for the solid samples the spectra were recorded in the diffuse reflectance mode using MgO as the reference.

In order to quantify the TiO_2 retained in the fibres, 0.1 g of the hybrid material was submitted to acid digestion (3 ml HCl + 1 ml HNO_3 + 0.5 ml HF), using 25 ml Teflon reactors, in a microwave oven. The resulting solution was diluted to 100 ml and analysed for its titanium content by Inductively Coupled Plasma (ICP), using a Jobin Yvon 70 Plus equipment.

Zeta potential and particle size measurements were performed using a Zeta Sizer Nano Series (Malvern) instrument. For the measurements, aqueous suspensions of TiO_2 nanoparticles were first submitted to sonication to promote a good dispersion of particles.

Nitrogen adsorption isotherms were measured at 77K, using a gravimetric adsorption apparatus equipped with a CI electronic MK2-M5 microbalance and an Eduards Barocel pressure sensor. Before measurements, the inorganic materials were outgassed at 200ºC and maintained at this temperature overnight to a residual pressure of ca. 10^{-4} mbar. The values of

BET specific surface area (S_{BET}, determined in the p/p_0 range 0.03-0.13) and specific total pore volume V_p, were estimated from N_2 adsorption isotherms.

The thermogravimetric (TGA) assays were carried out with a Shimadzu TGA 50 analyser equipped with a platinium cell. Samples were heated at a constant rate of 10ºC/min from room temperature up to 800 ºC in static air.

Contact angles with water were measured with a "Surface Energy Evaluation System" commercialized by Brno University (Czech Republic). Each θ value was the average of five determinations.

Solid-state magic-angle-spinning (MAS) NMR spectra were recorded at 79.49 MHz for ^{29}Si on Bruker Avance 400/500 spectrometers. ^{29}Si MAS NMR spectra were recorded with 40º pulses, spinning rates of 5.0-5.5 kHz and 60 s recycle delays.

The ^{1}H NMR spectra were acquired in D_2O, at 300.13 MHz using a Bruker AMX 300 spectrometer. All chemical shifts were expressed as parts per million downfield from tetramethylsilane (TMS).

7.2- Materials

Wood cellulose fibres (Eucalyptus globulus), ECF bleached kraft pulp, composed essentially of cellulose (~85%) and glucuronoxylan (~15%) supplied by Portucel (Portugal) was disintegrated and washed with distilled water before use.

All chemicals used in the synthesis procedure are resumed in the next list:

Solvents:

Distilled water

Absolut ethanol (99.8 % Riedel-de Haen)

Salts:

Urea (Panreac 99.0%)

Titanium tetrachloride (Fluka 98.0%)

Titanium tetraethoxide (Aldrich 97.0%)

Potassium chloride (Panreac 99.5%)

Sodium chloride (Panreac 99.5%)

Polyelectrolytes:

Poly(diallydimethylammonium chloride) (Aldrich, 20wt% in water Mw~100000-200000)

Poly(sodium 4-styrenesulfonate) (Aldrich Mw~70000)

Silanes:

Tetraethoxysilane (Aldrich 98.0%)

Octyltrimethoxysilane (Fluka purum)

Phenyltrimethoxysilane (Fluka purum)

For the photocatalysis experiments, the dye utilized is methylene blue (Aldrich purum). The pigment used as comparing sample is TiO_2 P25 supplied by Degussa (~50m^2/g, average particle size 30nm and in a proportion of 4:1 of anatase to rutile).

7.3- Synthesis

7.3.1- Synthesis of nanocomposite materials by hydrolysis of $TiCl_4$ in water

Typical synthesis involved the addition of 1 mL of $TiCl_4$ to 50 mL of ice-cold distilled water under vigorous stirring. After homogenization of the solution, urea was dissolved according to the quantities described in Table 1. Cellulose fibres (0.5 g) were then added to the solution and the mixture was heated at 70 ºC during 6 hours. The pH was measured in the final mixture. The nanocomposite fibres were then collected by filtering, washed thoroughly with distilled water and finally dried at 50°C over 24 h. All the samples were prepared in duplicate.

7.3.2- Synthesis of complex $TiCl_4(NH_2CONH_2)_2$

All the synthesis procedure was performed inside globe box. The urea (3g) is added to 50 mL of dichloromethane. This solvent do not dissolves urea that is the reason because that reaction is named a solid state reaction. After that an excess of $TiCl_4$ is added to the solution by stirring. After two days of reaction the solid stays yellow. The solid is well washed with dichloromethane to remove the excess of $TiCl_4$ that not reacts.

7.3.3- Synthesis TiO_2/Cellulose nanocomposites based on hydrolysis of $TiCl_4(NH_2CONH_2)_2$

Complex $TiCl_4(NH_2CONH_2)_2$ (2.8g) is dissolved in 50 mL of destillated water, after a few seconds the yellow colour disappear. Cellulose fibres (0.5 g) were then added to this solution and the mixture was heated at 70 ºC, during 6 hours. The nanocomposite fibres were filtered thoroughly washed with distilled water and finally dried at 50°C over 24 h.

7.3.4- Preparation of monodispersed titanium dioxide particles

Monodisperse round and rough particles were prepared by controlled hydrolysis of titanium tetraethoxide in ethanol solution. For a total volume of 100 mL of ethanol 0.7 mL of KCl salt solution were added, followed by the addition of 1.7 mL of titanium tetraethoxide solution. The reaction was performed at three different temperatures, 10ºC, 20ºC and 30ºC. The solution was stirred during all the reaction time (24 hours), in order to get more uniform particles. The nucleation started after a few seconds or minutes depending on the reaction temperature. The changing colour of the solution indicates the starting mechanism of the nucleation; formation of a white suspension (**sol**) during the reaction time increases the viscosity which indicates the growth of particles (**gel**).

After the reaction time, the solvents were removed by the centrifugation process for 10000 rpm 10 minutes and, after that particles were cleaned with ethanol three times, and water also three times. To get high densities and high crystalline particles, calcination was performed at 500ºC during four hours.

7.3.5- Assembly of nanocomposite containing colloidal TiO_2 particles and cellulosic fibres

For the adsorption tests, aqueous dispersions of spherical TiO_2 particles within the size range ~300nm were prepared by sonication. The following aqueous solutions of the polyelectrolytes were prepared: 1%(wt/v) of PDDA in NaCl 0.5 mol dm^{-3} and 1%(wt/v) of PSS in NaCl 0.5 mol/dm^{-3}. The so-called layer-by-layer (LbL) technique was applied to coat the fibres by alternately dipping of the fibres in PDDA, PSS and again in the PDDA solutions. The time for each emersion was 10 min, and after each immersion step, the fibres were rinsed with deionised water to remove the excess of electrolyte and finally, the fibres were dried at room conditions. For the cellulose fibres treated with the

polyelectrolites, they were sequentially immersed in the TiO_2 nanoparticles suspension. The fibres were then washed and dried as described above.

7.3.6- Synthesis of SiO_2/cellulose nanocomposites

For this synthesis, 0.5 g of fibres was used per synthesis and the consistency of the suspension was 1%. In a typical synthesis of SiO_2 in the presence of cellulosic fibres, the fibres were added to a mixture of ethanol, H_2O and NH_4OH under moderate stirring in a 100 mL flask. Then, TEOS was added to the ethanolic solution and the mixture was allowed to stand under constant agitation at room temperature for 24 h. The final fibres were then collected by filtering, washed thoroughly with distilled water and finally dried at 50 ºC.

7.3.7- Synthesis of Silanes/cellulose and Silanes /SiO_2/cellulose nanocomposites

To prepare cellulose surface modified with silanes, 0.5 g of cellulose fibres (blank or silica pre-coated fibres) were added to a mixture containing 2.0 mL of silane reagent, 1.9 mL of NH_4OH, 5.4 mL of H_2O and 44.6 mL of CH_3CH_2OH under vigorous stirring. This mixture was left under stirring during 6 hours at room temperature. The silane treated cellulose fibres were filtered, thoroughly washed with distilled water and ethanol to remove the excess of silane, and finally dried at 110°C overnight. The treatment for preparing Silanes/SiO_2/cellulose hybrids was similar.

7.4- Photoactivity evaluation

The photocatalytic activity of TiO_2/cellulose nanocomposite was evaluated by measuring the decrease of the methylene blue (**MB**) concentration in the reaction solution. Prior to commencing illumination, a suspension containing the appropriated amount of the nanocomposite in order to attain 5 $g \cdot L^{-1}$ of TiO_2 in 100 mL of an aqueous solution of 50 ppm of **MB** was stirred continuously for 60 min in the dark. This pre-treatment was made in order to saturate the fibres with the MB solution to avoid absorption effects during the experiment. After this treatment, the fibres were filtered and added to 100 mL of a fresh solution of **MB**. Degussa P-25 titanium dioxide was used as the reference photocatalyst, which was studied using equivalent concentration of TiO_2

The reactions were performed in a double-walled glass container (ϕ 350 mm) with water circulation from a thermostatized bath at 25 ºC under constant stirring. A 700 W UV lamp was placed at 25 cm distance from the reactor. The solution samples were withdrawn using a syringe at regular time intervals and filtered trough millipore filters. The UV visible absorbance spectra of the samples with respect to irradiation time were recorded. To determine the concentration of **MB** in the solutions, a calibration curve for **MB** was plotted by determining the absorbance at the maximum wavelength (658 nm) of **MB**.

7.5- Antibacterial tests

The fibre samples were placed in contact with selected bacteria in favourable conditions for the bacterial growth. During bacteria contact the fibres were subjected to photo-activation under a lamp reproducing complete solar light spectra. At 0 and 24h contact times, specimens of the fibres samples were extracted with a neutralising solution and the bacteria concentration (CFU/ml) of the extraction solution has been determined by plating serial dilution on Plate Count Agar to obtain the overall number of bacteria (CFU) recovered from the specimens. Testing method, Antibacterial Finishes on Textiles Materials: Assessment of (Modified AATCC Test Method 100-1998).

Testing conditions:

- Microorganisms: *Staphylococcus aureus* ATCC 6538, *Klebsiella pneumoniae* ATCC 4352, *Escherichia coli* ATCC 10536.
- Sample incubation: 24 h at 23 ±1°C under 4000-5000 Lux light lamp.
- Quantity of test material: 62 mg.
- Quantity of inoculated buffer: 1 ml of inoculum in 12.5% nutrient broth in physiological saline solution.
- Extraction solution. Neutralizing solution: Azolectin 3 g/l, Polysorbate 80 30 g/l, sodium thiosulphate 5 g/l, L-Hystidine 1 g/l, KH_2PO_4 0.68 g/l, (pH a 7.2 ± 0.2).
- The samples were not subjected to sterilization.

The antibacterial activity (% reduction of bacteria) of the sample was calculated as follows:

$$R= (B – A) / B \times 100$$

Where:

A = CFU/sample, bacteria recovered from the test sample after 24 h contact time.
B = CFU/sample, bacteria recovered from the test reference after 24 h contact time.
R = Percentage of reduction.
CFU: Colony Forming Units.

Due to the intrinsic variability of the antibacterial tests, at least 90% reduction (corresponding to 1 log reduction of CFU values) was considered necessary to claim an antibacterial effect.

8- Bibliography

1. Sjostrom, E., *In Wood Chemistry - Fundamentals and Applications*. 1993, London: Academic Press Limited. 21-69.
2. Lindström, T., *Electrokinetics of the papermaking industry. In Paper Chemistry*. 2nd ed. 1996, Glasgow: Blackie Academic & Professional. 25-43.
3. Klemm, D., Heublein, B., Fink, H.P. and Bohn, A., *Cellulose: Fascinating biopolymer and sustainable raw material.* Angew Chem Internat Edit, 2005. **44**(22): p. 3358-3393.
4. Valadez-Gonzalez, A., CervantesU., J.M., Olayo, R. and Herrera-Franco, P.J., *Effect of fiber surface treatment on the fiber-matrix bond strength of natural fiber reinforced composites.* Composites Part B: Eng, 1999. **30**(3): p. 309-320.
5. Jahn, A., Schroder, M.W., Futing, M., Schenzel, K. and Diepenbrock, W., *Characterization of alkali treated flax fibres by means of FT Raman spectroscopy and environmental scanning electron microscopy.* Spectrochim Acta A, 2002. **58**(10): p. 2271-2279.
6. Van de Weyenberg, I., Ivens, J., De Coster, A., Kino, B., Baetens, E. and Verpoest, I., *Influence of processing and chemical treatment of flax fibres on their composites.* Compos Sci Technol, 2003. **63**(9): p. 1241-1246.
7. Belgacem, M.N. and Gandini, A., *The surface modification of cellulose fibres for use as reinforcing elements in composite materials.* Compos Interfaces, 2005. **12**(1-2): p. 41-75.
8. Czaja, W., Krystynowicz, A., Bielecki, S. and Brown, R.M., *Microbial cellulose - the natural power to heal wounds.* Biomaterials, 2006. **27**(2): p. 145-151.
9. Klemm, D., Schumann, D., Kramer, F., Hessler, N., Hornung, M., Schmauder, H.P. and Marsch, S., *Nanocelluloses as innovative polymers in research and application*, *Polysaccharides,* 2006. p. 49-96.
10. Buxbaum, G., *Industrial inorganic pigments*. 2 ed. 1997, Weinheim: Wiley-VCH. 43-70.
11. Diebold, U., *The surface of titanium dioxide.* Surf Sci Rep, 2003(48): p. 53-229.
12. Linsebigler, A.L., Lu, G.Q. and Yates, J.T., *Photocatalysis on TiO_2 Surfaces - Principles, Mechanisms, and Selected Results.* Chem Rev, 1995. **95**(3): p. 735-758.
13. Chen, X. and Mao, S.S., *Titanium dioxide nanomaterials: Synthesis, properties, modifications, and applications.* Chem Rev, 2007. **107**(7): p. 2891-2959.
14. Hoffmann, M.R., Martin, S.T., Choi, W.Y. and Bahnemann, D.W., *Environmental Applications of Semiconductor Photocatalysis.* Chem Rev, 1995. **95**(1): p. 69-96.
15. Mao, L.Q., Li, Q.L., Dang, H.X. and Zhang, Z.J., *Synthesis of nanocrystalline TiO_2 with high photoactivity and large specific surface area by sol-gel method.* Mater Res Bull, 2005. **40**(2): p. 201-208.
16. Yoon, K.H., Noh, J.S., Kwon, C.H. and Muhammed, M., *Photocatalytic behaviour of TiO_2 thin films prepared by sol-gel process.* Mater Chem Phys, 2006. **95**(1): p. 79-83.

17. Sugimoto, T., Zhou, X.P. and Muramatsu, A., *Synthesis of uniform anatase TiO_2 nanoparticles by gel-sol method 4. Shape control.* J Colloid Interf Sci, 2003. **259**(1): p. 53-61.

18. Sugimoto, T., Zhou, X.P. and Muramatsu, A., *Synthesis of uniform anatase TiO_2 nanoparticles by gel-sol method - 1. Solution chemistry of $Ti(OH)_{(n)(4-n)}$ complexes.* J Colloid Interf Sci, 2002. **252**(2): p. 339-346.

19. Sugimoto, T., Okada, K. and Itoh, H., *Synthesis of uniform spindle-type titania particles by the gel-sol method.* J Colloid Interf Sci, 1997. **193**(1): p. 140-143.

20. Schmidt, H., *Considerations about the sol-gel process: From the classical sol-gel route to advanced chemical nanotechnologies.* J Sol-Gel Sci Techn, 2006. **40**(2-3): p. 115-130.

21. Sugimoto, T., *Preparation of Monodispersed Colloidal Particles.* Adv Colloid Interf Sci, 1987. **28**(1): p. 65-108.

22. Sugimoto, T. and Zhou, X.P., *Synthesis of uniform anatase TiO_2 nanoparticles by the gel-sol method - 2. Adsorption of OH- ions to $Ti(OH)_4$ gel and TiO_2 particles.* J Colloid Interf Sci, 2002. **252**(2): p. 347-353.

23. Sugimoto, T., Zhou, X.P. and Muramatsu, A., *Synthesis of uniform anatase TiO_2 nanoparticles by gel-sol method 3. Formation process and size control.* J Colloid Interf Sci, 2003. **259**(1): p. 43-52.

24. Cozzoli, P.D., Kornowski, A. and Weller, H., *Low-temperature synthesis of soluble and processable organic-capped anatase TiO_2 nanorods.* J Am Chem Soc, 2003. **125**(47): p. 14539-14548.

25. Joo, J., Kwon, S.G., Yu, T., Cho, M., Lee, J., Yoon, J. and Hyeon, T., *Large-scale synthesis of TiO_2 nanorods via nonhydrolytic sol-gel ester elimination reaction and their application to photocatalytic inactivation of E. coli.* J Phys Chem B, 2005. **109**(32): p. 15297-15302.

26. Zhang, Z.H., Zhong, X.H., Liu, S.H., Li, D.F. and Han, M.Y., *Aminolysis route to monodisperse titania nanorods with tunable aspect ratio.* Angew Chem Int Edit, 2005. **44**(22): p. 3466-3470.

27. Chae, S.Y., Park, M.K., Lee, S.K., Kim, T.Y., Kim, S.K. and Lee, W.I., *Preparation of size-controlled TiO_2 nanoparticles and derivation of optically transparent photocatalytic films.* Chem Mater, 2003. **15**(17): p. 3326-3331.

28. Yang, S.W. and Gao, L., *Fabrication and characterization of nanostructurally flowerlike aggregates of TiO_2 via a surfactant-free solution route: Effect of various reaction media.* Chem Lett, 2005. **34**(7): p. 1044-1045.

29. Yoshida, R., Suzuki, Y. and Yoshikawa, S., *Syntheses of TiO_2 (B) nanowires and TiO_2 anatase nanowires by hydrothermal and post-heat treatments.* J Solid State Chem, 2005. **178**(7): p. 2179-2185.

30. Wang, X., Zhuang, J., Peng, Q. and Li, Y.D., *A general strategy for nanocrystal synthesis.* Nature, 2005. **437**(7055): p. 121-124.

31. Pinna, N., *The "benzyl alcohol route": an elegant approach towards organic-inorganic hybrid nanomaterials.* J Mater Chem, 2007. **17**(27): p. 2769-2774.

32. Wen, B.M., Liu, C.Y. and Liu, Y., *Bamboo-shaped ag-doped TiO_2 nanowires with heterojunctions.* Inorg Chem, 2005. **44**(19): p. 6503-6505.

33. Hong, S.S., Lee, M.S. and Lee, G.D., *Photocatalytic decomposition of p-nitrophenol over titanium dioxide prepared by reverse microemulsion method using nonionic surfactants with different hydrophilic groups.* React Kinet and Catal Lett, 2003. **80**(1): p. 145-151.

34. Li, Y.Z., Lee, N.H., Hwang, D.S., Song, J.S., Lee, E.G. and Kim, S.J., *Synthesis and characterization of nano titania powder with high photoactivity for gas-phase photo-oxidation of benzene from $TiOCl_2$ aqueous solution at low temperatures.* Langmuir, 2004. **20**(25): p. 10838-10844.

35. Lin, J., Lin, Y., Liu, P., Meziani, M.J., Allard, L.F. and Sun, Y.P., *Hot-fluid annealing for crystalline titanium dioxide nanoparticles in stable suspension.* J Am Chem Soc, 2002. **124**(38): p. 11514-11518.

36. Seifried, S., Winterer, M. and Hahn, H., *Nanocrystalline titania films and particles by chemical vapor synthesis.* Chem Vapor Depos, 2000. **6**(5): p. 239-244.

37. Ayllon, J.A., Figueras, A., Garelik, S., Spirkova, L., Durand, J. and Cot, L., *Preparation of TiO_2 powder using titanium tetraisopropoxide decomposition in a plasma enhanced chemical vapor deposition (PECVD) reactor.* J Mater Sci Lett, 1999. **18**(16): p. 1319-1321.

38. Park, D.G. and Burlitch, J.M., *Nanoparticles of Anatase by Electrostatic Spraying of an Alkoxide Solution.* Chem Mater, 1992. **4**(3): p. 500-502.

39. Peral, J., Domenech, X. and Ollis, D.F., *Heterogeneous photocatalysis for purification, decontamination and deodorization of air.* J Chem Technol Biot, 1997. **70**(2): p. 117-140.

40. Romero, M., Blanco, J., Sanchez, B., Vidal, A., Malato, S., Cardona, A.I. and Garcia, E., *Solar photocatalytic degradation of water and air pollutants: Challenges and perspectives.* Sol Energy, 1999. **66**(2): p. 169-182.

41. Anpo, M., *Utilization of TiO_2 photocatalysts in green chemistry.* Pure and Appl Chem, 2000. **72**(7): p. 1265-1270.

42. Roland Benedix, F.D., Jana Quaas, Marko Orgass, *Application of Titanium Dioxide Photocatalysis to Created Self-Cleaning Building Materials.* Lacer, 2000. **5**: p. 157-168.

43. Minero, C., Catozzo, F. and Pelizzetti, E., *Role of Adsorption in Photocatalyzed Reactions of Organic-Molecules in Aqueous TiO_2 Suspensions.* Langmuir, 1992. **8**(2): p. 481-486.

44. Ying, J.Y. and Sun, T., *Research needs assessment on nanostructured catalysts.* J Electroceram, 1997. **1**(3): p. 219-238.

45. Chen, P.H. and Jenq, C.H., *Kinetics of photocatalytic oxidation of trace organic compounds over titanium dioxide.* Environ Int, 1998. **24**(8): p. 871-879.

46. Ranjit, K.T., Willner, I., Bossmann, S. and Braun, A., *Modified titanium dioxide photocatalysts for the enhanced photodegradation of organic substrates.* Res Chem Intermediat, 1999. **25**(8): p. 733-756.

47. Senthilkumaar, S. and Porkodi, K., *Heterogeneous photocatalytic decomposition of Crystal Violet in UV-illuminated sol-gel derived nanocrystalline TiO_2 suspensions.* J Colloid Interf Sci, 2005. **288**(1): p. 184-189.

48. Tayade, R.J., Kulkarni, R.G. and Jasra, R.V., *Enhanced photocatalytic activity of TiO_2-coated NaY and HY zeolites for the degradation of methylene blue in water.* Ind Eng Chem Res, 2007. **46**(2): p. 369-376.

49. Peral, J. and Ollis, D.F., *TiO_2 photocatalyst deactivation by gas-phase oxidation of heteroatom organics.* J Mol Catal A-Chem, 1997. **115**(2): p. 347-354.

50. Kartal, O.E., Erol, M. and Oguz, H., *Photocatalytic destruction of phenol by TiO_2 powders.* Chem Eng Techn, 2001. **24**(6): p. 645-649.

51. Duan, X.D., Sun, D.Z., Zhu, Z.B., Chen, X.Q. and Shi, P.F., *Photocatalytic decomposition of toluene by TiO_2 film as photocatalyst.* J Enviro Sci and Health A, 2002. **37**(4): p. 679-692.

52. Cho, M., Chung, H.M., Choi, W.Y. and Yoon, J.Y., *Different inactivation Behaviors of MS-2 phage and Escherichia coli in TiO_2 photocatalytic disinfection.* Appl Environ Microbiol, 2005. **71**(1): p. 270-275.

53. Kim, B., Kim, D., Cho, D. and Cho, S., *Bactericidal effect of TiO_2 photocatalyst on selected food-borne pathogenic bacteria.* Chemosphere, 2003. **52**(1): p. 277-281.

54. Maness, P.C., Smolinski, S., Blake, D.M., Huang, Z., Wolfrum, E.J. and Jacoby, W.A., *Bactericidal Activity of Photocatalytic TiO_2 Reaction: toward an Understanding of Its Killing Mechanism.* Appl Environ Microbiol, 1999. **65**(9): p. 4094-4098.

55. Coleman, H.M., Marquis, C.P., Scott, J.A., Chin, S.S. and Amal, R., *Bactericidal effects of titanium dioxide-based photocatalysts.* Chem Eng J, 2005. **113**(1): p. 55-63.

56. Nalwa, H.S., *Handbook of Organic-Inorganic Hybrid and Nanocomposites*. 2003: ASP.

57. Sanchez, C., Julian, B., Belleville, P. and Popall, M., *Applications of hybrid organic-inorganic nanocomposites.* J Mater Chem, 2005. **15**(35-36): p. 3559-3592.

58. Romero, P.G, *Funtional Hybrid Materials*. 2004, Weinheim: Wiley-VCH.

59. Nakane, K., Kurita, T., Ogihara, T. and Ogata, N., *Properties of poly(vinyl butyral)/TiO_2 nanocomposites formed by sol-gel process.* Compos Part B: Eng, 2004. **35**(3): p. 219-222.

60. Zan, L., Tian, L.H., Liu, Z.S. and Peng, Z.H., *A new polystyrene-TiO_2 nanocomposite film and its photocatalytic degradation.* Appl Catal A-Gen, 2004. **264**(2): p. 237-242.

61. Yang, B.D. and Yoon, K.H., *Effect of nanoparticles on the conjugated polymer in the PPV/TiO_2 nanocomposites.* Synthetic Met, 2004. **142**(1-3): p. 21-24.

62. Marques, P., Trindade, T. and Neto, C.P., *Titanium dioxide/cellulose nanocomposites prepared by a controlled hydrolysis method.* Comp Sci Techn, 2006. **66**(7-8): p. 1038-1044.

63. Yamabi, S. and Imai, H., *Crystal phase control for titanium dioxide films by direct deposition in aqueous solutions.* Chem Mater, 2002. **14**(2): p. 609-614.

64. Neimo, L., *Papermaking Chemistry*. Vol. 4. 1999, Helsinki - Finland.

65. Fei, B., Deng, Z.X., Xin, J.H., Zhang, Y.H. and Pang, G., *Room temperature synthesis of rutile nanorods and their applications on cloth.* Nanotechnology, 2006. **17**(8): p. 1927-1931.

66. Chu, R.H., Yan, J.C., Lian, S.Y., Wang, Y.H., Yan, F.C. and Chen, D.W., *Shape-controlled synthesis of nanocrystalline titania at low temperature.* Solid State Commun, 2004. **130**(12): p. 789-792.

67. Park, H.K., Kim, D.K. and Kim, C.H., *Effect of solvent on titania particle formation and morphology in thermal hydrolysis of $TiCl_4$.* J Am Ceram Soc, 1997. **80**(3): p. 743-749.

68. Li, Y., White, T.J. and Lim, S.H., *Low-temperature synthesis and microstructural control of titania nano-particles.* J Solid State Chem, 2004. **177**(4-5): p. 1372-1381.

69. Seok, S.I. and Kim, J.H., *TiO_2 nanoparticles formed in silica sot-gel matrix.* Mater Chem Phys, 2004. **86**(1): p. 176-179.

70. Trung, T. and Ha, C.S., *One-component solution system to prepare nanometric anatase TiO_2.* Mater Sci Eng C-Bio, 2004. **24**(1-2): p. 19-22.

71. Lee, Y.C., Jung, Y.J., Park, P.Y. and Ko, K.H., *Preparation of TiO_2 powder by modified two-stage hydrolysis.* J Sol-Gel Sci Techn, 2004. **30**(1): p. 21-28.

72. Yu, K.F., Zhao, J.Z., Tian, Y.M., Jiang, M., Ding, X.F., Liu, Y.H., Zhu, Y.C. and Wang, Z.C., *Preparation of nanosized titanium dioxide from titanium n-butoxide modified with tartaric acid and its influence on the phase transformation.* Mater Lett, 2005. **59**(28): p. 3563-3566.

73. Wada, S., Chikamori, H., Noma, T. and Suzuki, T., *Synthesis of new titanium chelated complexes stabilized in aqueous solution and their stability on pH and temperature.* J Mater Sci Lett, 2000. **19**(20): p. 1855-1858.

74. Fang, C.S. and Chen, Y.W., *Preparation of titania particles by thermal hydrolysis of $TiCl_4$ in n-propanol solution.* Mater Chem Phys, 2003. **78**(3): p. 739-745.

75. Chen, K.Y. and Chen, Y.W., *Synthesis of spherical titanium dioxide particles by homogeneous precipitation in acetone solution.* J Sol-Gel Sci Techn, 2003. **27**(2): p. 111-117.

76. Abazovic, N.D., Comor, M.I., Dramicanin, M.D., Jovanovic, D.J., Ahrenkiel, S.P. and Nedeljkovic, J.M., *Photoluminescence of anatase and rutile TiO_2 particles.* J Phys Chem B, 2006. **110**(50): p. 25366-25370.

77. Guillard, C., Lachheb, H., Houas, A., Ksibi, M., Elaloui, E. and Herrmann, J.M., *Influence of chemical structure of dyes, of pH and of inorganic salts on their*

photocatalytic degradation by TiO_2 comparison of the efficiency of powder and supported TiO_2. J Photochem Photobio A, 2003. **158**(1): p. 27-36.

78. Gopal, M., Chan, W.J.M. and DeJonghe, L.C., *Room temperature synthesis of crystalline metal oxides.* J Mater Sci, 1997. **32**(22): p. 6001-6008.
79. Samuel, V., Pasricha, R. and Ravi, V., *Synthesis of nanocrystalline rutile.* Ceram Inter, 2005. **31**(4): p. 555-557.
80. Lencka, M.M. and Riman, R.E., *Thermodynamic Modeling of Hydrothermal Synthesis of Ceramic Powders.* Chem Mater, 1993. **5**(1): p. 61-70.
81. Sugimoto, T. and Zhou, X.P., *Synthesis of uniform anatase TiO_2 nanoparticles by the gel-sol method - 2. Adsorption of OH- ions to $Ti(OH)_4$ gel and TiO_2 particles.* J Colloid Interf Sci 2002. **252**(2): p. 347-353.
82. Sugimoto, T., Muramatsu, A. and Zhou, X., *Synthesis of uniform anatase TiO_2 nanoparticles by gel-sol method. 3. Formation process and size control.* J Colloid Interface Sci, 2003. **259**(1): p. 43-52.
83. Wei, Y., Wu, R.T. and Zhang, Y.F., *Preparation of monodispersed spherical TiO_2 powder by forced hydrolysis of $Ti(SO_4)_2$ solution.* Mater Lett, 1999. **41**(3): p. 101-103.
84. Sivakumar, S., Pillai, P.K., Mukundan, P. and Warrier, K.G.K., *Sol-gel synthesis of nanosized anatase from titanyl sulfate.* Mater Lett, 2002. **57**(2): p. 330-335.
85. Grdadolnik, J. and Marechal, Y., *Urea and urea-water solutions-an infrared study.* J Mol Struct, 2002. **615**(1-3): p. 177-189.
86. Rivest, R., *Coordination Complexes of Titanium (IV) Halides .3. Preparation and infrared spectra of complexes of titanium tetrachloride with urea, thiourea, and some of their derivatives.* Can J Chem, 1962. **40**(12): p. 2234-2241.
87. Decher, G., *Fuzzy nanoassemblies: Toward layered polymeric multicomposites.* Science, 1997. **277**(5330): p. 1232-1237.
88. Jiang, C.Y., Markutsya, S. and Tsukruk, V.V., *Collective and individual plasmon resonances in nanoparticle films obtained by spin-assisted layer-by-layer assembly.* Langmuir, 2004. **20**(3): p. 882-890.
89. Radtchenko, I.L., Papastavrou, G. and Borkovec, M., *Direct force measurements between cellulose surfaces and colloidal silica particles.* Biomacromolecules, 2005. **6**(6): p. 3057-3066.
90. Sousa, F.L., Ferreira, A., Ferreira, R.A.S., Cavaleiro, A.M.V., Carlos, L.D., Nogueira, H.I.S., Rocha, J. and Trindade, T., *Lanthanopolyoxotungstoborates: Synthesis, characterization, and layer-by-layer assembly of europium photoluminescent nanostructured films.* J Nanosc Nanotechno, 2004. **4**(1-2): p. 214-220.
91. Podsiadlo, P., Choi, S.Y., Shim, B., Lee, J., Cuddihy, M. and Kotov, N.A., *Molecularly engineered nanocomposites: Layer-by-layer assembly of cellulose nanocrystals.* Biomacromolecules, 2005. **6**(6): p. 2914-2918.

92. Kim, K.D. and Kim, H.T., *Synthesis of TiO_2 nanoparticles by hydrolysis of TEOT and decrease of particle size using a two-stage mixed method.* Powder Technol, 2001. **119**(2-3): p. 164-172.

93. Ding, X.Z. and Liu, X.H., *Synthesis and microstructure control of nanocrystalline titania powders via a sol-gel process.* Mater Sci Eng A-Struct, 1997. **224**(1-2): p. 210-215.

94. Zhang, H.Z. and Banfield, J.F., *Size dependence of the kinetic rate constant for phase transformation in TiO_2 nanoparticles.* Chem Mater, 2005. **17**(13): p. 3421-3425.

95. Kanie, K. and Sugimoto, T., *Shape control of anatase TiO_2 nanoparticles by amino acids in a gel-sol system.* Chem Commun, 2004(14): p. 1584-1585.

96. Zhong, Z.Y., Chen, F.X., Ang, T.P., Han, Y.F., Lim, W.Q. and Gedanken, A., *Impact of growth kinetics on morphology and pore structure of TiO_2-one-pot synthesis of macroporous TiO_2 microspheres.* Inorg Chem, 2006. **45**(12): p. 4619-4625.

97. Eiden-Assmann, S., Widoniak, J. and Maret, G., *Synthesis and characterization of porous and nonporous monodisperse colloidal TiO_2 particles.* Chem Mater, 2004. **16**(1): p. 6-11.

98. Barringer, E.A. and Bowen, H.K., *High-purity, monodisperse TiO_2 powders by hydrolysis of titanium tetraethoxide. 1. Synthesis and physical-properties.* Langmuir, 1985. **1**(4): p. 414-420.

99. Park, J.K., Myoung, J.J., Kyong, J.B. and Kim, H.K., *Reaction mechanism for the hydrolysis of titanium alkoxides.* B Kor Chem Soc, 2003. **24**(5): p. 671-673.

100. Barringer, E.A. and Bowen, H.K., *High-purity, monodisperse TiO_2 powders by hydrolysis of titanium tetraethoxide. 2. Aqueous interfacial electrochemistry and dispersion stability.* Langmuir, 1985. **1**(4): p. 420-428.

101. Pelton, R., Brook, M. and Geng, X., *Photocatalytic paper from colloidal TiO_2-fact or fantasy.* Adv Colloid Interface Sci, 2006. **127**(1): p. 43-53.

102. Iguchi, Y., Ichiura, H., Kitaoka, T. and Tanaka, H., *Preparation and characteristics of high performance paper containing titanium dioxide photocatalyst supported on inorganic fiber matrix.* Chemosphere, 2003. **53**(10): p. 1193-1199.

103. Gao, X.T. and Wachs, I.E., *Titania-silica as catalysts: molecular structural characteristics and physico-chemical properties.* Catal Today, 1999. **51**(2): p. 233-254.

104. Atik, M., Neto, P.L., Avaca, L.A., Aegerter, M.A. and Zarzycki, J., *Protection of 316L stainless steel against corrosion by SiO_2 coatings.* J Mater Sci Lett, 1994. **V13**(15): p. 1081-1085.

105. Stober, W., Fink, A. and Bohn, E., *Controlled growth of monodisperse silica spheres in micron size range.* J Colloid Interf Sci, 1968. **26**(1): p. 62-69.

106. Pinto R. J. B., M.P.A.A.P., Timmons A. M. B., Trindade T., Neto C. P. , *Novel SiO_2/cellulose nanocomposites obtained by in situ syntheses and LbL technique.* Submitted, 2007.

107. Witucki, G.L., *Silane Primer - Chemistry and Applications of Alkoxy Silanes.* J Coatings Tech, 1993. **65**(822): p. 57-60.

108. Abdelmouleh, M., Boufi, S., ben Salah, A., Belgacem, M.N. and Gandini, A., *Interaction of silane coupling agents with cellulose.* Langmuir, 2002. **18**(8): p. 3203-3208.

109. Salon, M.C.B., Abdelmouleh, M., Boufi, S., Belgacem, M.N. and Gandini, A., *Silane adsorption onto cellulose fibers: Hydrolysis and condensation reactions.* J Colloid Interf Sci, 2005. **289**(1): p. 249-261.

110. Casserly, T.B. and Gleason, K.K., *Density functional theory calculation of ^{29}Si NMR chemical shifts of organosiloxanes.* J Phys Chem B, 2005. **109**(28): p. 13605-13610.

111. Takada, S., Hata, N., Hayamizu, K., Murakami, M., Deguchi, K., Ohki, S., Tansho, M. and Shimizu, T., *Skeletal Si-O-Si network connectivity of self-assembled porous silica for low-k dielectrics depending on organoalkoxysilane concentration in precursor solutions.* J Appl Phys, 2007. **101**(6).

112. Ma, Z.R., Dunn, B.C., Turpin, G.C., Eyring, E.M., Ernst, R.D. and Pugmire, R.J., *Solid state NMR investigation of silica aerogel supported Fischer-Tropsch catalysts.* Fuel Process Technol, 2007. **88**(1): p. 29-33.

113. Fadeev, A.Y., Helmy, R. and Marcinko, S., *Self-assembled monolayers of organosilicon hydrides supported on titanium, zirconium, and hafnium dioxides.* Langmuir, 2002. **18**(20): p. 7521-7529.

114. Colthup N.B., D.L.H., Wiberley S.E., *Introduction to infrared and raman spectroscopy*. 3rd ed. 1990, Boston: Academic Press.

115. Matinlinna, J.P., Areva, S., Lassila, L.V.J. and Vallittu, P.K., *Characterization of siloxane films on titanium substrate derived from three aminosilanes.* Surf Interface Anal, 2004. **36**(9): p. 1314-1322.

116. Pietak, A., Korte, S., Tan, E., Downard, A. and Staiger, M.P., *Atomic force microscopy characterization of the surface wettability of natural fibres.* Appl Surf Sci, 2007. **253**(7): p. 3627-3635.

117. Jesionowski, T. and Krysztafkiewicz, A., *Preparation of the hydrophilic/hydrophobic silica particles.* Colloid Surfaces A, 2002. **207**(1-3): p. 49-58.

118. Dahiya, J.B. and Rana, S., *Thermal degradation and morphological studies on cotton cellulose modified with various arylphosphorodichloridites.* Polym Inter, 2004. **53**(7): p. 995-1002.

119. Wang, Q.F. and Shi, W.F., *Photopolymerization and thermal behaviors of acrylated benzenephosphonates/epoxy acrylate as flame retardant resins.* Eur Polym J, 2006. **42**(10): p. 2261-2269.

120. Al-Ghamdi, R.F., Fahmi, M.M. and Mohamed, N.A., *Thermal stability and degradation behavior of novel wholly aromatic azopolyamide-hydrazides.* Polym Degrad Stabil, 2006. **91**(7): p. 1530-1544.

121. Herrmann, J.M., *Heterogeneous photocatalysis: State of the art and present applications.* Top Catal 2005. **34**(1-4): p. 49-65.

122. Fujishima, A., Rao, T.N. and Tryk, D.A., *Titanium dioxide photocatalysis.* J Photochem Photobio C, 2000. **1**(1): p. 1-21.

123. Tayade, R.J., Kulkarni, R.G. and Jasra, R.V., *Enhanced Photocatalytic Activity of TiO_2-Coated NaY and HY Zeolites for the Degradation of Methylene Blue in Water.* Ind Eng Chem Res, 2007. **46**(2): p. 369-376.

124. Minero, C., Catozzo, F. and Pelizzetti, E., *Role of adsorption in photocatalyzed reactions of organic-molecules in aqueous TiO_2 suspensions.* Langmuir, 1992. **8**(2): p. 481-486.

125. Zhang, T., Oyama, T., Aoshima, A., Hidaka, H., Zhao, J. and Serpone, N., *Photooxidative N-demethylation of methylene blue in aqueous TiO_2 dispersions under UV irradiation.* J Photochem Photobio A, 2001. **140**(2): p. 163-172.

126. Thevenet, F., Guaitella, O., Herrmann, J.M., Rousseau, A. and Guillard, C., *Photocatalytic degradation of acetylene over various titanium dioxide-based photocatalysts.* Appl Catal B, 2005. **61**(1-2): p. 58-68.